

STORAGE AND HANDLING OF BULK SOLIDS

Greg Mehos, Ph.D., P.E.

Storage and Handling of Bulk Solids

FOR MORE INFORMATION CONTACT:

Greg Mehos, Ph.D., P.E.

4 Crusade Road

Westford, MA 01886

www.mehos.net

About this book

When I became an adjunct professor at the University of Rhode Island, I realized that most books on the subject of bulk solids testing and hopper design were either very terse or rather intense for readers who did not have a mechanical engineering background. I began preparing my course notes when I worked at Cabot Corporation and improved them when I joined Jenike & Johanson, Inc. While at both Cabot and J&J, I wrote a number of articles for *Chemical Engineering*, *Chemical Engineering Progress*, and other rags. They really came in handy when I was asked to write the subsection on powder flow and hopper design of the ninth edition of Perry's Chemical Engineers' Handbook. Jenike & Johanson encouraged me to write, provided that I only disclosed design methods that were published in the open literature. I carefully adhered to those guidelines when writing this book. Yes, some of the text was taken from my prior publications, but I figure that it isn't plagiarism when you Ctrl+C and Ctrl+V your own material. (If I were a faculty member or administrator at Harvard, I could copy and paste anyone's material.) A few of the formulas I derived on my own, but they were all based on fundamental engineering principles. Consequently, some of the analyses that I present may be slightly different from what you might find published elsewhere, so use them with caution.

I always advise my students to keep this book in the bathroom. That way they can read about hoppers when they are sitting on the hopper, and if they run out of toilet paper, there isn't a crisis.

I have found that when teaching, it is best to start with the fundamentals and then use them to derive the equations that can be used to predict bulk solids

flow behavior and design systems for reliable flow. When you read this work, I encourage you to understand the first fundamental equation, know how to apply the final one, and then appreciate that someone who was much smarter than us¹ was able to come up with all the equations in between. Fundamentals are fun!

I've always said that handling powders is a lot like electricity – sometimes a little knowledge is more dangerous than none at all. In the real world, there is almost always more than one answer to a problem. For challenging problems, I encourage you to contact me, Jenike & Johanson, Solids Handling Technologies, or other engineering firms that specialize in the storage and handling of bulk solids. Andrew Jenike developed his test and design methods in the 1960's; yet his principles have withstood the test of time and are still used today. When analyses are based on fundamentals rather than empiricism, an engineer can have great confidence in his or her designs, and formulators can be confident that their powders can be handled reliably in their available equipment.

Engineers are adept at solving equations, and as a consultant, I rely on the following formula:

Happiness Equals Reality Minus Expectations

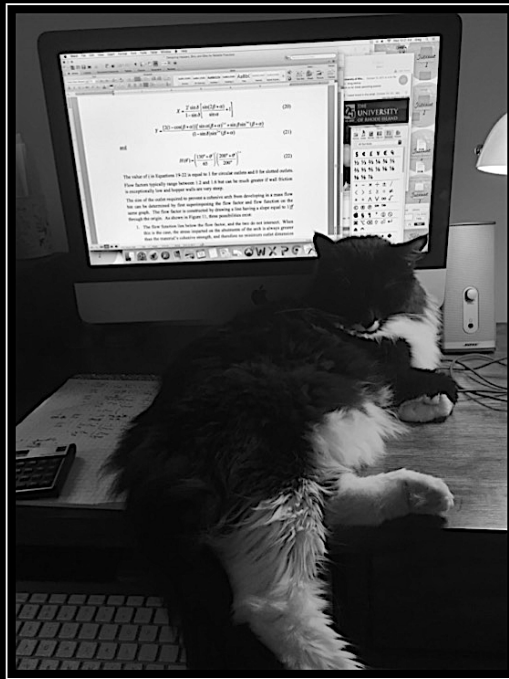
Note that there are three terms. If the last term is larger than the middle one, the first one is negative. My goal as a consultant is to understand the reality of bulk solids handling. That way I can exceed my clients' expectations, they'll be happy and eager to pay me, and I can eke out a miserable existence.

Greg Mehos, Ph.D., P.E.²

¹ To be grammatically correct, this sentence should be written as “smarter than we.” I checked with Mrs. Sanchez, my high-school English teacher. She agrees and she has pardoned me.

² I am excited to have both Ph.D. and P.E. after my name although my nephew thinks I'm a physical education teacher.

DEDICATION



TO TOMMY

Without you, I'd have finished sooner!

TABLE OF CONTENTS

1. INTRODUCTION	6
Some definitions	9
Thank you, Dr. Andrew Jenike	10
Flow problems	11
Flow patterns	13
So how do we define flowability?	16
The classic Rand Corporation study	22
2. ANALYSIS OF STRESS	24
Continuum model	26
Transformation of stress and Mohr's circles	28
3. STRESSES IN HOPPERS, BINS, AND SILOS	35
Cylinder (vertical) section	36
Hopper (converging) section – mass flow	42
Funnel flow hoppers	47
4. BULK SOLIDS FLOW PROPERTIES TESTING	48
Cohesive strength and internal friction	49
Bulk density/compressibility	63
Wall friction	65
<i>FFC</i>	70
Permeability	71
Hopper tests	76
Particle size	79

5. BIN DESIGN	82
Mass flow hopper angle	82
Jenike's flow - no flow postulate	88
Critical mass flow outlet dimensions to prevent arching	88
Solids discharge rates	101
Funnel flow outlet size to prevent arching and ratholing	110
Expanded flow dimensions	113
Inserts	114
Converging/diverging walls	120
Over-pressurization	121
Flow channel angle	124
Capacity	126
Be careful how you regress the data!	128
Bin selection	130
Example bin design	130
There is always more than one answer	136
6. FEEDERS AND FLOW AIDS	144
Rotary valves	145
Screw feeders	146
Other feeders	152
Flow aids	155
Air assist and fluidization	157
Reclaim systems	158
7. OTHER STUFF	161
Segregation	161
Caking	178
Process vessels – not in abridged version	
Pneumatic conveying	183
Transfer chutes	198
8. BETTER REFERENCES THAN THIS ONE	204

1. INTRODUCTION

Designing systems for reliable handling of bulk solids or determining if a vessel is appropriate for a bulk solid that is to be handled can pose challenges that do not typically arise when tackling assignments that involve the transport of fluids. More often than not, the information needed for predicting fluid behavior is readily accessible. A fluid's viscosity and density can usually be found in a reference book or a website; otherwise, correlations, estimation methods, or equations of state detailed in textbooks can be used to calculate the necessary physical properties. Given the diameter of a transfer line, the fluid's flow behavior, *e.g.*, laminar or turbulent flow, can then be confidently predicted. From the length and layout of the line and knowing the roughness of the pipe, information that is also readily found in print, the pump required to transfer the fluid at the desired rate can be specified. If cavitation is a concern, the pump's net positive suction head requirements can be readily determined as the fluid's vapor pressure is likely available from data or correlations. You know the drill. Gather the physical properties, specify a velocity, assume a pipe diameter, and then calculate a Reynolds number. Then calculate a ΔP , which will allow you to calculate an hp and size your pump. Easy as π !

Designing a system for handling solids, however, may be more trying as the fundamental properties required to predict flow behavior may not be immediately obvious and any necessary data may not be readily available. In fact, a property as simple as a material's bulk density is highly dependent on the particles' shape, size, and porosity, and therefore any published data providing the bulk density of a powder may not necessarily be representative of the material that will be handled. In addition, because bulk solids are compressible, the bulk density of a material inside a hopper, bin, or silo will vary due to consolidation stresses. Without proper training, one may be resigned to select a conical hopper that has an aesthetically pleasing

slope or recommend a pyramidal vessel that is inexpensive to fabricate, size the outlet to fit the valve that a supplier recommended, and propose the installation of vibrating equipment to promote flow. Perhaps that is why identifying equipment and lines that handle bulk solids is often easy – they are the ones with the hammer marks (see Figure 1.1).



Figure 1.1. Examples of “bin rash”.

Many geometries are used in the design of hoppers, bins, and silos, including conical, pyramidal, wedge, chisel, and transition (round to rectangular). Common designs are shown in Figure 1.2.

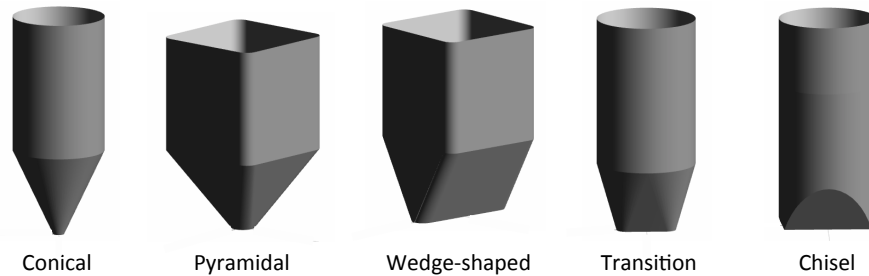


Figure 1.2. Common hopper designs.

Frequently, the size and geometry of a hopper or bin are based on ease of fabrication rather than with consideration of the solids’ flow behavior. Sometimes, bulk solids are stored in flat-bottomed vessels, some equipped with agitators. These vessels are appropriate for storing liquids, but bulk solids behave differently. A liquid spreads when it is poured onto a flat

surface. A bulk solid forms a pile. Liquids are nearly incompressible. Most bulk solids are highly compressible. With liquids, the resistance to shear, *i.e.*, its viscosity, is independent of normal pressure but is dependent on shear rate. For bulk solids, the shear stress is dependent on normal stress and independent of shear rate. Liquids are isotropic, that is, their properties such as pressure are the same in all directions. Bulk solids are anisotropic; their stresses vary with direction. Unlike liquids, bulk solids have friction and can generate shear stresses at wall boundaries.

Designing vessels for storing or handling bulk solids by following methods established for fluids is a risk that is too often taken. Unfortunately, compared to liquids and gases, training in bulk solids is frequently lacking for scientists and engineers. For many, bulk solids fit into the four categories presented in Table 1-1 [Woodcock, C.R. and J.S. Mason, Bulk Solids Handling: An Introduction to the Practice and Technology, Chapman & Hall, London, 1987].

Table 1-1	
Classification of Bulk Solids	
Neurotic	Move awkwardly - Poor flowability - Sticky or tacky
Sadistic	Attack their surroundings - Abrasive - Explosive
Masochistic	Suffer from their surroundings - Friable - Degradable
Schizophrenic	Change their behavior - Hygroscopic - Electrostatic

This book attempts to summarize the fundamental principles behind bulk solids handling, test methods for measuring their fundamental flow properties, and methods for designing systems for reliable flow or predicting flow behavior in existing equipment, *e.g.*, determining if an existing bin or hopper will be able to handle a powder without difficulties.

Some definitions

Now is a good time to define a few terms that are used in the discussion of bulk solids handling.

Bulk solid – a material consisting of discrete solid particles, handled in bulk form. There really is no limit to their size. The material must be made up of separate particles. The term bulk solid does not apply to muds, pastes, or slurries. The terms *bulk solids* and *powders* are sometimes used interchangeably.

Hopper, bin, or silo – storage vessels for bulk solids. The terms are often used interchangeably. Silos usually refer to tall vessels that store several tons of material. Hoppers and bins usually refer to smaller vessels. The converging section of a storage vessel is often called the hopper section. For the most part, this book will refer to storage vessels as bins.

Cylinder – vertical part of a bin. It may be round or rectangular, and it has a constant cross section.

Expanded flow – flow pattern inside a bin, where all the bulk material is in motion in the bottom portion of the vessel when discharged, but flow only occurs in a central flow channel in the top portion of the vessel.

Feeder – device for modulating the withdrawal rate of bulk material. Examples include rotary valves, screw feeders, and belt feeders. Often, a valve or gate is used to stop and start flow, but such devices in general should not be used to control the discharge rate of bulk solids.

Flow channel – the space in a bin in which the bulk solid is actually flowing during withdrawal.

Funnel flow – flow pattern inside a bin, where the bulk material only moves in a flow channel above the outlet when withdrawn.

Hopper section – the converging part of a storage vessel that has sloped walls and a variable cross section.

Major principal stress – the maximum normal stress on a bulk solid. The terms major principal stress, major consolidation stress, and major consolidation pressure may be used interchangeably.

Mass flow – flow pattern inside a bin where all material is in motion when withdrawn.

Shear cell tester – device that measures the cohesive strength, compressibility, and wall friction of bulk solids.

Unconfined yield strength – a fancy way to say cohesive strength.

Thank you, Dr. Andrew Jenike

Andrew W. Jenike began his work on the development of the theory of bulk solids flow in the early 1950s and published his classic bulletins in the mid 1960s [Jenike, A.W., Gravity Flow of Bulk Solids, Bulletin 108, University of Utah Engineering Station, 1961; Jenike, A.W., Storage and Flow of Solids, Bulletin 123³, University of Utah Engineering Station, 1964 (revised, 1976)]. Until then, the walls of hoppers, bins, and silos were usually 30° or 45° from vertical because those were the angles of common triangles that engineers of that era used to carry. (Yes, engineers had a reputation for being nerdy back then, not that anything is different today!) An advantage of specifying a 30° from vertical cone was that its fabrication from a flat sheet of metal generated the least amount of waste material. Of course, in the days without calculators, choosing an angle whose sine was equal to 0.5 was an added bonus.

Andrew Jenike was born in Poland in 1914 and graduated from Warsaw Polytechnic Institute with a B.S. in mechanical engineering in 1939. Jenike joined the military and fought the Nazis until Poland was overrun. He escaped to England where he continued his education, receiving his doctorate in structural engineering from the University of London in 1949. Later, he immigrated to Canada and then the United States. He eventually settled in Salt Lake City, Utah.

Jenike was a bookworm, and so in his spare time, he enjoyed browsing the literature at the University of Utah library. He was surprised to find that bin design at the time was a black art. Storage equipment for bulk solids was pretty much taken for granted. Designs were based on rules of thumb or methods that made the math stress-free and fabrication easy. He approached

³ <https://digital.library.unt.edu/ark:/67531/metadc1067072/?q=Bulletin%20123> has a pdf copy of Bulletin 123 that you can download. It really is a classic. It's a bit confusing because the number 13 seems to appear everywhere. Jenike presented his expressions in terms of force rather than stress, and the number 13 is the reciprocal of the cross-sectional area of his 3/4 inch diameter cell in square feet.

the NSF (National Science Foundation, not Not Safe for Work), who agreed that storage and flow of bulk solids fundamentals was a subject worthy of research. To be funded, however, he would have to be affiliated with a college or university. He contacted the University of Utah with a proposal; If the University were to hire him, he would work for no salary. NSF would provide the funding. All Jenike needed was a lab and some students. (Come to think of it, I have a similar arrangement at the University of Rhode Island where I am an adjunct professor. I don't get paid, but I am able to embellish my LinkedIn profile.)

Using a solids mechanics continuum approach, Jenike developed a theoretical approach to solids flow. The critical fundamental flow properties of a bulk solid were found to be its cohesive strength, internal friction, wall friction, and bulk density. Testing methods and shear cells along with design techniques were developed, and experiments were run to confirm and refine the analysis. Knowing the bulk solid's cohesive strength and bulk density, the dimensions of a hopper outlet that would prevent the development of obstructions to flow could be calculated. Wall friction data could be used to determine the slope of hopper walls that prevented ratholes from developing when a powder was discharged from a hopper.

Jenike eventually left the University of Utah and moved to Massachusetts to live nearer to the ocean and pursue full-time consulting. Jerry Johanson, one of his Ph.D. students, later joined him, and in 1966, the two founded Jenike & Johanson, Inc. John Carson, who had worked in Jenike's basement as a co-op student, was hired after receiving his Ph.D. from Massachusetts Institute of Technology and eventually became president. Jenike's test and design methods that were developed in the 1960s still form the primary bases for the design of hoppers, bins, and silos for reliable flow of bulk materials. The advancement of computers has allowed the development of automated testers for measuring solids flow properties; however, they only are able to gain acceptance if the test results agree with data obtained from Jenike's original direct shear cell. By measuring the fundamental properties of a bulk solid, the flow behavior of the material can be predicted, and reliable hoppers, bins, and silos can be designed.

Flow problems

Many storage vessels are fabricated from architectural or fabrication viewpoints. However, designing equipment without regard to the bulk

material being handled often leads to flow problems. Common solids flow problems include:

No flow. If a stable dome, bridge, or arch forms over the outlet of a bin, the bulk solid will not flow when the feeder is started or gate is opened. If a stable rathole forms in a vessel in which flow only occurs in a narrow channel above the outlet, material will stop flowing when the flow channel empties. Obstructions to flow are illustrated in Figure 1.3.

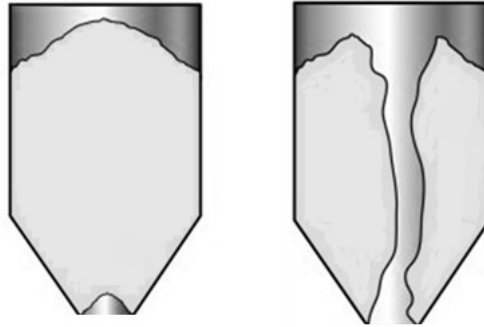


Figure 1.3. Obstructions to flow – cohesive arch (left), stable rathole (right).

Erratic flow. Erratic flow occurs when both arching and ratholing occurs. If a rathole collapses due to external vibration, the bulk solid may arch as it impacts the outlet. After the arch fails due to vibration or operator intervention, the flow channel will empty leaving a rathole momentarily stopping flow until it eventually collapses, reforming a cohesive arch.

Flooding. If a stable rathole develops and fresh material is added or if a rathole collapses and falls into the channel, it may become aerated or fluidized. Since most feeders are designed to handle solids and not fluids, the fluidized material may flood, that is, discharge uncontrollably in a fluidized state from the bin, and the feeder will not be able to control the rate of discharge.

Limited discharge rate. As a fine powder dilates as it flows toward the outlet, vacuum will naturally develop inside the hopper above the outlet. As a consequence, air will flow counter to the solids, disrupting flow. Increasing the speed of the feeder will no longer increase the discharge rate of powder as the discharge rate has become limited.

Caking. Some materials will readily flow from a bin if handled continuously. Other materials, however, will exhibit flow problems if allowed to remain at rest for a period of time. Given enough time at rest, some powders will gain additional cohesive strength, and obstructions to flow such as arches and ratholes may become exceptionally difficult to remove.

Segregation. Some materials, when transferred into a bin, will segregate, that is, particles of different size will separate. For some powders, once a pile is formed, larger particles, which are relatively free flowing, will roll down the surface towards the periphery of the vessel; smaller particles will percolate through the bed and concentrate in the center. When the piles avalanche, the momentum of the larger particles causes them to travel farther than the finer particles (see Figure 1.4). Lyn Bates refers to this as “Christmas tree segregation” [Bates, L., User Guide to Segregation, Bartham Press, London, 1997]. If flow only occurs in a central channel during discharge, the particle size distribution of the powder leaving the bin will be considerably different than that of the feed.

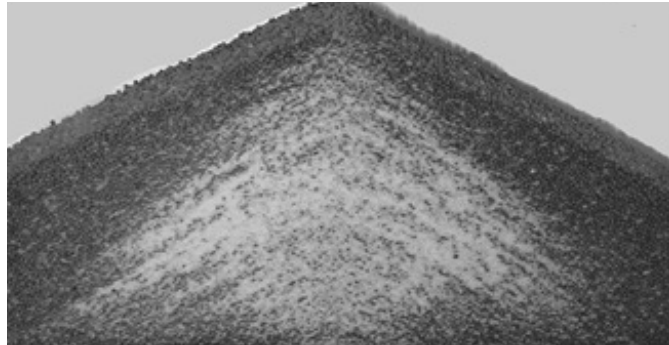


Figure 1.4. Sifting segregation.

Flow patterns

The likelihood of a solids flow problem often depends on the flow pattern present inside a bin. There are three primary flow patterns that can occur: *mass flow*, *funnel flow*, and *expanded flow*. In mass flow, the entire bed of solids is in motion when material is discharged from the outlet, including material along the walls. Mass flow hoppers typically have steep and/or low-friction walls. Provided that the outlet is large enough to prevent

arching, all material will be discharged from the bin, as ratholes will not form. Mass flow is illustrated in Figure 1.5.

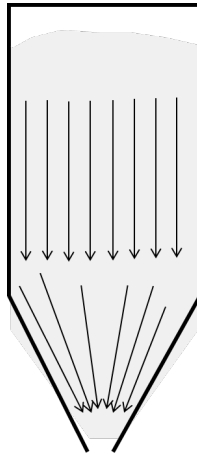


Figure 1.5. Mass flow pattern.

Mass flow bins are characterized by a first-in, first-out flow sequence and therefore are suitable for handling materials that degrade with time or are prone to caking. The steep hopper walls provide a more uniform flow, making mass flow hoppers suitable for process vessels. Discharge rates are predictable and likely more steady, since the bulk density of the material is nearly independent of the head of the material inside the vessel. Sifting segregation is minimized, as fine and coarse particles separated during filling are remixed at the outlet during discharge.

A disadvantage of a mass-flow hopper is that it requires relatively more headroom due to its steep hopper section. This is especially the case for conical hoppers.

In *funnel flow*, an active flow channel forms above the outlet, with stagnant material remaining at the periphery (*i.e.*, ratholes). This occurs when the walls of the hopper section of the storage vessel are not steep enough or have low enough friction to allow flow along them. The size of the resultant flow channel is approximately the largest dimension of the outlet. It is equal to the diameter of a round outlet or the diagonal of a slotted outlet. For a conical funnel flow hopper, the fraction of its volume that is active can be dramatically small. If the bulk material is cohesive, the ratholes may be

stable and the effective capacity of the bin will be just a small fraction of the intended capacity. Funnel flow is illustrated in Figure 1.6.

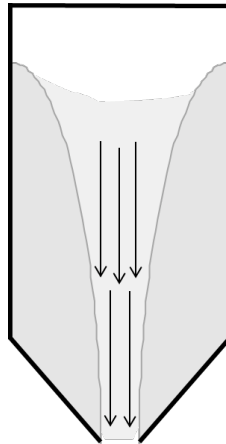


Figure 1.6. Funnel flow pattern.

A funnel flow bin typically exhibits a first-in, last-out flow sequence. Therefore, materials that readily cake or degrade over time should not be handled in funnel flow hoppers. Funnel flow can cause erratic flow and induce high loads (depending on vessel size) on the structure and downstream equipment due to collapsing ratholes and eccentric flow channels. If the powder is cohesive, ratholes may become stable, and the vessel will not empty.

Funnel flow bins are best suited for bulk solids that are free flowing and do not degrade or gain strength over time. They should not be used if segregation is a concern. Funnel flow vessels require less headroom and in general are less expensive to build since they can have shallower walls.

Expanded flow is characterized by mass flow in the lowermost section of a bin and funnel flow in the upper section. An expanded flow bin is essentially a mass flow bin with a funnel flow hopper section above it. An expanded flow bin is illustrated in Figure 1.7.

The outlet of the funnel flow hopper section must be large enough to prevent stable ratholes from developing. Because the bottom section is designed for mass flow, discharge rates are uniform and predictable. Expanded flow bins are frequently used when large bin diameters are required.

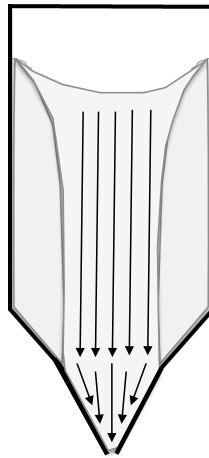


Figure 1.7. Expanded flow hopper.

Designing systems for bulk solids can be challenging since they have a wide range of characteristics, *e.g.*, cohesive or free-flowing; fine or coarse; fluffy or dense; adhesive to surfaces or surface repellent; easily aerated or nearly impermeable; and highly compressible or nearly incompressible. Defining a particle size, density, or permeability may be straightforward. The best metric for cohesion or adhesion, however, might not be as obvious. These characteristics or a combination of them ought to be useful in defining a bulk material's ease of flow or "flowability".

So how do we define flowability?

Several methods exist for measuring the relative flowability of bulk materials. The simplest is to determine the powder's angle of repose by pouring the material onto a horizontal surface and measuring the surcharge angle of the pile that is formed. A powder that forms a steeper pile is believed to be less flowable than one that is shallow. However, as stated by [Andrew Jenike](#) [[Storage and Flow of Solids](#), Bulletin 123, Utah Experimental Station, 1964]:

"The angle of repose is not a measure of the flowability of solids. In fact, it is useful only in the determination of the contour of a pile, and its popularity among engineers and investigators is due not to its usefulness but to the ease with which it is measured."

Compressibility tests, such as those in which a sample of bulk solid is vibrated or tapped inside a cylinder, are often used. The Hausner ratio is the

ratio of the “tapped” density to the aerated or loose bulk density. The Carr ratio is determined by dividing the difference between the tapped and freely settled volumes of a given mass of material by the freely settled volume. A low Hausner ratio or low Carr ratio indicates that the material is easy to handle. These ratios might be useful for comparing the relative cohesiveness of similar materials; however, the ratios reveal no fundamental information that can be used to predict how a powder will flow or if a powder will flow in a bin.

Hausner and Carr ratios are frequently used in the pharmaceutical industry in an attempt to quantify flowability. The indices are of limited use, however, since at best, these ratios can be only loosely correlated to the flow behavior of similar powders. In addition, these methods are deficient as the stress applied to the sample of powder is unknown, the tests do not replicate the degree of consolidation that takes place when a powder is stored in a vessel, and the gain in the material’s strength during rest cannot be determined.

Another flowability test involves a series of tests, including angle of repose, angle of spatula, bulk density before and after vibration, and particle size distribution, to establish a flow index. This index is known as the Carr index, which is determined by summing scores that depend on the outcomes of each test [Carr, R., *Chem. Eng.*, 72, 163 (1965)]⁴. The maximum possible score for each test was 25, and any powder scoring a Carr index of 100 won a prize. Interpretations of the Carr index are given in Table 1-2.

The Carr index may indeed qualitatively compare the likelihoods of solids flow problems of similar materials, but after the tests have been completed and a flow index has been determined, the investigator will not know what size hopper outlet dimension will prevent blockages, how steep the hopper walls must be to avoid ratholing, what outlet size is required to achieve the desired discharge rate, and whether or not storage at rest will lead to flow stoppages.

Investigators often find comfort in a Carr index, as its result is usually consistent with experience, *e.g.*, when a flow aid is added to improve the flowability of a powder, the flow index indeed increases. Table 1-3 gives

⁴ In Carr-speak, a high ratio is bad, whereas a high index is good. It can be confusing; it’s best to use neither.

flow index results for mixtures of a polyolefin powder, pigment, and fumed silica that were provided in a technical bulletin published by the silica manufacturer. Indeed, addition of silica improved the flowability of the powder. By adding a small amount of silica, the Carr index of a powder that *sans* silica was equal to 44.3, indicating poor flowability, increased to as high as 59.5, which was still poor, but perhaps better than before. Hey, at least it wasn't very poor or very, very poor!

Table 1-2
Carr's Flow Index

Score	Flowability and Performance
90-100	Excellent
80-89	Good
70-79	Fair
60-69	Passable
40-59	Poor
20-39	Very Poor
0-19	Very, Very Poor

Table 1-3
Carr Index Example

Silica	Angle of Repose	Aerated Bulk Density	Cohesiveness (%)	Flow Index
None	49.0	0.384	16.5	49.3
A	42.0	0.384	4.1	54.0
B	41.0	0.737	5.4	56.0
C	46.1	0.388	8.0	59.0
D	50.4	0.388	6.0	59.5

The tests that must be conducted to obtain a powder's Carr index are tedious and time consuming. The index is frequently used in the toner industry as a measure of flowability. Tribocharge properties of toners are also important. Fortunately, laboratories equipped with instruments that measure the Carr index also have tribocharge testers. After spending a day in the lab obtaining angle of repose, angle of spatula, compressibility, and particle size data to obtain results that have questionable utility, investigators are able to get some badly needed electroshock therapy.

Solids rheometers of various designs are sometimes used to quantify the flowability of powders. The material is placed in a cell equipped with an impeller, and the torque or energy required to rotate the agitator either upward or downward is measured. In some instruments, the vertical force on the agitator can also be directly measured. Flowability is deemed to correlate with the torque or the power drawn by the agitator.

Unfortunately, the stresses acting in the shear zone during testing are unknown, and therefore the results cannot be applied to actual process conditions. In addition, both fluidization and agglomeration can occur inside the test cell, confounding the results [Schulze, D., Powders and Bulk Solids – Behavior, Characterization, Storage, and Flow, Springer, Berlin, 2007]. The “basic flow energy”, in which the impeller pushes the powder downward, roughly correlates with the material’s compressibility (compressible powders require less energy to compact), while the “specific energy”, where the impeller rotates upward, weakly correlates with its cohesive strength (more effort is required to cause a powder to yield if it is cohesive). High torque or energy consumption may be the result of high internal friction or friction between the bulk material and the walls of the cell, rather than an indication of the material’s cohesive strength or compressibility. It is better to determine a powder’s cohesive strength and compressibility directly as they are fundamental flow properties whereas methods based on stirred vessels do not provide results that have any fundamental solids flow basis. They are often used for quality control or acceptance criteria for raw materials and are reported to be able to pick up differences in powders that other testers cannot.

Funnel tests are also frequently used. In such a test, a powder is placed in a cylinder with interchangeable bottom lids that have an orifice of various sizes. Flowability is defined as the minimum size of the orifice for which flow occurs, or alternatively, the time required to discharge the powder.

Very little practical information is obtained from such a test. The funnel flow pattern that results from such a test ensures variability of the test results. In addition, the discharge rate will be greatly influenced by the permeability of the bulk solid, since powder introduced into the flow channel from collapsing ratholes may be aerated if the air cannot flow through the powder quickly.

The pharmaceutical industry frequently uses a parameter known as the flow function coefficient or *FFC*. It is the ratio of the major principal stress to the unconfined yield strength as determined from a shear cell test. (Shear cell testing will be discussed later. The major principal stress is the maximum level of stress imparted on the material during a shear cell test. Unconfined yield strength is a measure of a powder's cohesive strength.) Interpretation of *FFC* values is summarized in Table 1-4.

Ratio	Flowability
< 2	Very Cohesive
2 – 4	Cohesive
4 – 10	Easy-flowing
> 10	Free-flowing

FFC is often abused. The *FFC* value and therefore its interpretation (*e.g.*, cohesive, easy-flowing) depend on the major principal stress, and the appropriate value of that stress to use when defining *FFC* is not immediately known. Because the major principal stress imparted on the powder during the test is not known *a priori*, the *FFC* for a desired major principal stress cannot be determined by performing only one test. Conclusions from the comparison of *FFC* values of two powders must be made carefully. Two materials may have identical *FFC* values, but the powder that has the higher bulk density will discharge from hoppers with smaller outlets. So, FFS, don't use *FFC*!

Researchers often have the task of optimizing the composition of a powder both for performance (in the case of pharmaceuticals, potency, dissolution rate, *etc.*) and flow behavior. Because typical experimental designs look for the response of a set of dependent variables due to changes in independent variables, defining flowability by one numerical value is tempting. Such a strategy certainly allows one's statistical software to do its job. Unfortunately, one number cannot readily define flowability.

An optimal test method is one where the consolidation pressures used while conducting a test simulate those expected when a bulk solid is stored and quantifiably measures the fundamental flow properties of the material. Results can then be applied with confidence since tests conducted with small

samples of material will replicate conditions present in real systems. For example, the solids-stress profile inside a bin can be readily determined if the material's bulk density, internal friction, and wall friction are known. Therefore, test methods that measure these properties along with the strength of the bulk material over the applicable range of stress are advantageous.

The test results should allow investigators to be able to (1) predict the flow pattern inside a bin, (2) determine the minimum outlet dimension that can prevent an obstruction to flow from developing, and (3) allow calculation of the outlet size that will provide the desired discharge rate. A material that has the best flowability is therefore one that will not arch or develop a stable rathole in a hopper with the smallest outlet, is able to flow along the walls of a bin with the shallowest hopper angle and will discharge from a hopper steadily at the highest rate. Hence, it is beneficial to define a powder's flowability by the size of the outlet required to prevent flow obstructions and to achieve the desired discharge rate and the hopper angle required to allow flow along the hopper walls. To determine these critical outlet dimensions and hopper angles, the following *fundamental* solids flow properties must be measured:

1. *Cohesive strength*. The relationship between the cohesive strength of a bulk material and consolidation pressure is called the material's *flow function*. The flow function can be analyzed to determine the minimum outlet size of a bin that prevents arching or stable rathole formation. Cohesive strength is best measured by shear cell testing.
2. *Internal friction*. Internal friction is a result of solid particles flowing against each other. Internal friction is expressed as an angle of internal friction. Instruments that measure cohesive strength also measure angles of internal friction.
3. *Wall friction*. Wall friction results when solid particles flow along a surface. Like internal friction, wall friction is expressed as an angle of friction. Wall friction can also be measured using a shear cell; alternatively, instruments that measure shear and normal forces as a sample of material slides along a wall material are available. Wall friction test results, together with knowledge of the material's internal friction, can be used to predict the flow pattern inside a bin. Wall

friction test data are used to determine hopper angles that ensure mass flow.

4. *Bulk density or compressibility.* The bulk density of a powder varies with the applied consolidation pressure. Bulk density test results are used to calculate stress profiles in and capacities of hoppers, bins, and silos and in the calculation of critical outlet dimensions. The relationship between bulk density and consolidation pressure is called the compressibility.
5. *Permeability.* Pressure gradients within a bed of powder are created when voids within the powder expand during flow in the converging section of a vessel. This results in the flow of gas counter to the flow of solids at the outlet, which can hinder solids flow and limit solids discharge rates. Permeability test results along with compressibility can be used to determine the outlet size required to achieve a desired solids discharge rate.

With fundamental solids flow property data, investigators can determine outlet dimensions that will prevent obstructions to flow from developing, hopper angles required for mass flow, and outlet sizes necessary to achieve desired discharge rates. A bulk material's flowability therefore depends on the bin that is currently in place or will be used to handle the material. A material perceived to be easy flowing may rathole or arch in an inappropriate hopper, whereas one that is considered to flow poorly will flow unhindered from a hopper that was properly designed.

The classic Rand Corporation study

Specifying solids-handling equipment without regard to the fundamental flow properties of the bulk solids can have dire consequences. A study performed in the 1980s by the Rand Corporation [Morrow, E.W., *Chem. Eng.*, 95 (18), 89 (1985)] found a significant difference between the start-up times of new plants that handled fluids and those that handled bulk solids. Figure 1.8 shows the average planned start-up times and actual start-up times for nearly 40 new plants that handled fluids and bulk solids. The average start-up time for a new plant handling liquids and gases was about three months, and the start-up typically proceeded as planned. The project engineers who managed these projects received large bonuses, as their Gantt charts required very few revisions. Project engineers on average anticipated

a six-month start-up for plants handling bulk solids. (After all, some of the materials were neurotic.) Instead, the plants that handled solids on average required nearly two years.

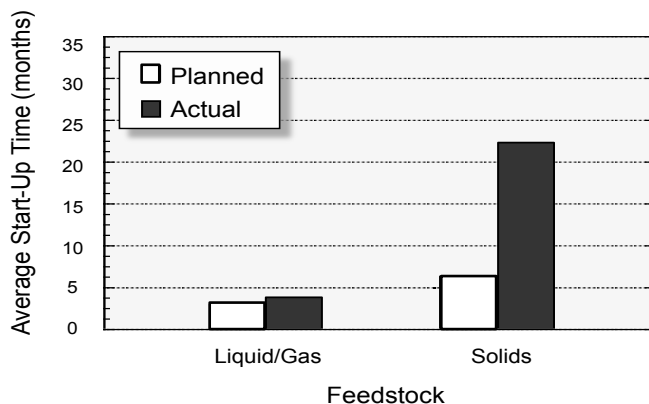


Figure 1.8. Planned and actual start-up times for new plants.

Capacity also suffered for the plants that handled bulk solids. On average, the capacity of plants that processed fluids was 90 percent of design, compared to about 50 percent for plants handling solids. And what was the solution? Frequently, capacity was increased by adding a second, equally crappy, parallel line!

Morrow followed up his study in 2000 using a larger database of over 500 companies [Morrow, E.W., *Chem. Innov.*, 30 (1), 35 (2000)]. The performance of new plants improved, but the same trends from the previous study were observed. Start-up times were shorter and performance was significantly better for plants that received liquids and gases as raw materials.

With proper training, engineers can design bulk solids handling plants with the same level of confidence they have when designing processes for liquids and gases. The key is to measure the fundamental bulk solids flow properties: cohesive strength, internal friction, bulk density or compressibility, wall friction, and permeability. Find a laboratory that has a shear cell tester and a permeability tester. If you are adventurous, set up your own powder-testing lab. Then follow Jenike's testing and design recipes, and you will never need a hammer again.

2. ANALYSIS OF STRESS

Let's start with the obvious: liquids and solids are different. Liquids are *isotropic*; that is, their properties are uniform in all directions. For example, if a pressure probe were inserted into a cylinder containing a liquid and its orientation were then varied, its reading would not change. The static pressure of the fluid is the same in all directions. This is illustrated in Figure 2.1.

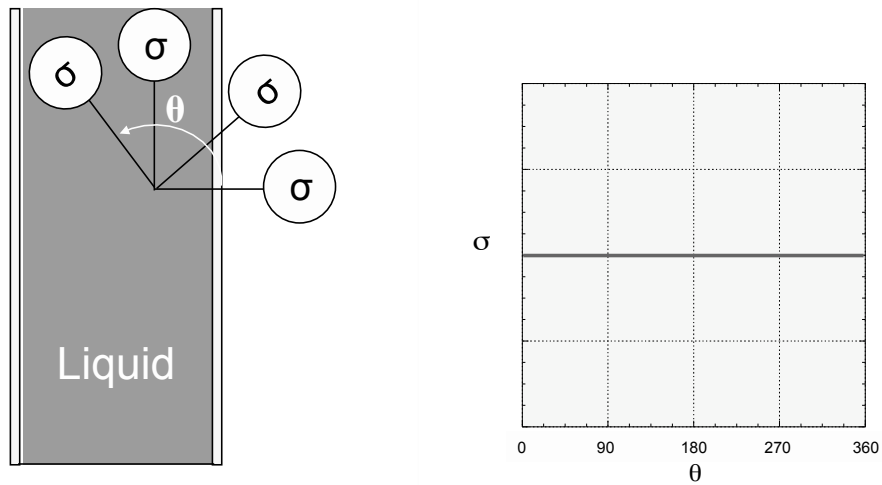


Figure 2.1. Stresses inside a cylinder of liquid.

On the other hand, bulk solids are *anisotropic*. If the liquid were replaced with a bulk solid and the probe then inserted into the cylinder, the measured stress would depend on its orientation. In the vertical direction, the probe would measure the normal stress applied on the bulk solid, and the stress

measured in this direction would be its maximum. If the probe were rotated, the measured normal stress would become lower, following a sinusoidal pattern and reaching a minimum when the direction of the probe was close to horizontal (see Figure 2.2). The maximum normal stress is called the major principal stress σ_1 . The minimum normal stress, which acts perpendicular to σ_1 , is called the minor principal stress σ_2 .

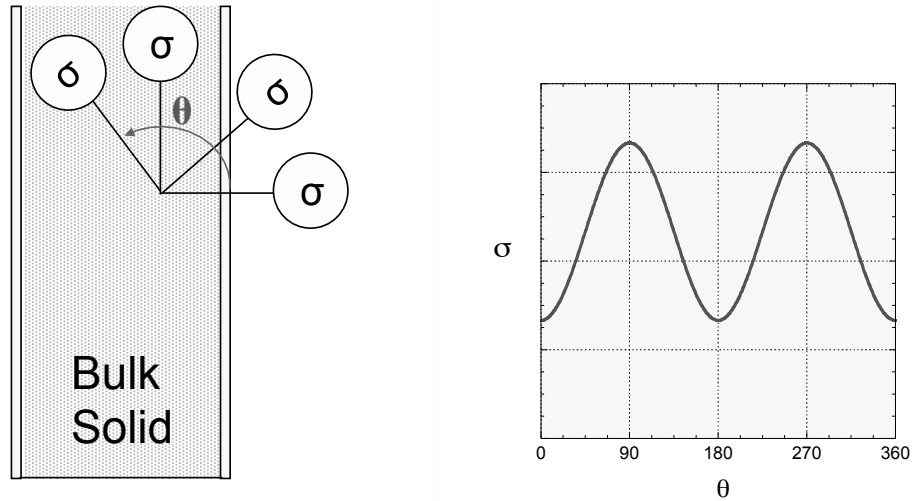


Figure 2.2. Stresses inside a cylinder containing a bulk solid.

If the cylinder were replaced with a rigid solid, and a probe was inserted and its orientation somehow changed, the maximum normal stress again would be measured when the probe was directed vertically. In this case, the stress would be nearly zero when the probe reached horizontal.

The ratio of the horizontal stress to the vertical stress in a bulk solid is the stress ratio k . For liquids, the stress constant is equal to one. For an ideal, rigid solid, the stress constant is zero. Not surprisingly, the stress ratio for bulk solids is somewhere in between, typically between 0.4 and 0.6.

Transforming the stresses in bulk solids can be stressful (pun intended). Fortunately, there are graphical techniques that an engineer or scientist can use to determine the stress with respect to a convenient reference plane when the state of stress is known or has been measured with respect to another less useful plane of reference.

Continuum model

Although a bulk solid consists of individual particles, they are generally treated as if they were a continuum when the flow of bulk solids is analyzed. The forces associated with individual particles are not considered. Rather, the forces on the boundary areas of individual volume elements are described.

Figure 2.3 illustrates a volume element in the form of an infinitesimal cube. On each plane, three stress components are specified. One acts into to the plane; the other two act along the plane. Stress components acting perpendicular are termed normal stresses; those acting parallel are shear stresses.

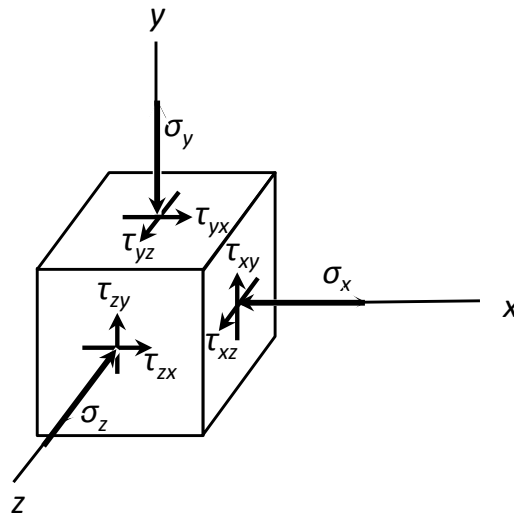


Figure 2.3. Stresses on bulk solid element.

Consider the stresses acting on a plane that lies perpendicular to the x -axis. The normal stress is denoted σ_x . The shear stress acting in the y direction is denoted τ_{xy} ; the shear stress that acts in the z direction is denoted τ_{xz} . Figure 2.3 provides descriptions of stresses acting on the other planes.

The following sign convention is used. When both the normal and shear components face in a positive direction with respect to the coordinate axes, the stress is positive. When both components face in a negative direction with respect to the axes, the stress is positive. When the normal stress

points in the positive direction while the shear stress points to the negative and *vice versa*, the stress is positive. Note that in this convention, tensile stresses, which act to pull on the volume element, are negative, while compressive forces, which push against the volume element, are positive.

Rotational equilibrium of the element is established by taking moments about its center. For example, taking moments of the forces in the z direction yields the following:

$$\tau_{xy}(dydz)dx = \tau_{yx}(dxdz)dy \quad (2.1)$$

and hence

$$\tau_{xy} = \tau_{yx} \quad (2.2)$$

Likewise,

$$\tau_{xz} = \tau_{zx} \quad (2.3)$$

and

$$\tau_{yz} = \tau_{zy} \quad (2.4)$$

In the case of two-dimensional or plane stress, all stresses act parallel to the x and y axes. For convenience, often only a two-dimensional view of the element is sketched, as shown in Figure 2.4.

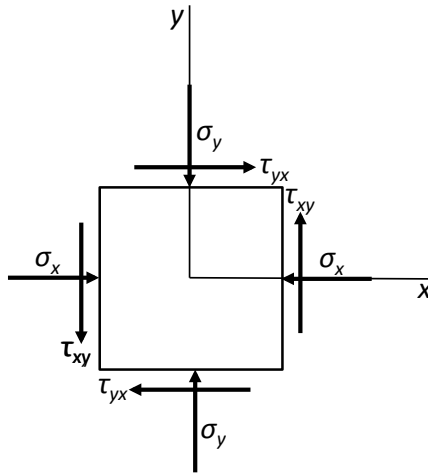


Figure 2.4. Plane stress.

Often, geometry considerations are the basis of the coordinate directions chosen to ensure that principal stresses line up with system boundaries, *e.g.*, the walls of the vessel in which the bulk material is handled. For example, to analyze a bin, one of the coordinate axes is lined up with the straight-walled section of the vessel. As a result, the normal and shear stress components are associated with this direction. In the converging hopper section, radial coordinates are generally used.

Additionally, recall that bulk solids are anisotropic. The solids stresses depend on direction. How we define the stress will depend on to what plane the force is acting. Given a state of stress, the magnitude of the normal and shear stresses acting on the bulk material will depend on the coordinate system used to describe the direction of these stresses. It will be convenient to define the axes such that the normal stresses acting on planes perpendicular to the axes are at their maximum or minimum. These stresses are called the principal stresses, and they act in the direction of the principal axes. A somewhat obvious example might be a cylinder with vertical walls that contains a bulk solid. We would expect the maximum normal stress, at least on average, to act vertically on a cross section of the cylinder. This stress is called the major principal stress. The minor principal stress or minimum normal stress will be directed 90 degrees from the direction of the major principal stress.

Transformation of stress and Mohr's circles

Consider the case of two-dimensional stress on an infinitesimal element of powder as shown in Figure 2.5. Normal and shear stresses acting on planes perpendicular to the x and y axes are assumed known. Our task is to determine the stresses acting on the element with a new set of axes formed by rotating the original set about the origin. We can define a new set of axes, denoted by x' and y' . The angle θ formed between the x and x' is positive when measured from the x axis toward the y axis in the counterclockwise direction (anticlockwise if you're a Brit). It should be obvious that if we are looking at stresses on walls inclined by an angle equal to θ , the analysis will prove to be useful.

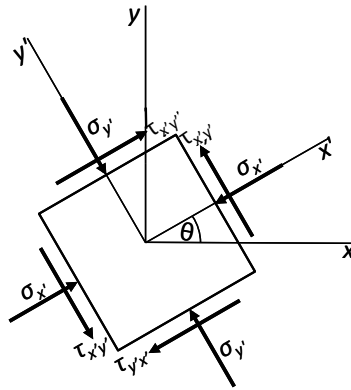


Figure 2.5. Stresses on a rotated element.

The area of each face of the infinitesimal element is equal to dA . Applying the equations of static equilibrium to the wedge-shaped element shown in Figure 2.6 in the x' direction gives

$$\begin{aligned} \sigma_{x'} dA \sec \theta - \sigma_x dA \cos \theta - \tau_{xy} dA \sin \theta \\ - \sigma_y dA \tan \theta \sin \theta - \tau_{yx} dA \tan \theta \cos \theta = 0 \end{aligned} \quad (2.5)$$

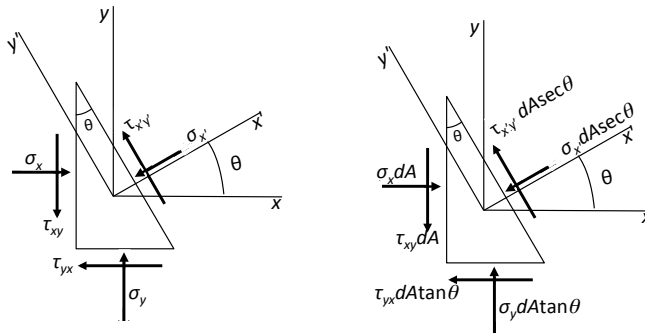


Figure 2.6. Stresses on a wedge-shaped element (left); forces on a wedge-shaped element (right).

Let's examine how we derived this force balance. Remember, force is equal to the product of stress and area. If the cross sectional area of the left side of the differential element is dA , then the cross-sectional area that $\sigma_{x'}$ acts against is equal to $dA/\tan \theta$ or $dA \sec \theta$. The force is equal to the product of

the stress and the area, *i.e.*, $\sigma_x dA \sec \theta$, the first term of Equation 2.5⁵. The component of the stress σ_x in the x' direction is equal to $\sigma_x \cos \theta$; hence the force is equal to $\sigma_x \cos \theta dA$, which is the second term of Equation 2.5. You get the idea. Lots of trigonometry is applied as necessary to each of the stress and differential area terms.

So, on your mark! Get set! Derive!

Equation 2.5 can be rewritten as

$$\sigma_{x'} = \sigma_x \cos^2 \theta + \sigma_y \sin^2 \theta + 2\tau_{xy} \sin \theta \cos \theta \quad (2.6)$$

Substitution of the trigonometric identities

$$\cos^2 \theta = \frac{1 + \cos 2\theta}{2} \quad (2.7)$$

and

$$\sin^2 \theta = \frac{1 - \cos 2\theta}{2} \quad (2.8)$$

into Equation 2.6 yields

$$\sigma_{x'} = \frac{\sigma_x + \sigma_y}{2} + \frac{\sigma_x - \sigma_y}{2} \cos 2\theta + \tau_{xy} \sin 2\theta \quad (2.9)$$

Figure 2.7 is an example of the application of Equation 2.9. Note that as the element is rotated, the normal stress with respect to the transformed coordinate system varies in a sinusoidal pattern. (Recall the experiment where a pressure probe was inserted into a cylinder of powder and rotated.)

Equation 2.9 does not seem too challenging to solve, but can you imagine how painful analysis of stress was before calculators and engineers and scientists relied on trig tables and slide rules? Actually, we'll see that it wasn't so bad because in the late 1800s, Otto Mohr continued to drink and derive.

A similar balance of the forces acting in the y' direction gives

⁵ I once entered a trigonometry competition. I finished in secant place.

$$\tau_{x'y'} = -\frac{\sigma_x - \sigma_y}{2} \sin 2\theta + \tau_{xy} \cos 2\theta \quad (2.10)$$

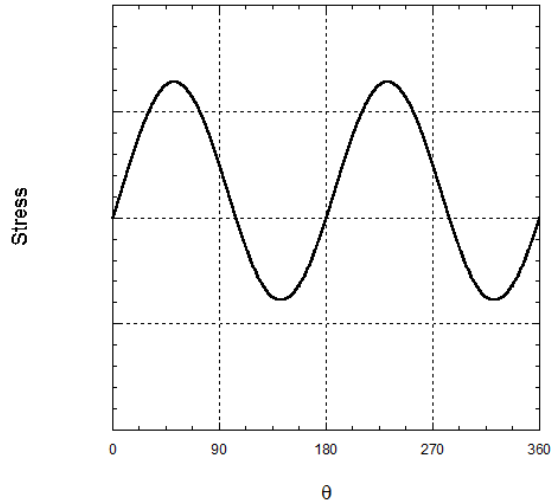


Figure 2.7. Transformation of stress.

The normal stress in the direction of the y' axis can be derived by replacing θ with $\theta + \pi/2$ (i.e., $\theta + 90^\circ$), which yields

$$\sigma_{y'} = \frac{\sigma_x + \sigma_y}{2} - \frac{\sigma_x - \sigma_y}{2} \cos 2\theta - \tau_{xy} \sin 2\theta \quad (2.11)$$

Squaring Equations 2.9 and 2.10 and adding the results gives

$$(\sigma_{x'} - \sigma_{avg})^2 + \tau_{x'y'}^2 = R^2 \quad (2.12)$$

where

$$\sigma_{avg} = \frac{\sigma_x + \sigma_y}{2} \quad (2.13)$$

and

$$R^2 = \left(\frac{\sigma_x - \sigma_y}{2} \right)^2 + \tau_{xy}^2 \quad (2.14)$$

Equation 2.12, together with Equations 2.13 and 2.14, is a circle with radius R and center $(\sigma_{avg}, 0)$ and is appropriately called a Mohr's circle. A Mohr's circle can be used to determine stresses in directions that do not line up with the original coordinate set. A Mohr's circle represents all possible combinations of σ_x , σ_y , and τ_{xy} that act on a rotated coordinate system, *i.e.*, one acting on a differently oriented plane. No slide rules or trigonometric tables are needed. Just pull out your compass and draw a circle! A Mohr's circle is illustrated in Figure 2.8.

Additionally, the Mohr's circle allows the direction of principal axes and major and minor principal stresses to be calculated. A Mohr's circle that gives the principal axes is illustrated in Figure 2.9.

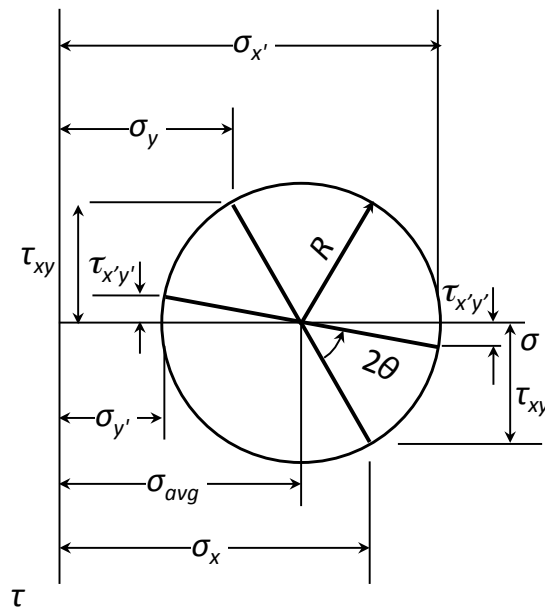


Figure 2.8. Stress transformation using a Mohr's circle.

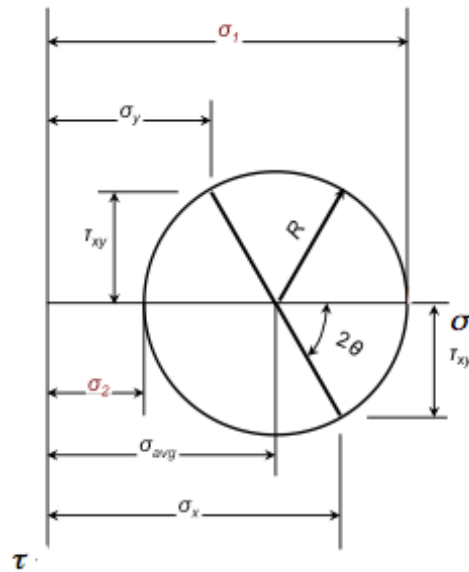


Figure 2.9. Determination of principal stresses by application of Mohr's circle.

The maximum and minimum values of the normal stresses, *i.e.*, the major and minor principal stresses, respectively, can be determined from the two intersection points of the Mohr's circle and the horizontal axis. The major principal stress σ_1 and minor principal stress σ_2 can therefore be calculated from

$$\sigma_1 = \sigma_{avg} + R \quad (2.15)$$

$$\sigma_2 = \sigma_{avg} - R \quad (2.16)$$

Note that the Mohr's circle is centered at σ_{avg} and the two points (σ_x, τ_{xy}) and $(\sigma_y, -\tau_{xy})$ lie on opposite sides of the circle. To determine the stresses with respect to the rotated or transformed axes, the line connecting the two points (σ_x, τ_{xy}) and $(\sigma_y, -\tau_{xy})$ is rotated 2θ . The transformed axes have been rotated by θ .

In summary, the major and minor principal stresses are the highest and lowest values, respectively, of the normal stresses possible on a material. If the normal and shear stresses are known, the principal stresses can be conveniently determined using a Mohr's circle. We'll find Mohr's circles

useful when analyzing results from shear cell testers, which measure the cohesive strength of a powder. During a shear cell test, a sample is sheared while under a normal load. Mohr's circles are used to determine what is known as the material's unconfined yield strength at the major principal stress applied to a sample during a test. Mohr's circles are also used to determine solids and wall stresses at a bin outlet, which come into play when calculating outlet dimensions required to prevent obstructions to flow and recommending hopper angles for mass flow. While computers have all but rendered compasses, trig tables, rulers, and slide rules obsolete, Mohr's circles remain a useful tool for analyzing stresses of bulk solids.

3. STRESSES IN HOPPERS, BINS, AND SILOS

The geometry of the bin, which determines the solids flow pattern, and the solids flow properties, in particular wall friction, bulk density, and internal friction, influence the pressure profiles that develop within the bulk solids handled in a bin. A typical bin consists of a vertical (cylinder) section followed by a converging (hopper) section. Solids stresses are illustrated in Figure 3.1.

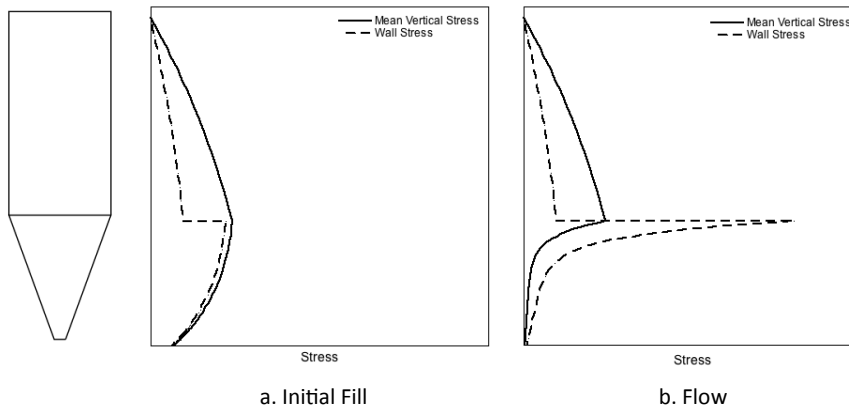


Figure 3.1. Representative stress profiles in a mass flow bin.

In the cylindrical section, the stresses increase with depth, approaching a maximum asymptotically. The wall stresses are smaller than the vertical stresses by a factor equal to k . In the cylinder, the major principal stress σ_1 is directed downward, parallel to the vertical walls. As the silo walls are

approached, the direction of the major principal stress begins to diverge from vertical.

When a previously empty bin is initially filled with a bulk solid, the major principal stresses in the converging section also act downward. This stress state after initial fill is termed the active stress state. Note that a discontinuity exists in the wall stress profile. Both the wall stresses and vertical stresses decrease as the hopper outlet is approached.

When the bulk solid is discharged from the bin, changes in the stress conditions in the hopper section occur. In order for flow to take place, the bulk solid is compressed laterally and expands vertically. As a result, the major principal stresses act horizontally instead of vertically. This state of stress is called the passive state. A peak stress, called the switch, occurs at the hopper-cylinder interface.

Cylinder (vertical) section

The stresses in the vertical section of a silo were originally calculated by Janssen in 1895 [Janssen, H.A., *Zeitschr. d. Vereines deutscher Ingenieure*, 39, 1045 (1895)] when he was investigating wall stresses in corn and grain silos. His analysis is still used today!

Consider a volume element as shown in Figure 3.2, which has the same cross-sectional area A as the vertical section of the silo. Assuming a constant vertical stress and constant bulk density across the cross-section, an equilibrium force balance in the z direction gives:

$$A\sigma_v + \rho_b g A dz = A(\sigma_v + d\sigma_v) + \tau_w C dz \quad (3.1)$$

where A is the cross-sectional area of the element (equal to cross-sectional area of the cylinder), C is its perimeter, z is the distance from the top of the bed of solids, dz is the height of the infinitesimal element, σ_v is the vertical stress, τ_w is the wall stress, ρ_b is the bulk density, and g is equal to the acceleration due to gravity⁶.

⁶ We all know that $g = 9.8 \text{ m/s}^2$ or 32.2 ft/s^2 . There are two types of units: metric units and units used by the only country to have ever landed a man on the moon. When the bulk density is given in lb/sq ft, g is built in and you don't have to multiply by 32.2.

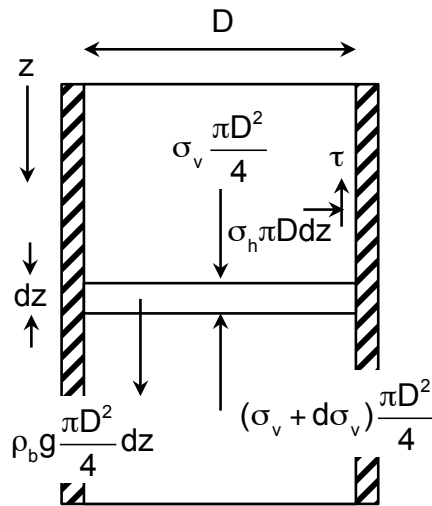


Figure 3.2. Stresses on element of bulk solid inside cylinder.

The wall friction coefficient μ_w can be defined as

$$\mu_w = \frac{\tau_w}{\sigma_w} \quad (3.2)$$

where σ_w is equal to the stress normal to the wall. Wall friction is typically expressed as an angle of wall friction ϕ' , which is the inverse tangent of the friction coefficient, *i.e.*,

$$\mu_w = \tan \phi' \quad (3.3)$$

Expressing friction as an angle may at first appear peculiar, but in the analysis of stresses in bulk solids in bins, angles appear everywhere, such as hopper angles, angles referenced to normal, *etc.* We'll learn that the math becomes a bit cleaner if angles are used in place of inverse tangents of friction coefficients.

Recall that the ratio of the horizontal stress to the vertical stress, *i.e.*, the stress ratio k , is given by:

$$k = \frac{\sigma_h}{\sigma_v} \quad (3.4)$$

The stress ratio is also known as the Janssen coefficient and is typically in the range of 0.4 to 0.6⁷. Noting that σ_h is equal to $k\sigma_v$, Equation 3.1 can be rewritten as

$$\frac{d\sigma_v}{dz} + \tan \phi' \frac{k\sigma_v}{R_H} = \rho_b g \quad (3.5)$$

where the hydraulic radius R_H is given by

$$R_H = \frac{A}{C} \quad (3.6)$$

Equation 3.5 is an ordinary differential equation, which we all know how to solve provided that we have a boundary condition. At the top of the solids bed, the solids stress is zero, *i.e.*,

$$\sigma_v(0) = 0 \quad (3.7)$$

Solving Equation 3.5 yields the Janssen equation:

$$\sigma_v(z) = \frac{\rho_b g R_H}{k \tan \phi'} \left[1 - \exp\left(\frac{-k \tan \phi' z}{R_H}\right) \right] \quad (3.8)$$

The stress in the horizontal direction, *i.e.*, the stress on the walls, is therefore

$$\sigma_h(z) = \frac{\rho_b g R_H}{\tan \phi'} \left[1 - \exp\left(\frac{-k \tan \phi' z}{R_H}\right) \right] \quad (3.9)$$

The dependence of solids stress on depth is illustrated in Figure 3.3. Note that the maximum stress is proportional to the cylinder's hydraulic radius and is independent of its height if the cylinder is tall.

⁷ The lateral stress constant k can be estimated by the relation $k = 1.2(1 - \sin \phi)$ where ϕ is the kinematic angle of internal friction, which is determined from shear cell testing. Powder flow property testing is discussed in Chapter 4. Structural engineers often choose a stress ratio equal to 0.6.

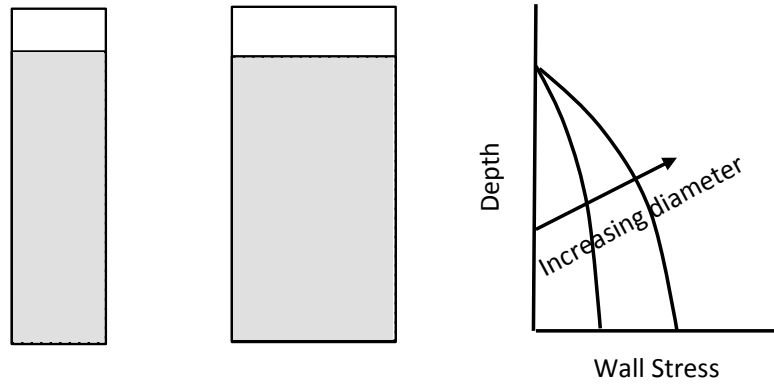


Figure 3.3. Stresses on cylinder walls filled with bulk solid.

The pressure distribution for a bulk solid in a cylinder is very different from the stress (*i.e.*, pressure) profile for a liquid. If the cylinder were instead filled with a liquid instead of a bulk solid, the vertical and horizontal stresses would both be equal to the hydrostatic pressure, which is proportional to the depth of the liquid:

$$\sigma_v = \sigma_h = \rho g z \quad (3.10)$$

where ρ is the density of the liquid.

If a load σ_{v0} were placed on the top of the solids bed inside the cylinder, then the solution to Equation 3.5 with the new boundary condition is

$$\sigma_v(z) = \frac{\rho_b g R_H}{k \tan \phi'} \left[1 - \exp\left(\frac{-k \tan \phi' z}{R_H}\right) \right] + \sigma_{v0} \exp\left(\frac{-k \tan \phi' z}{R_H}\right) \quad (3.11)$$

The horizontal stress is then

$$\sigma_h(z) = \frac{\rho_b g R_H}{\tan \phi'} \left[1 - \exp\left(\frac{-k \tan \phi' z}{R_H}\right) \right] + k \sigma_{v0} \exp\left(\frac{-k \tan \phi' z}{R_H}\right) \quad (3.12)$$

Figure 3.4 illustrates the effect of an additional load on the solids stress profile in a cylinder. When analyzing the stresses in silos, the additional load is often the surcharge or pile formed when a bulk solid is filled from the center as shown in Figure 3.5. Note that (for long cylinders) the maximum stress is independent of the load. This is of course not the case

for fluids, where applying a load on the liquid will increase the hydrostatic pressure.

The additional load is calculated from the hydrostatic head:

$$\sigma_{v0} = \rho_b g h \quad (3.13)$$

where h is the height of the pile (see Figure 3.5). Figure 3.6 compares the stress on the walls of a cylinder filled with a liquid to those of a cylinder filled with a bulk solid that has a bulk density equal to the density of the liquid. Since bulk solids are capable of supporting a shear stress, the wall stresses are significantly lower.

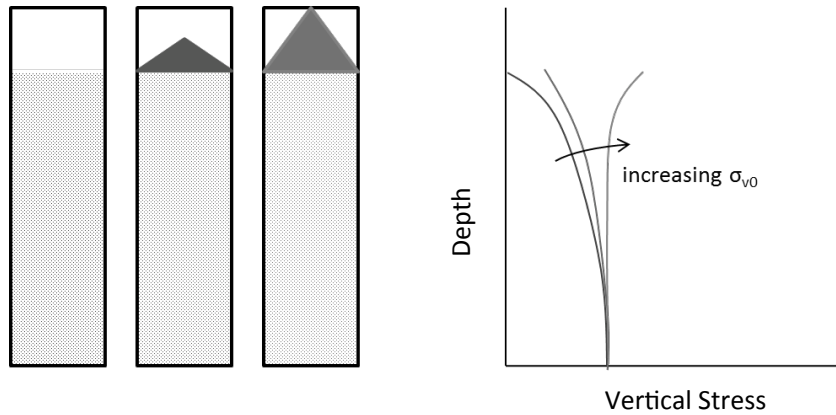


Figure 3.4. Effect of load on vertical stress on bulk solids in cylinder.

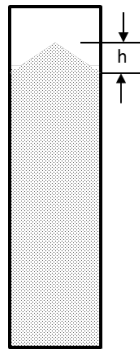


Figure 3.5. Surcharge of powder on cylinder.

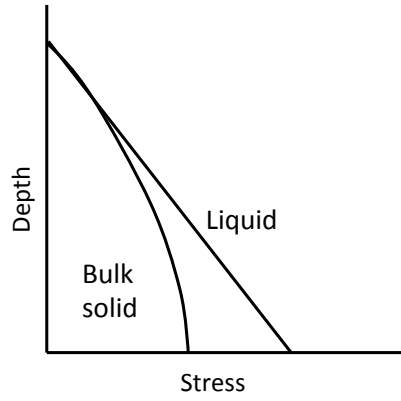


Figure 3.6. Comparison of stresses in a cylinder containing a bulk solid or a liquid.

Note that bulk density and wall friction are dependent on consolidation pressure, and therefore average values for ρ_b and μ_w must be used in the analytical expressions given above. Alternatively, the differential form of the Janssen equation can be used:

$$\frac{d\sigma_v}{dz} = \rho_b g - \mu_w \frac{k\sigma_v}{R_H} \quad (3.14)$$

Equation 3.14 can be integrated numerically from the top of the cylinder with the boundary condition

$$\sigma_v(0) = \sigma_{v0} \quad (3.15)$$

Numerical integration can be readily accomplished by expressing Equation 3.14 as a difference equation and using Euler's method of integration:

$$\sigma_v^{i+1} - \sigma_v^i = \left(\rho_b^i g - \mu_w \frac{k\sigma_v^i}{R_H} \right) \Delta z \quad (3.16)$$

where the superscript i is related to the distance from the top of the solids bed, *i.e.*,

$$z = (i - 1)\Delta z \quad (3.17)$$

Because pressures generated by liquids are proportional to the level of material, efforts are made to minimize the height of a vessel used to store

liquids to reduce the wall thickness required for structural stability. For solids, the maximum stress is independent of height but instead proportional to the diameter. To reduce the wall thickness of a silo, the diameter is kept as small as possible. This is why tanks that store liquids tend to be short and squat whereas silos tend to be tall and thin. Isn't that interesting?

Hopper (converging) section – mass flow

The cross-sectional area varies in the converging hopper section. Walker [*Chem. Eng. Sci.* 21, 11, 975 (1966)] and Walters [*Chem. Eng. Sci.*, 28, 1, 13 (1973)] analyzed the stresses in the hopper section by performing an equilibrium force balance on an elemental volume with converging sides as shown in Figure 3.7.

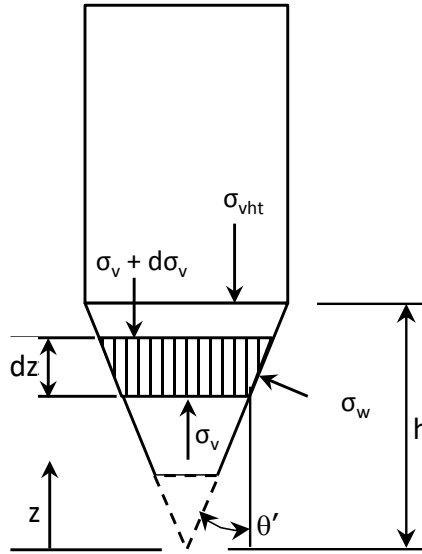


Figure 3.7. Forces acting on a differential slice of bulk material in a hopper.

Johanson [*Powder Technol.*, 140, 122 (2004)] provides a rather intimidating version of the force balance:

$$\frac{d\sigma_v}{dz} = -\rho_b g - \frac{1}{A} \frac{dA}{dz} + \frac{1}{A} \oint_p [k(\tan(\theta' + \tan \phi'))] dp \quad (3.18)$$

where p denotes the perimeter of a differential section and for the hopper analysis, θ' is the hopper angle (from vertical), and z is the distance from the vertex.

At the hopper-cylinder junction, *i.e.*, at $z = h$,

$$\sigma_v(h) = \sigma_{vht} \quad (3.19)$$

where σ_{vht} is the mean vertical stress on the solid at the transition after filling (as determined by the Janssen equation).

For conical or wedge-shaped hoppers, Schulze [*Chem. Eng. Sci.*, 49, 13, 2047 (1994)] presents a simpler form:

$$\frac{d\sigma_v}{dz} - n \frac{\sigma_v}{z} = -g\rho_b \quad (3.20)$$

where

$$n = (m+1) \left[k \left(1 + \frac{\tan \phi'}{\tan \theta'} \right) - 1 \right] \quad (3.21)$$

where m is equal to 1 for a conical hopper and equal to 0 for a straight-walled hopper having a slotted outlet.

Integration of Equation 3.20 yields the following:

$$\sigma_v = \frac{\rho_b g h}{n-1} \left[\frac{z}{h} - \left(\frac{z}{h} \right)^n \right] + \sigma_{vht} \left(\frac{z}{h} \right)^n \quad (3.22)$$

Average values of the bulk density and stress ratio are used in Equation 3.22. As with the Janssen equation, Equation 3.20 can be integrated numerically if the properties vary strongly with solids stress.

Methods to calculate the stress ratio k are given in the Eurocode standard [European Committee for Standardization, EN 1991-4:2006]. The value of the stress ratio depends on the flow properties of the bulk material handled and the slope of the hopper walls. Different values of k are used when determining initial filling loads and discharge loads.

According to the Eurocode, the stress ratio for initial fill is

$$k = 1 - \frac{0.2}{1 + \frac{\tan \theta'}{\tan \phi'}} \quad (3.23)$$

For discharge, the Eurocode recommends the larger of Equations 3.24 or 3.26:

$$k = \frac{1 + \sin \delta \cos \varepsilon}{1 - \sin \delta \cos(2\theta' + \varepsilon)} \quad (3.24)$$

where

$$\varepsilon = \phi' + \sin^{-1} \left(\frac{\sin \phi'}{\sin \delta} \right) \quad (3.25)$$

or

$$k = \left(\frac{1}{1 + \frac{\tan \phi'}{\tan \theta'}} \right) \left\{ 1 + 2 \left[1 + \left(\frac{\sin \delta}{1 + \sin \delta} \right) \left(\frac{\cos \varepsilon \sin(\varepsilon - \theta')}{\sin \theta'} \right) \right] \right\} \quad (3.26)$$

where

$$\varepsilon = \theta' + \frac{1}{2} \left[\phi' + \sin^{-1} \left(\frac{\sin \phi'}{\sin \delta} \right) \right] \quad (3.27)$$

Equation 3.24 was derived by Walker [*Chem. Eng. Sci.*, 21, 975 (1966)]. Equation 3.26 is based on a more complete theory described by Enstad [*Chem. Eng. Sci.*, 30, 1273 (1975)]. Note that the Eurocode uses different definitions of the angle ε in its stress ratio equations. (Don't shoot the messenger!)

The wall stress σ_w is calculated from:

$$\sigma_w = k \sigma_v \quad (3.28)$$

and the frictional traction τ is calculated from

$$\tau = \sigma_w \tan \phi' \quad (3.29)$$

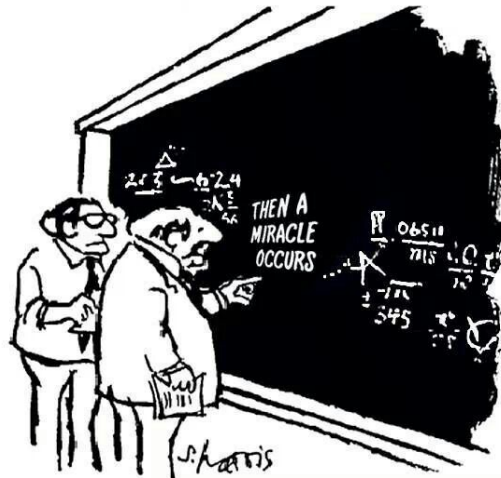
The wall friction angle ϕ' is a function of the stress normal to the wall σ_w , while the bulk density is a function of the major principal stress σ_1 . The major principal stress and the wall stress are related by:

$$\sigma_1 = \frac{\sigma_v}{\cos \beta} \quad (3.30)$$

where β can be calculated from

$$2\beta = \phi' + \sin^{-1} \left(\frac{\sin \phi'}{\sin \delta} \right) \quad (3.31)$$

A derivation of the equations that describes the solids stresses in a mass flow hopper is shown in Figure 3.8 [Larson, G., The Far Side Gallery, Warner, London, 1992].



“I think you should be more explicit here in step two”

Figure 3.8. Derivation of the equation for solids stresses in the converging section of a mass flow hopper⁸.

⁸ Actually, a fairly easy-to-follow derivation can be found in Shamiou, P.A., Handling of Bulk Solids – Theory and Practice, Butterworths, Boston, 1988.

Transition hoppers have both flat side walls and round end walls, and as such, the analysis is a bit more tedious. Going back to Equation 3.18, the cross-sectional area A can be calculated from

$$A = \frac{\pi b^2}{2} + (l - b)b \quad (3.32)$$

with

$$b = 2z \tan \theta'_{side} \quad (3.33)$$

and

$$l = 2z \tan \theta'_{end} \quad (3.34)$$

where b and l are the hopper width and length, respectively, and *side* and *end* of course denote the sides and ends, respectively (see Figure 3.9). Also,

$$\frac{dA}{dz} = 2 \left[\left(\frac{\pi b}{2} + l - 2b \right) \tan \theta'_{side} + b \tan \theta'_{end} \right] \quad (3.35)$$

That oddball integral term in Equation 3.18 can be replaced by

$$\oint_p [k(\tan(\theta' + \tan \phi'))] dp = 2(l - b)(\tan \theta'_{side} + \tan \phi')k_{side} + 2\pi b k_{end}(\tan \theta'_{end} + \tan \phi') \quad (3.36)$$

These terms can be inserted into Equation 3.18, which can then be integrated numerically to calculate the solids stresses inside a transition hopper.

The values of the stress constants k_{side} and k_{end} in Equation 3.36 should be those recommended by the Eurocode with m equal to 0 (planar flow) and 1 (axisymmetric flow), respectively. For transition hoppers with vertical end walls, k_{end} can be set equal to the value of the stress ratio used in the cylinder load calculations.

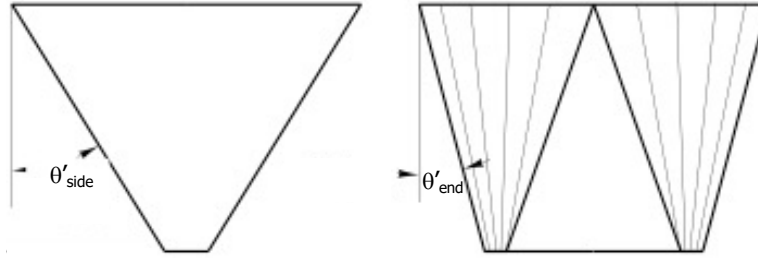


Figure 3.9. Side and end wall angles.

A qualified structural engineer should be assigned the task of performing solids-induced load calculations, using appropriate safety factors as needed. Otherwise, the bin may one day resemble the one shown in Figure 3.10.



Figure 3.10. Example of silo failure.

Funnel flow hoppers

In a funnel flow silo, flow of material takes place in a flow channel surrounded by stagnant zones. Eventually, the flow channel may expand and reach the silo walls. A stress peak may then form at that point. The location is difficult to predict, however, and therefore the cylinder section of a funnel flow hopper should be designed to withstand peak stress. Methods for calculating solids stresses in funnel flow silos are given in the Eurocode.

4. BULK SOLIDS FLOW PROPERTIES TESTING

When designing systems for handling fluids, an engineer must find or measure the material's viscosity, density, and if cavitation is a concern, its vapor pressure. For bulk solids, there are five fundamental flow properties that an engineer uses to design a bin for reliable flow: cohesive strength, internal friction, bulk density, wall friction, and permeability.

Unlike fluids, bulk solid materials that have the same composition often have considerably different fundamental flow properties. The solids flow properties are frequently dependent on the material's particle size, shape, porosity, and particle size distribution. In addition, temperature, moisture content, purity, surface energy, and morphology all can affect the flow behavior of a bulk solid. In some cases, the flow properties may change dramatically when a bulk solid is stored at rest.

Using flow property data from the literature or assuming that the properties are the same as those of other bulk materials whose properties are known is exceptionally risky. Tests should be conducted on the materials that will actually be used, and measurements should be taken over the range of temperatures, moisture contents, relative humidity levels, time at rest, and stress levels for which the bulk solid will be stored and handled. A material that is free flowing under ambient conditions may become cohesive or frictional at actual handling conditions. The addition of moisture generally causes powders to become more cohesive, although high levels of moisture

can reduce cohesiveness due to lubrication. Smooth wall surfaces often allow lower wall friction, but sometimes a rougher surface is better due to less contacts between the powder and the wall. The number-one rule of powder properties is that there are exceptions to every rule.

Cohesive strength, internal friction, and wall friction tests are performed using a shear cell tester⁹. Permeability testing is performed by measuring the pressure drop that results from passing a fluid through a bed of bulk material.

Cohesive strength and internal friction

The size of the outlet of the vessel that will prevent arching or the formation of a stable rathole depends greatly on the bulk material's cohesive strength. Knowing a bulk material's strength is therefore an important fundamental solids flow property.

Consider a snowball. If you were to “pre-consolidate” it by packing it tightly together with your hands, you'll have made yourself a snowball with a lot of strength. If you were to throw it, the snowball would likely cause damage once it hit a target. I know, because I have been the target of such a snowball. Now if *I* were to make a snowball, it might not have as much strength because I do not have the ability to pre-consolidate it with a great amount of stress. In fact, the snowball may be so weak that when I throw it, the drag forces from the air may be great enough to cause it to fail. Obviously there is a relationship between the strength of the snowball and the pre-consolidation stress applied to it when forming it.

⁹ When process conditions are severe, a Jenike direct tester should be used, as its electronics are isolated from the cell in which the sample resides during testing. Modern annular ring shear testers can be used in high-temperature environments, but only once. Then another tester must be purchased! Shear cell testers are rather pricey, so this is probably not advised. Jenike & Johanson has a modified tester that can measure the properties of bulk solids at furnace temperatures. Dietmar Schulze can also customize his tester so that it can be used at extreme temperatures. Anton-Paar offers a tester that can be operated at über-high temperatures.

Figure 4.1 is a schematic of a uniaxial compressive strength tester. In a uniaxial test, a sample is placed in a cell with low-friction walls and is then consolidated by applying a normal load equal to σ_1 . The load and cell are removed, and increasing loads are applied to the compacted, unconfined specimen until it breaks apart, *i.e.*, fails. The failure stress is termed the material's cohesive strength or the unconfined yield strength f_c .

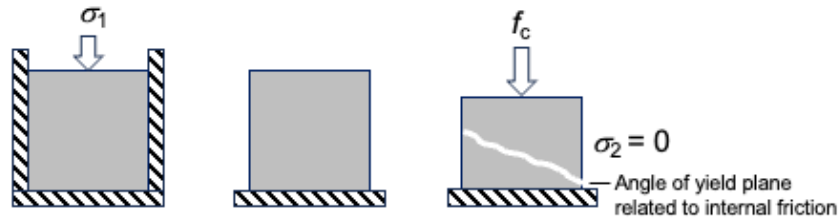


Figure 4.1. Uniaxial compressive strength test.

Uniaxial compressive strength test results are often highly variable. The stresses are not uniform inside the sample, and the location of the failure varies greatly from one test to the next. In addition, the cell walls should ideally be frictionless, but in reality, wall friction does exist. Improvements have been made to uniaxial strength testers to reduce their variability; however, uniaxial compression tests usually do not provide a bulk material's true unconfined yield strength. That being said, Ajax Equipment Company in the U.K. offers a decent one that is good for comparative tests where the intention does not involve designing a bin.

The cohesive strength of a bulk solid is therefore best measured by shear cell testing. Translational (Jenike), annular (ring), and torsional testers are frequently used. They are described in ASTM standards D-6128 (translational), D-6773 (annular), and D-6682 or D7891 (torsional). Schematics of the testers are given in Figure 4.2.

The direct translational shear tester was originally developed by Andrew Jenike [Storage and Flow of Solids, Bulletin 123, University of Utah, 1964 (revised, 1976)]. This tester is particularly hearty in that its cell can be placed in extreme environments allowing a material's cohesive strength to be measured over a sizeable range of process conditions. Its disadvantage is that significant operator training and experience are usually required to be able to obtain reliable results. Good health insurance with mental health

coverage is also recommended. Figure 4.3 is a photograph of a Jenike tester.

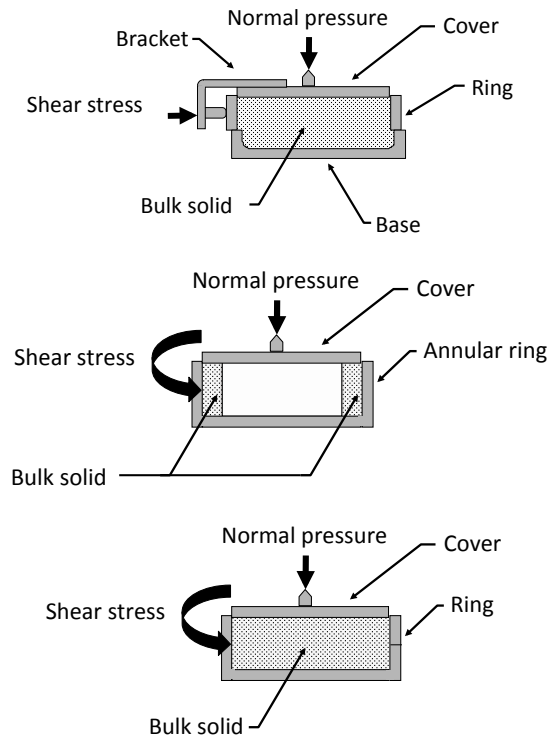


Figure 4.2. Shear cell testers – Jenike direct (top), annular (center) and torsional (bottom).



Figure 4.3. Jenike direct shear cell tester.

Modern annular and torsional shear testers are computer controlled and are thus straightforward to operate and less prone to operator error. The automated shear testers have been validated by conducting tests on multiple bulk solids and obtaining results that were within experimental error equal

to those determined using a Jenike tester. Annular and torsional shear testers are shown in Figure 4.4.



Figure 4.4. Automated testers; left to right: Schulze, Brookfield Engineering and Anton-Paar annular ring shear testers, Freeman Technology and E&G Associates (Peschl) torsional testers.

Most manufacturers of shear cell testers confirm that their results from testing a BCR limestone (CRM-116) standard powder are similar to those of a Jenike direct tester.

To measure cohesive strength, a sample of bulk material is placed in a cell and then “pre-sheared”, that is, consolidated by applying a normal stress and then shearing it until the measured shear stress is steady. A shear plane develops, in which a moving layer of bulk material is sheared against a stationary layer. Next, the “shear” step is conducted, in which the normal compacting load is replaced with a smaller load, and the sample is again sheared until it fails. These pre-shear and shear steps are repeated at the same consolidation level for a number of reduced normal stresses. The test history is illustrated in Figure 4.5. Some shear cell testers perform the pre-shear step by rotating the cell and then periodically reducing the shear stress to zero by retracting it, and then again shearing the sample until steady state is reached.

The failure shear stress is plotted against the normal stress together with the steady-state results. This plot is called the yield locus and is illustrated in Figure 4.6. The yield locus gives the shear stress that must be applied to a previously consolidated sample as a function of normal stress. The yield locus terminates at the steady-state values of normal stress and shear stress. For a given normal load, any shear stress below the yield locus will not be great enough to cause the bulk solid to fail. Instead, it will deform elastically. Shear stresses above the yield locus are not possible. The material has already yielded.

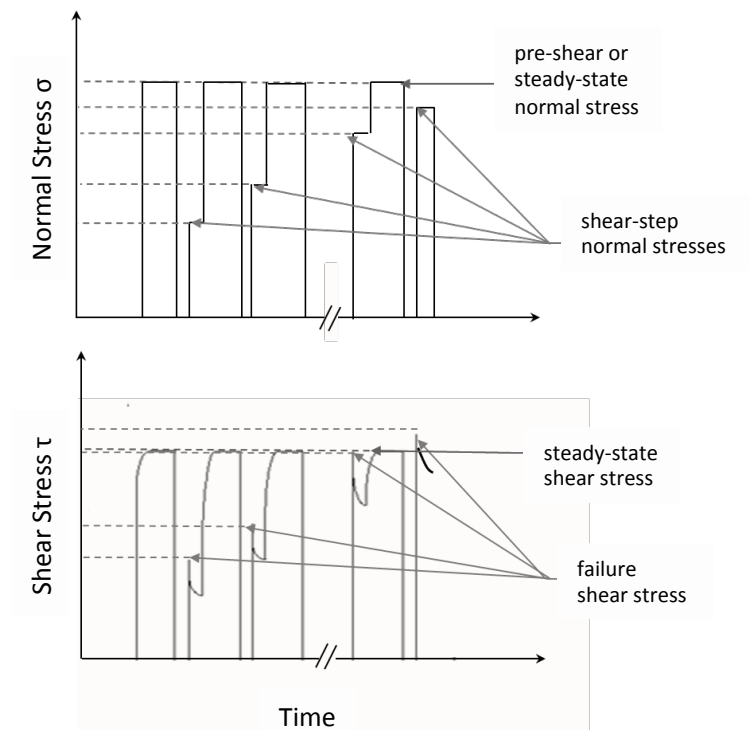


Figure 4.5. Pre-shear and shear steps.

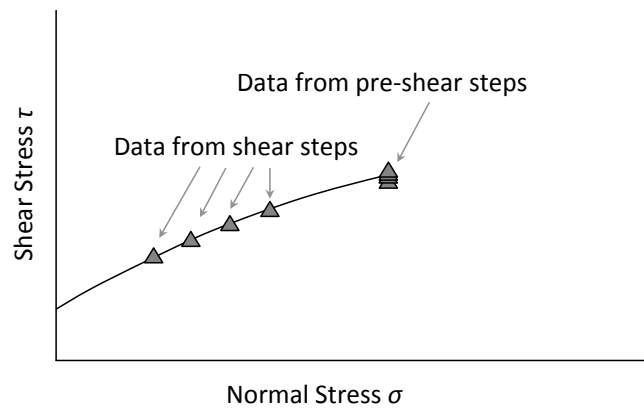


Figure 4.6. Yield locus.

Ideally, all measurements of the pre-shear shear stress τ_{ss} should be identical. However, because of unavoidable variability during testing and occasional attrition along the shear plane, there is inevitably scatter in the τ_{ss} values. *Prorating* is used to account for the variability of the data. Prorated values of the shear stress measured during each shear step are calculated by dividing the measured shear stress by the ratio $\bar{\tau}_{ss}/\tau_{ss}$ where $\bar{\tau}_{ss}$ is equal to the average of the measured pre-shear shear stresses. Prorating assumes that the variations in the shear stress measured during a shear step are proportional to the corresponding variation in the measured pre-shear shear stress.

To determine the major principal stress σ_1 (also called the major consolidation stress or the major consolidation pressure) and the unconfined yield shear strength f_c from the yield locus, a line is drawn through the shear test data. The major principal stress can be determined using a Mohr's circle analysis. At steady state, the state of stress is represented by the points (σ_{ss}, τ_{ss}) on the yield locus. To construct a Mohr's circle, we need one more point. We know that the Mohr's circle cannot lie above the yield locus. Therefore, we draw a Mohr's semicircle through the steady-state result (σ_{ss}, τ_{ss}) that is tangent to the yield locus line (see Figure 4.7). The intersection points of the semicircle with the horizontal axis give the values of the major principal stress σ_1 and the minor principal stress σ_2 .

We also know that when a sample is unconfined, its minor principal stress is equal to zero. The unconfined yield strength f_c is therefore determined by drawing a Mohr's semicircle tangent to the yield locus and passing through the origin. The point of intersection of this circle and the horizontal axis is the major principal stress associated with the condition where the bulk solid has failed. The major stress is called the unconfined yield strength, which can be considered the cohesive strength of the bulk solid. Note that all points on the yield locus must lie to the right of the point of tangency to the smaller Mohr's circle. Data points to the left should be discarded.

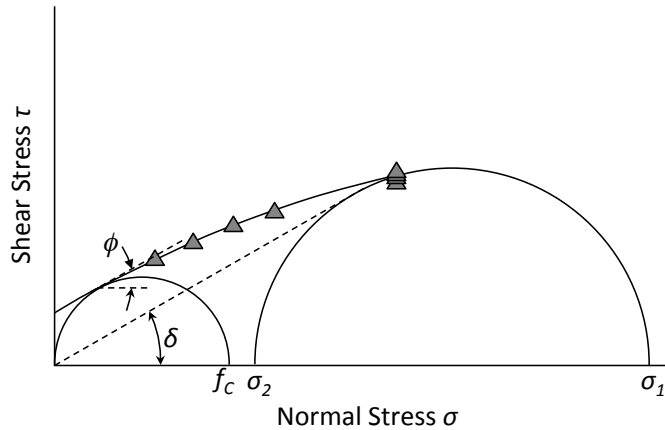


Figure 4.7. Determination of the major and minor principal stresses, unconfined yield strength, effective angle of friction, and the kinematic angle of internal friction from the yield locus.

Also determined are the effective angle of friction δ and kinematic angle of internal friction ϕ . The effective angle of friction is found by constructing a line through the origin and tangent to the larger Mohr's semicircle. The kinematic angle of internal friction is the angle formed between a line that is horizontal and one drawn tangent to the smaller Mohr's circle at its intersection with the yield locus (see Figure 4.7). The effective angle of friction δ is useful in the design of mass flow hoppers and is an indication of the anisotropy of the powder. The kinematic angle of internal friction ϕ is used to design funnel flow hoppers.

The yield locus generally is slightly concave downward. However, if the yield locus is approximated as linear with respect to the consolidation pressure, the major principal stress and unconsolidated shear strength can be calculated explicitly.

Now if you insist on a nonlinear curve fit, Wolfram has a computer tool for fitting the data to a Warren Spring equation [Peleg, M., M. Normand, and M. Corradini, "Interactive software for calculating the principal stresses of compacted cohesive powders with the Warren-Spring equation", *Powder*

Technology, 197, 268-27 (2009)]. But why bother? A linear approximation gives conservative results; that is, the unconfined yield strength determined from a linear approximation of the yield locus will be higher than its true strength. (What is the difference between a scientist and an engineer? A scientist will say, “ $f = ma$ ”, whereas an engineer will say, “ $f = ma + 25\%$, just to be safe.”)

The (prorated) shear data that make up the yield locus (*i.e.*, all data points *sans* the steady-state or pre-shear data) are regressed to give the following linear relation:

$$\tau = c + \sigma \tan \phi \quad (4.1)$$

where τ is the shearing stress and σ is the normal load. Equation 4.1 is the Coulomb equation. The slope of the line is equal to the tangent of the kinematic angle of internal friction ϕ , and the intercept is equal to c , which is called the material’s cohesion. The cohesion c should not be confused with the cohesive strength or unconfined yield strength f_c . In fact, the state of stress in which the normal stress equals zero and the shear stress is equal to the cohesion c does not exist when a bulk solid is flowing inside a hopper. While some investigators tabulate c as a metric for powder flowability, it really has very little utility.

The unconfined yield strength and major principal stress are calculated from:

$$f_c = \frac{2c(1 + \sin \phi)}{\cos \phi} \quad (4.2)$$

and

$$\sigma_1 = \left(\frac{A - \sqrt{A^2 \sin^2 \phi - \tau_{ss}^2 \cos^2 \phi}}{\cos^2 \phi} \right) (1 + \sin \phi) - \frac{c}{\tan \phi} \quad (4.3)$$

respectively, where

$$A = \sigma_{ss} + \frac{c}{\tan \phi} \quad (4.4)$$

The major principal stress represents the maximum amount of stress applied to the sample during the shear test. The minor principal stress σ_2 can be calculated from

$$\sigma_2 = \sigma_{SS} - \frac{\tau_{ss}^2}{(\sigma_1 - \sigma_{SS})} \quad (4.5)$$

Finally, the effective angle of friction δ is calculated from:

$$\delta = \sin^{-1} \left(\frac{\sigma_1 - \sigma_2}{\sigma_1 + \sigma_2} \right) \quad (4.6)$$

The larger Mohr's circle can be constructed by drawing a circle centered at $(\sigma_1 + \sigma_2)/2$ on the horizontal axis having a radius R . The radius R is given by

$$R = \frac{\sigma_1 - \sigma_2}{2} \quad (4.7)$$

Plotting values of f_c against the major principal stress σ_1 gives the flow function FF of the bulk solid. The flow function describes the relationship between a bulk material's cohesive strength and its consolidation stress. Construction of the flow function from a number of yield locus measurements is illustrated in Figure 4.8. The effective yield locus EYL is an envelope of the larger Mohr's semicircles, as illustrated in Figure 4.9.

Some bulk materials gain cohesive strength if stored at rest. Unless a bin is expected to be operated continuously, the time unconfined yield strength of the bulk material should be measured. To conduct a time test, a sample of bulk material is placed inside a cell and pre-sheared using a normal stress σ_{ss} used during instantaneous testing. After pre-shear, the sample is then kept consolidated at that state of stress, typically by applying a vertically-acting load equal to the major principal stress σ_1 associated with the corresponding instantaneous test. After the appropriate amount of time has passed (*e.g.*, 2-3 days if the bulk material is to be stored at rest over a weekend), the vertical compacting load is replaced with a lighter load, and the shear step is conducted, in which the shearing force again is applied until the sample fails.

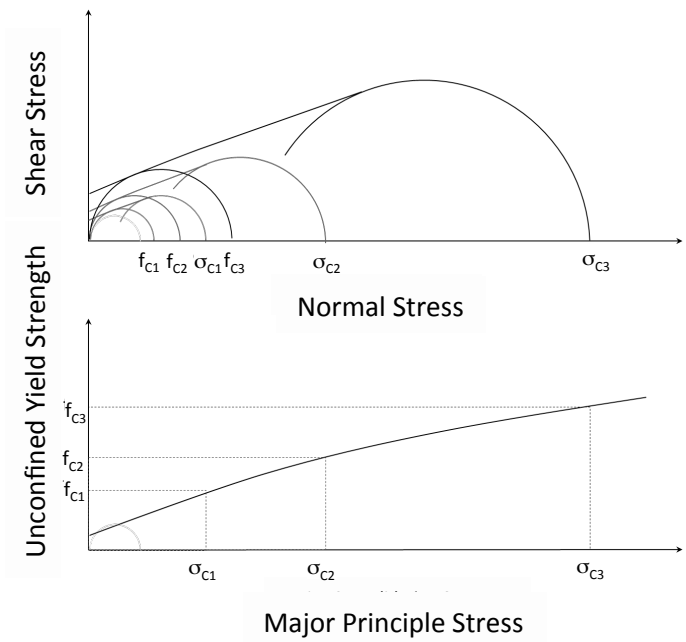


Figure 4.8. Construction of flow function from yield loci.

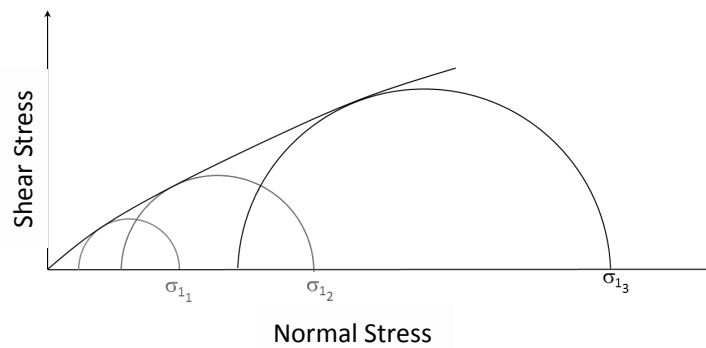


Figure 4.9. Construction of the effective yield locus.

The pre-shear, time under consolidation, and shear steps are repeated at the same normal stress σ_{ss} for a number of normal stresses, and the time yield locus (TYL) is then determined by plotting the failure shear stress against normal stress. An example of a time yield locus is given in Figure 4.10.

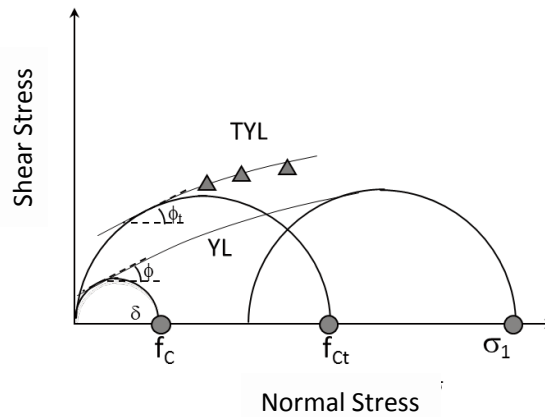


Figure 4.10. Construction of the time yield locus.

To calculate the time unconfined yield strength, a Mohr's circle is drawn through the origin and tangent to the time yield locus. The point of intersection with the horizontal axis is the material's time unconfined yield strength f_{ct} . This value, along with the value of the major consolidation stress for instantaneous flow σ_1 , becomes one point on the *time* flow function (FF_t).

The time angle of internal friction ϕ_t is the angle formed between a horizontal line and a line drawn tangent to the smaller Mohr's circle at its intersection with the time yield locus (see Figure 4.10).

As with the yield locus, the time yield locus is often approximated as a line, and Equation 4.2 can be used to calculate f_{ct} . Frequently time tests are conducted by performing one test only, that is, conducting a pre-shear step, consolidating it under a normal stress equal to the major consolidation stress determined from the instantaneous test, and then performing only one shear step at a reduced normal load. A line whose slope is the same as that of the instantaneous yield locus is drawn through the point, and the time unconfined yield strength is calculated using Equation 4.2.

The time flow function is determined by plotting the time unconfined yield strength f_{ct} against major principal stress σ_1 after measuring time yield loci using other normal stress levels and corresponding major principal stresses. If a bulk material gains strength when stored at rest in a bin over time, its time flow function will lie above its instantaneous flow function, as illustrated in Figure 4.11.

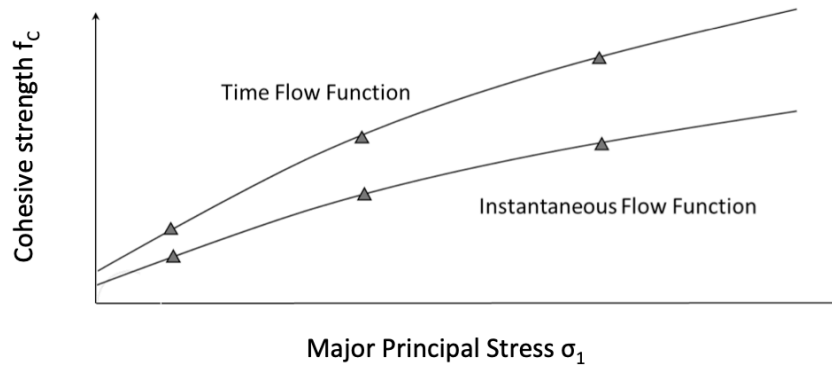


Figure 4.11. Instantaneous and time flow functions.

Solving the equations that allow the major principal stress, effective angle of friction, and the unconfined yield strength to be determined from the yield locus or time yield locus can be painful, but the formulas can be readily input into spreadsheets. Most modern automated shear cell testers perform this analysis. The user should confirm that prorating is used and in general, a linear approximation to the yield locus is acceptable.

Note that in a torsional shear cell, shear deformation of the specimen varies with radius in the cell: at the perimeter it is at its maximum, while at the center it is zero. This can result in data that differ from results obtained using a Jenike (translational) or annular shear cell. Rotational and annular shear cells permit infinite travel, so they are better suited than a Jenike shear cell for testing bulk solids that require large shear strain to reach steady state. The Jenike shear cell tester can be relatively easily modified to operate at extremely high or low temperatures, whereas this is more difficult with the other two types of testers. In addition to the Jenike direct tester, Jenike & Johanson uses Schulze ring shear testers to measure the cohesive strength of powders, which is an *über* endorsement of Schulze's tester.

The normal stress values that should be used when conducting a shear cell test depend on the bulk density of the powder tested and the size of the storage vessel that is under consideration. Typically three yield locus tests are conducted, which allows three points on a flow function to be determined. The tests should provide values of the material's cohesive strength that are expected in the cylinder and the hopper section of the vessel.

The maximum solids stress in the cylinder $\sigma_{1\max}$ can be calculated using the Janssen equation (Equation 3.8). A very approximate value can be estimated from

$$\sigma_{1\max} = \frac{1}{2} \rho_b g h \quad (4.8)$$

where h is the cylinder height. Because the major principal stress σ_1 calculated from the yield locus is roughly double the normal stress used during the pre-shear step of the yield locus test, the value of the pre-shear normal load σ_{pre} used to create the highest-stress data point on the flow function is

$$\sigma_{pre} = \frac{1}{4} \rho_b g h \quad (4.9)$$

Subsequent tests can be performed using the lowest normal stress allowed by the tester and one near the middle. Most shear cell testers have a lower limit to the normal stress that can be used during a yield locus test. Because the solids stress at the outlet of a mass flow hopper is low, it's best to have a test conducted in the neighborhood of this lower limit. If you are fortunate and have a Schulze RST-XS.s, RST-01.pc, or RST MK II, you will be able to measure shear stresses at very low normal stresses.

Wall friction and compressibility tests should be conducted over a similar range of normal stresses.

Example yield locus calculation

A shear cell test was performed on a sample of powder. The target pre-shear normal stress was 1.6 kPa, and shear-step normal stress set points were 20, 30, 40, 50, and 60 percent of the pre-shear normal stress setting. Test data are summarized in Table 4-1.

The average steady-state shear stress measured during the pre-shear steps is 1.286 kPa. This value is used to adjust the shear-step failure shear stress values by prorating. The prorated data are given in Table 4-2 and plotted in Figure 4.12.

Table 4-1			
Shear Cell Test Data – Measured			
Pre-Shear Step		Shear Step	
Normal Stress (kPa)	SS Shear Stress (kPa)	Normal Stress (kPa)	Failure Shear Stress (kPa)
1.602	1.363	0.961	1.112
1.601	1.261	0.801	0.899
1.598	1.262	0.642	0.755
1.599	1.261	0.481	0.599
1.605	1.281	0.320	0.477

Table 4-2			
Pro-rated Shear Cell Data – Prorated			
Pre-Shear Step		Shear Step	
Normal Stress (kPa)	SS Shear Stress (kPa)	Normal Stress (kPa)	Failure Shear Stress (kPa)
1.601	1.286	0.961	1.049
1.601	1.286	0.801	0.917
1.601	1.286	0.642	0.769
1.601	1.286	0.481	0.611
1.601	1.286	0.320	0.479

Regression of the shear-step data gives an intercept equal to 0.186 kPa and a slope equal to 0.903. The slope is equal to $\tan \phi$; hence $\phi = 42^\circ$. Solving Equation 4.2 gives $f_c = 0.84$ kPa. Solving Equation 4.3 gives $\sigma_1 = 3.01$ kPa. From Equation 4.6, $\delta = 49^\circ$.

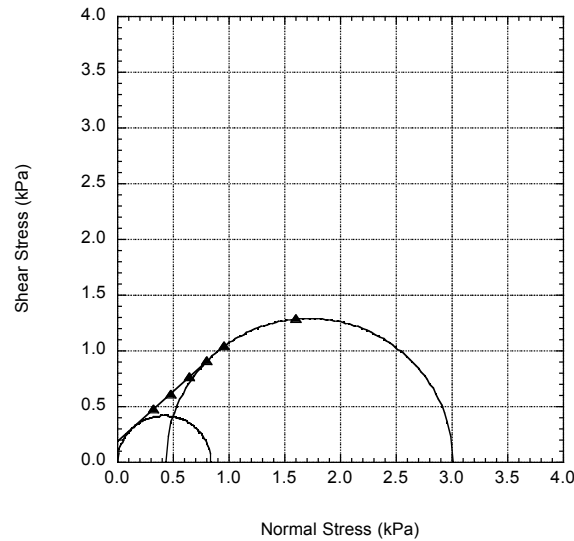


Figure 4.12. Prorated shear cell data and yield locus.

Bulk density/compressibility

A method to measure the bulk density of a material as a function of compressive stress (*i.e.*, pressure) is given in ASTM D6683. A sample is placed in a cylinder of known volume and its mass is recorded. A lid with a known weight is placed on the specimen and the displacement is logged, allowing an updated volume to be calculated. The compressive stress is equal to the weight placed on the sample divided by the cross-sectional area of the cylinder. The bulk density is equal to the mass of sample divided by the volume. Increasing loads are placed on the lid, and the displacement is recorded for each load. From the data, the bulk density as a function of consolidation pressure, *i.e.*, its compressibility, is determined. A typical compressibility curve is shown in Figure 4.13.

The relationship between bulk density and consolidation pressure is nonlinear. The bulk density increases with increasing consolidation pressure, varying rapidly at low stress and less so at high stress. Data can be fit to a number of equations that describe the relationship between bulk density and consolidation pressure. Frequently, a power-law relationship is used:

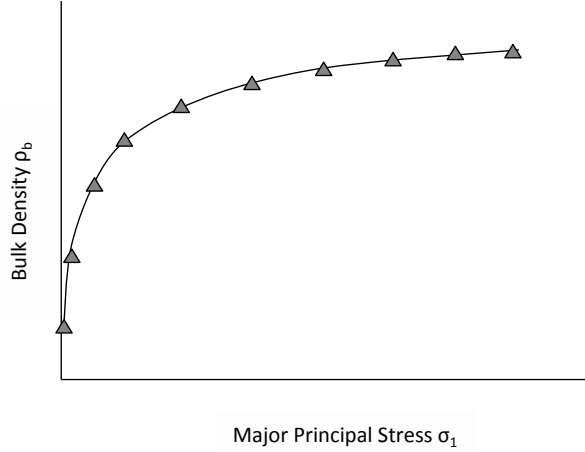


Figure 4.13. Typical bulk density – consolidation stress relationship.

$$\rho_b = \rho_{b0} \left(\frac{\sigma}{\sigma_0} \right)^\beta \quad (4.10)$$

where σ is the consolidation pressure, σ_0 is an arbitrarily chosen reference consolidation level, ρ_{b0} is the bulk density at that consolidation, and β is called the compressibility. A limitation of the model is that it does not provide a value of the bulk density at zero stress. Alternative bulk density-consolidation stress relations are [Gu *et al.*, *Powder Techn.*, 72, 39 (1992)]:

$$\rho_b = \rho_{b\min} (1 + \alpha\sigma)^\beta \quad (4.11)$$

$$\rho_b = \rho_{b\min} + \alpha\sigma^\beta \quad (4.12)$$

$$\begin{aligned} \rho_b &= \rho_{b\min}, & \sigma &= 0 \\ \rho_b &= \rho_{b\min} + \frac{(\rho_{b0} - \rho_{b\min})\sigma}{\rho_{b0}}, & 0 < \sigma < \sigma_0 \end{aligned} \quad (4.13)$$

$$\rho_b = \alpha\sigma^\beta, \quad \sigma \geq \sigma_0$$

$$\rho_b = \rho_{b\max} - (\rho_{b\max} - \rho_{b\min}) \exp(-\alpha\sigma) \quad (4.14)$$

$$\rho_b = \rho_{b\min} \rho_{b\max} \frac{1 + \alpha \sigma}{\rho_{b\max} + \rho_{b\min} \alpha \sigma} \quad (4.15)$$

where α and β are empirical constants and $\rho_{b\min}$ and $\rho_{b\max}$ are the material's minimum (loose-fill) and maximum bulk density, respectively.

Wall friction

The flow pattern inside a bin depends on the friction between the bulk solid and the wall material. Therefore, measuring wall friction is a critical step when designing mass flow bins.

Suppose we were to place a bulk material in a dump truck and then raise the front of the bed. When the slope is great enough, the contents will begin to slide on the floor of the bed. We then lower it until the material stops sliding. We note the angle of incline referenced from horizontal to equal α , as shown in Figure 4.14.

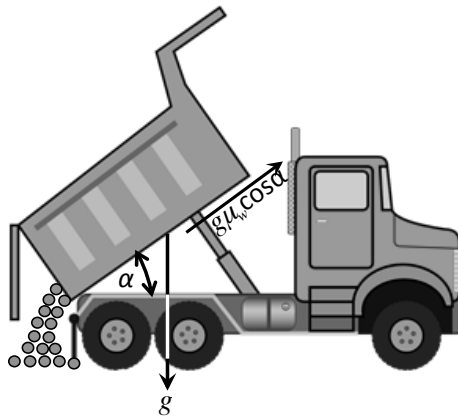


Figure 4.14. Element of bulk solid sliding on a straight surface.

A force balance gives

$$g \sin \alpha - \mu_w g \cos \alpha = 0 \quad (4.16)$$

where g is the acceleration due to gravity and μ_w is the friction coefficient. Solving for μ_w gives

$$\mu_w = \tan \alpha \quad (4.17)$$

It turns out that the friction coefficient is equal to the tangent of the angle of the incline where the bulk material stopped sliding.

One would expect that for some materials, such as coarse sand, the angle of incline would be fairly shallow. However, if carbon black were loaded onto a dump truck (not recommended!), the bed would have to be very steep before sliding begins.

A better way to measure the friction between a bulk solid and a wall material is described in ASTM D-6128. The test is best conducted using a direct translation shear tester. A sample of bulk solid is placed inside a retaining ring on a flat coupon of wall material (see Figure 4.15), and a normal load is then applied to the bulk solid. The bulk solid in the ring is forced to slide along the stationary wall material, and the resulting steady shear stress is measured as a function of the applied normal load. The normal load is then reduced, and the test is continued until a new steady shear stress is measured. The test is repeated for various normal loads.

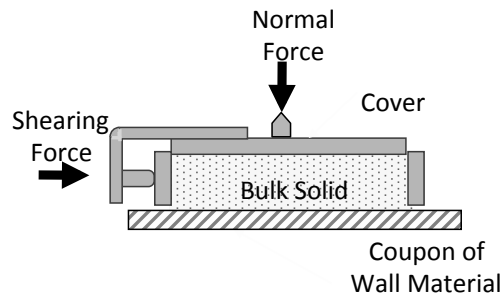


Figure 4.15. Wall friction test equipment.

The wall coupon should be located beneath the bulk solid sample. After all, this is what occurs in most commercial equipment. If a material is allowed to slide against a coupon of wall material located above the sample, low values of the wall friction will be measured if fine particles percolate through the sample and away from the coupon.

After a number of steady shear stress values have been recorded for a range of normal loads, the *instantaneous wall yield locus (WYL)* is constructed by plotting shear stress against normal stress. The angle of wall friction ϕ' is the angle that is formed when a line is drawn from the origin to a point on the wall yield locus. A typical wall yield locus is shown in Figure 4.16.

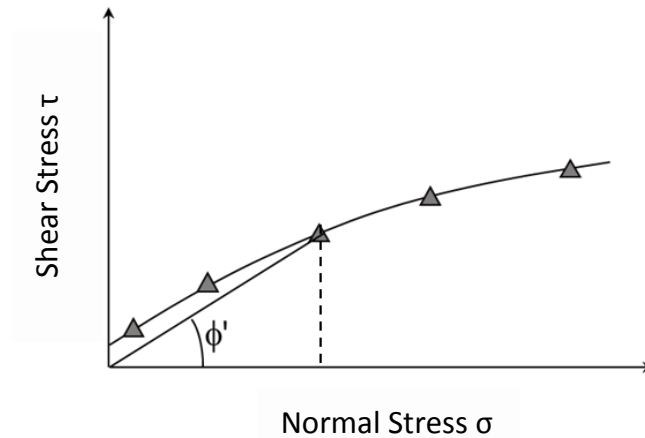


Figure 4.16. Wall yield locus.

Guess what? The angle of wall friction is the inverse tangent of the ratio of the shear stress to the normal stress, *i.e.*, the inverse tangent of the friction coefficient. That is, the angle of wall friction ϕ' is the same as α , the angle at which material stopped sliding in the dump truck. The higher the friction coefficient, the higher the value of the angle of wall friction or the angle required to stop material from sliding on an inclined wall. It is convenient to use an angle of wall friction ϕ' rather than a friction coefficient μ_w . Again, angles appear everywhere in the analysis of solids stresses inside hoppers. The math is less hostile if angles of wall friction are used rather than inverse tangents of friction coefficients.

The wall yield locus is frequently concave downward. In addition, the wall yield locus does not always intersect the origin, as many bulk materials adhere to a wall surface in the absence of a normal stress. As a consequence, ϕ' is often higher at lower applied stresses. This is important in the design of hoppers, since for mass flow the stresses at the hopper outlet are low and the angle of wall friction is therefore usually higher near the outlet. The wall friction angle is constant only when the wall yield locus is a straight line that passes through the origin.

Because wall friction is a critical parameter in the design of mass flow hoppers, tests are often performed in triplicate, and the highest values of the wall friction angle are used in the calculation of critical mass flow hopper

angles. Stresses on bin walls are maximized when low wall friction angle values are used in load calculations.

To measure the static friction between a wall surface and a bulk solid after storage at rest, wall friction *time* tests are performed. A sample is sheared under a normal load until a steady shear load is observed. The normal load is then reduced by 10-20 percent, and shearing is continued until steady state is again reached. The shear is then reduced to zero and the sample is stored in the cell for the suitable period of time. Afterwards, the sample is again sheared, and the maximum shear stress is reported.

The pair of normal stress and maximum shear stress values provide one point on the *time wall yield locus (TWYL)*. Repeating the test over a range of normal loads completes the time wall yield locus. The time angle of wall friction is the angle obtained by drawing a line from the time wall yield locus to the origin (see Figure 4.17).

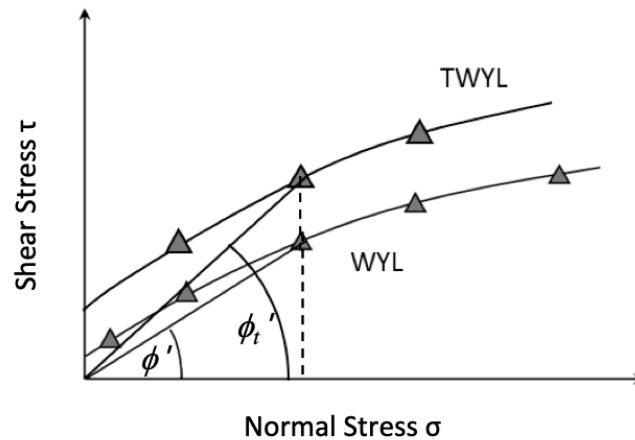


Figure 4.17. Time wall yield locus.

Note that the measured friction between a powder and a “smooth” surface will not always be lower than that for a “rougher” surface. There are two components that lead to the measured friction between the bulk material and wall material: friction and adhesion. While friction is independent of contact area, adhesion is not. Smoother surfaces should lead to reduced friction but also increased wall adhesion due to greater contact area and reduced intermolecular separation between the wall and solid particles.

Therefore, the measured wall friction may be considered an “effective wall friction.”

Wall friction can also be measured in annular and torsional ring shear testers. A limitation is when friction is dependent on the grain direction of the wall material. The sample of bulk material slides circumferentially along the wall coupon in annular and torsional testers. For this reason, direct shear testers are preferable. Figure 4.18 gives an example in which wall friction angle is strongly dependent on the direction of powder flow with respect to the grain of the wall material (Schulze, D., “How to Deal with Orientation-Dependent Wall Friction”, presented at the 2012 CHoPS meeting, Friedrichshafen, Germany).

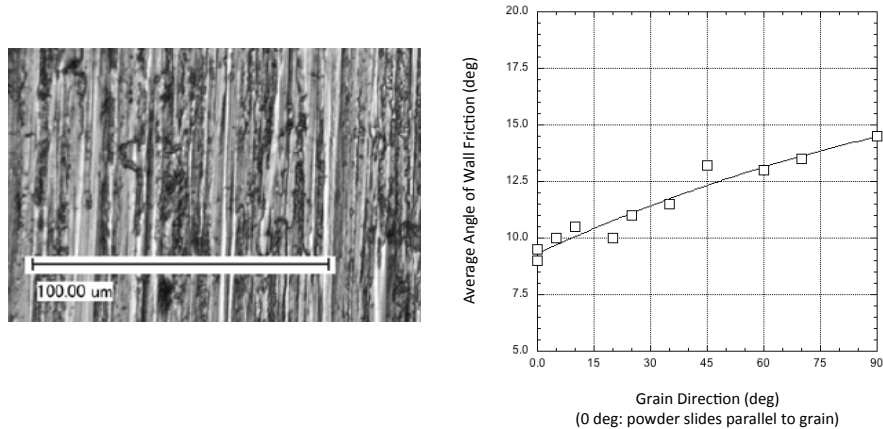


Figure 4.18. Influence of grain direction on wall friction angle.

Wall friction depends on the roughness of the surface, which is generally indicated by its Ra value. 2B finish is typically 0.3 - 1 μm depending on the gauge of the metal. A #1 finish, sometimes called hot rolled, annealed, and pickled (HRAP), typically ranges from 3.2 to 12.5 μm . The Ra of a metal with a #4 or ‘brushed’ finish is around 0.8 μm , while a #8 finish is mirror-like and is around 0.025 μm . Table 4-3 compares grit size and Ra values.

Note that the surface designations encompass rather large ranges of surface roughness values. Wall materials from different suppliers can have considerably different roughness characteristics. It is always prudent to conduct wall friction tests on the actual material in use or that will be used to fabricate a bin.

Grit Size	<i>Ra</i> (μm)
80	1.80
120	1.32
150	1.06
180	0.76
240	0.38
320	0.30
500	0.18
600	0.13

FFC

Frequently, *FFC*, the ratio of the major principal pressure σ_1 to the unconfined yield strength f_c is used as a metric for flowability, *i.e.*, $FFC = \sigma_1/f_c$. Because the unconfined yield strength appears in the denominator, small values of *FFC* are believed to indicate poor flowability.

In his Bulletin 123, Jenike generalized the flowability of powders as shown in Table 4-4:

$10 < FF$	free-flowing
$4 < FF < 10$	easy-flowing
$2 < FF < 4$	cohesive
$FF < 2$	very cohesive and non-flowing

The ratio is often erroneously referred to as the flow function or the flow factor. In Bulletin 123, Jenike first defined the term *FF* as the ratio of the major principal stress to the cohesive strength. He also defined *FF* as the flow function, the relationship between the material's strength (f_c) and the major principal stress σ_1 . *FF* can therefore be either the ratio of the major principal stress to the cohesive strength or the flow function. Jenike defined the flow factor *ff* as the ratio of the major principal stress to the stress on the

abutments of an arch of powder at the hopper outlet $\bar{\sigma}$. We will learn how the flow factor is used to calculate the size of a hopper outlet required to prevent arching. *FFC* should never be referred to as the flow function or flow factor. *FFC* is equal to σ_1/f_c , the ratio of the major principal stress to the cohesive strength. It is best to refer to *FFC* as the flow function coefficient or the flowability coefficient. Actually, it's probably better not to use *FFC* at all.

FFC can be a poor metric for flowability as it ignores the effects of bulk density and wall friction on flow behavior. Instead, cohesive strength tests should be conducted over a range of consolidation pressures. The test results, together with those from wall friction and compressibility tests, can then be used to determine the size of a hopper outlet that must be exceeded to prevent flow obstructions and the recommended hopper angle to ensure mass flow. The results can also be used to determine if an existing bin is appropriate for the powder tested.

FFC can be confusing because it more times than not depends on the major principal stress. This is illustrated in Figure 4.19 where a flow function is plotted along with flowability defined by *FFC*. At high solids stresses, *FFC* may suggest that a material is easy-flowing, but at low stresses, the powder may be deemed very cohesive. In fact, we will learn that if the size of the outlet is the minimum dimension required to prevent arching, *FFC* at the outlet solids stress will be equal to the flow factor ff , which typically ranges between 1.1 and 1.5.

Permeability

Because of vacuum that naturally develops above a hopper outlet when the voids in fine powders expand as the material discharges, the resulting counter flow of gas may hinder the solids flow and a limiting discharge rate will exist. The ease at which a gas flows through a bed of solids therefore greatly influences the maximum attainable discharge rate of a bulk material from a hopper, bin, or silo.

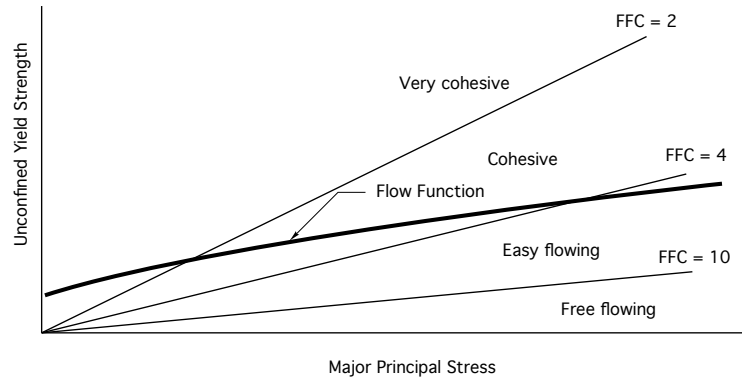


Figure 4.19. Flowability changing with major principal stress.

If the particle diameter, its particle sphericity, and the void fraction of the bed of bulk solids are known, the Kozeny-Carman equation can be used to calculate the pressure drop of a gas flowing through the bed. The equation is only valid for laminar flow and is given by

$$\frac{\Delta P}{L} = \frac{180u_g \eta (1-\varepsilon)^2}{\Phi_s^2 D_p^2 \varepsilon^3} \quad (4.18)$$

where ΔP is the pressure drop (formally, this term should be negative, but for now, we'll let this slide for convenience), L is the height of the bed, u_g is the gas slip velocity (*i.e.*, the superficial gas velocity relative to the solids velocity), η is the viscosity of the fluid, ε is the porosity of the bed, Φ_s is the sphericity of the particles in the bed, and D_p is the diameter of the related spherical particle. The sphericity of a particle is the ratio of the surface area of a sphere (with the same volume as the given particle) to the surface area of the particle and is given by

$$\Phi_s = \frac{\pi^{1/3} (6V_p)^{2/3}}{A_p} \quad (4.19)$$

where A_p and V_p are the particle surface area and volume, respectively. Equation 4.19 can be rearranged to solve for the slip velocity:

$$u_g = \frac{\Phi_s^2 D_p^2 \varepsilon^3}{180\eta(1-\varepsilon)^2} \frac{\Delta P}{L} \quad (4.20)$$

Inspection of Equation 4.20 shows that under laminar flow, the gas slip velocity is proportional to the pressure drop across a moving bed of solids. This is the basis of Darcy's law (or D'Arcy's Law if you are a Francophile), which mathematically can be expressed as

$$u_g = \frac{K}{\rho_b g} \frac{\Delta P}{L} \quad (4.21)$$

where K is the powder's permeability. Comparison of Equations 4.20 and 4.21 shows that

$$K = \frac{\Phi_s^2 D_p^2 \rho_b g \varepsilon^3}{180 \eta (1 - \varepsilon)^2} \quad (4.22)$$

Note that the units of K are length/time, which are those of velocity. If the gas slip velocity is equal to the powder's permeability, then

$$\frac{\Delta P}{L} = \rho_b g \quad (4.23)$$

and the pressure gradient is equal to the body forces. In other words, there's just enough pressure force to overcome gravity, and the powder is fluidized. The permeability is therefore related to the powder's minimum fluidization velocity.

Frequently, Darcy's Law is expressed as

$$u_g = \frac{k}{\eta} \frac{dP}{dz} \quad (4.24)$$

where k is the Darcy permeability. Equation 4.24 is just an empirical form of the Kozeny-Carman equation. K and k are related by:

$$K = \frac{\rho_b g}{\eta} k \quad (4.25)$$

Unless dealing with powders comprised of mono-disperse spherical particles, the Kozeny-Carman equation unfortunately is of little practical use. The sphericity of the particles is difficult to measure, and if the powder is made up of particles with a distribution of sizes, which diameter to use in the calculations is unclear.

The permeability of a bulk solid is best measured directly. Permeability is determined by passing a gas through a bed of powder contained in a cylinder as shown in Figure 4.20. During a test, the sample mass and volume are recorded, which allows its bulk density to be calculated. The pressure drop between two locations of the bed and the gas flow rate are measured, from which the permeability can be calculated from Darcy's Law:

$$q_g = \frac{KA}{\rho_b g} \frac{\Delta P}{h} \quad (4.26)$$

where q_g is the volumetric gas flow rate, A is the cross-sectional area of the bed, and h is the distance between pressure measurements (see Figure 4.20).

Typically, the test is conducted by measuring the flow rate of air that results in a target pressure drop. The permeability is then calculated from the formula

$$K = \frac{q_g h \rho_b g}{A \Delta P} \quad (4.27)$$

To determine the relationship between permeability and bulk density, the test is conducted over a range of bulk densities by adjusting the bed height downward and determining the flow rate of air that results in the same pressure drop.

Alternatively, for a given bed height (*i.e.*, bulk density), the flow rate can be varied, recording the pressure drop for each flow rate as shown in Figure 4.21. The data for which the pressure drop varies linearly with flow rate (*i.e.*, where Darcy's Law holds) are regressed, and the permeability can be determined from the slope of the line passing through the origin.

Permeability is a strong function of the powder density. As a powder is compacted, its void fraction decreases, which results in a greater pressure drop for a given flow rate. Permeability and bulk density tend to have a power-law relationship, as shown in Figure 4.22. Permeability results are therefore frequently regressed to fit the expression

$$K = K_0 \left(\frac{\rho_b}{\rho_{b0}} \right)^{-\alpha} \quad (4.28)$$

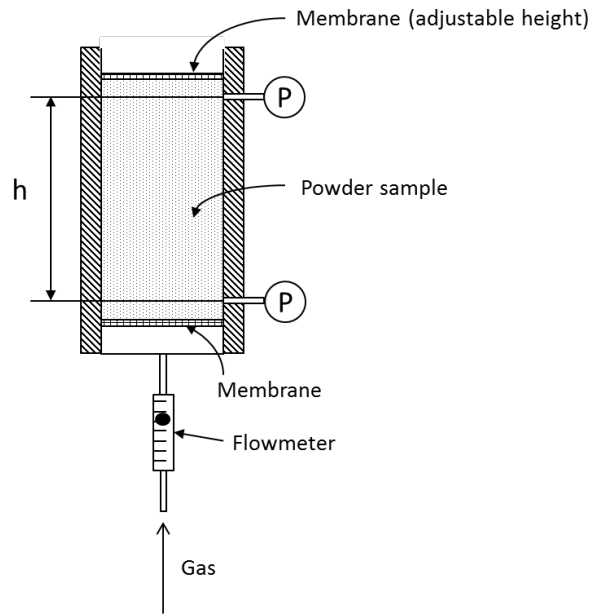


Figure 4.20. Permeability tester.

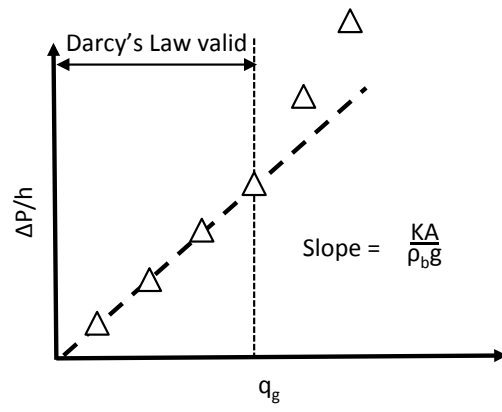


Figure 4.21. Determination of K from permeability test results.

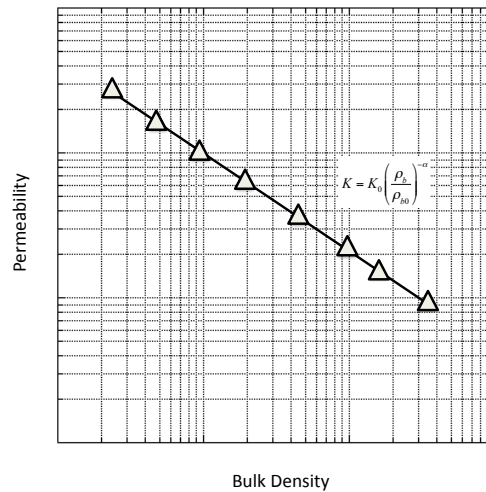


Figure 4.22. Bulk density – permeability relationship.

where ρ_{b0} is an arbitrary reference bulk density, K_0 is the powder's permeability at that bulk density, and α is an empirical constant determined by regression. For convenience, the reference bulk density can be the loose-fill bulk density, *i.e.*, ρ_{bmin} .

The permeability factor K is inversely proportional to the viscosity of the gas (see Equation 4.25). Results from permeability tests performed at ambient temperature can be adjusted to elevated temperatures and to other gases by multiplying the constant K_0 by the ratio of the viscosity of air at room temperature to that of the gas at the temperature in question.

For many purposes, only the value at the material's minimum bulk density is critical. Values of K at higher stresses are important in the design of process vessels if a gas is injected into a moving bed of solids.

Hopper tests

Some bulk materials, *e.g.*, solids that are fibrous, composed of rod-like particles with a high aspect ratio or that readily interlock, are not amenable for shear cell testing. For these materials, relatively large-scale hopper tests should be performed.

To conduct a hopper test, a planar hopper made up of removable wedge sections similar to that illustrated in Figure 4.23 is fabricated. A hopper angle of 15° from vertical is preferred. The hopper is filled with the bulk

solids, and then sections are removed from the bottom until the material discharges. The width of the outlet that allowed the bulk solid to flow can be considered the critical arching span of a planar mass flow hopper with a slotted outlet. The critical arching diameter of a conical mass flow hopper can be assumed to be equal to twice that value.

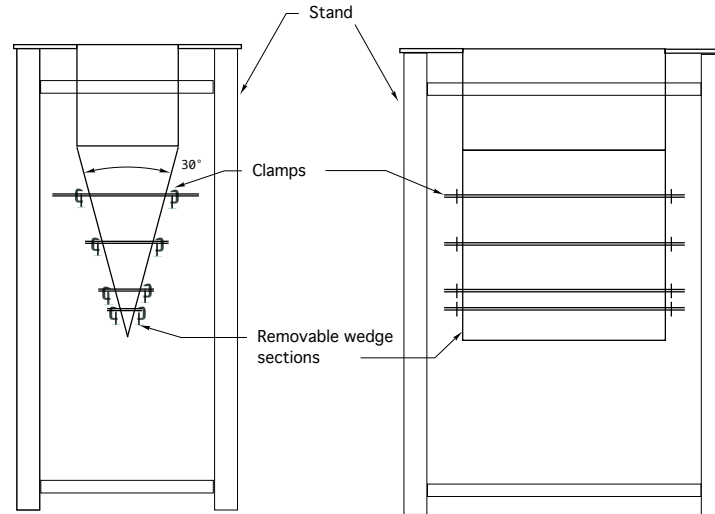


Figure 4.23. Hopper test apparatus.

Additional tests are then performed in which a normal stress is applied to consolidate the bulk material. The lowermost wedge section is then filled with material, and a weight is applied briefly and then removed. The next wedge section is then filled with powder, and again a weight is applied and then removed. The weight added is such that the applied stress is the same as that which was used previously by accounting for the increase in the cross-sectional area. The process of filling a wedge section with bulk material and applying and removing a weight that gives a constant stress is continued until the top wedge section has been filled. The cylinder section is then filled, but no weight is applied. Wedge sections are then removed until material discharges. Typically, two series of tests in which the bulk material is consolidated are performed to be able to generate a flow function.

The major principal stress associated with the outlet at which material discharged is calculated from

$$\sigma_1 = ff \frac{\rho_b g B}{H(\theta')} \quad (4.29)$$

where B is the width of the wedge section outlet for which failure occurred. A value of ff of 1.3 and $H(\theta')$ equal to 1.1 are typically used. (The flow factor ff and the geometry function $H(\theta')$ will be defined in Chapter 5.) The unconfined yield strength is then calculated from

$$f_c = \frac{\rho_b g B}{H(\theta')} \quad (4.30)$$

A plot of the unconfined yield strength against the major principal stress gives the flow function.

For biomass and other strange materials, the Wolfson Centre recommends conducting a simple test to determine whether or not the material can be handled in a conventional hopper with inclined walls. Material is placed inside a *ca.* 8-in. diameter tube, taking care not to consolidate it during filling. The tube is then slowly lifted vertically. If the material expands and forms a pile while it leaves the cylinder, it can be handled in a hopper with converging walls provided that its outlet is large enough to prevent obstructions to flow. If it discharges and remains as a plug, then bins with straight vertical walls or diverging walls are recommended. Figure 4.24 illustrates the Wolfson Centre's test method.

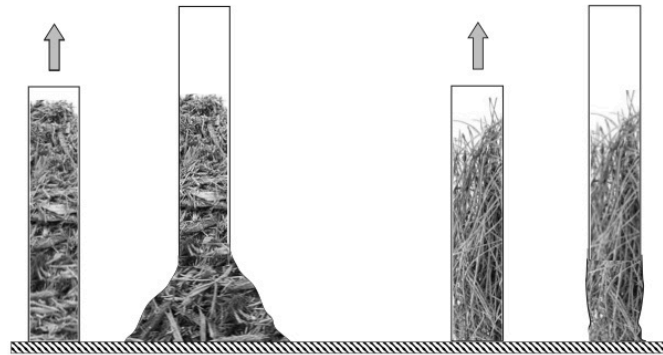


Figure 4.24. Wolfson Centre test; surcharge formation (left) and plug formation (right).

Particle size

While particle size and shape measurements by themselves cannot be used to predict the flow behavior of bulk solids, measurement is still useful, as size and shape greatly influence flowability. In general, fine powders have greater cohesive strength (due to a greater number of inter-particle contacts and greater specific surface area), higher wall friction (due to greater contact between the wall surface and surface of the powder particles), and lower permeability (due to reduced void volume). Particles with high aspect ratios tend to be less flowable. Numerous methods and instruments are available to measure particle size, including sieving, laser diffraction, and image analysis. Frequently, particle size is expressed in terms of mesh size. Standard mesh sizes are given in Table 4-5.

Various mean diameters are used to characterize powders with a particle size distribution. (Note that for volume and weight averages to be equal, particle density must be independent of particle diameter.) Mean diameters can be calculated from the following formulae:

Arithmetic (linear) mean diameter d_{AM} :

$$d_{AM} = \frac{\sum_i d_i f(d_i) \Delta d_i}{\sum_i f(d_i) \Delta d_i} \quad (4.31)$$

Geometric mean diameter d_{GM} :

$$\log d_{GM} = \sum_i df(d_i) \log d_i \quad (4.32)$$

Surface mean diameter d_{SM} :

$$d_{SM} = \frac{\sum_i d_i^2 f(d_i) \Delta d_i}{\sum_i f(d_i) \Delta d_i} \quad (4.33)$$

Weight (volume) mean diameter d_{VM} :

$$d_{SM} = \frac{\sum_i d_i^3 f(d_i) \Delta d_i}{\sum_i f(d_i) \Delta d_i} \quad (4.34)$$

Surface-volume (Sauter) mean diameter d_{SM} :

$$d_{SM} = \frac{\sum_i d_i^3 f(d_i) \Delta d_i}{\sum_i d_i^2 f(d_i) \Delta d_i} \quad (4.35)$$

The Sauter mean is appropriate for analyses that involve heat and mass transfer. In Equations 4.31 through 4.35, $f(d_i)$ is the fraction of all powder particles whose particles are within the range Δd_i .

Different methods, including sieving, laser diffraction, and photographic, can be used to measure particle size. Results obtained using one method generally should not be compared to results obtained by another. You'll be comparing apples to oranges, and you may just end up with fruit salad.

Particle shape is less straightforward to define. One approach is to define the sphericity of a particle Φ_S as the ratio of the surface area of a sphere having the same volume as the particle to the surface area of the particle, (see Equation 4.19). For most powders, Φ_S ranges between 0.65 and 0.98.

**Table 4-5
Standard Sieve Sizes**

U.S. MESH	INCHES	MICRONS	MILLIMETERS
3	0.2650	6730	6.730
4	0.1870	4760	4.760
5	0.1570	4000	4.000
6	0.1320	3360	3.360
7	0.1110	2830	2.830
8	0.0937	2380	2.380
10	0.0787	2000	2.000
12	0.0661	1680	1.680
14	0.0555	1410	1.410
16	0.0469	1190	1.190
18	0.0394	1000	1.000
20	0.0331	841	0.841
25	0.0280	707	0.707
30	0.0232	595	0.595
35	0.0197	500	0.500
40	0.0165	400	0.400
45	0.0138	354	0.354
50	0.0117	297	0.297
60	0.0098	250	0.250
70	0.0083	210	0.210
80	0.0070	177	0.177
100	0.0059	149	0.149
120	0.0049	125	0.125
140	0.0041	105	0.105
170	0.0035	88	0.088
200	0.0029	74	0.074
230	0.0024	63	0.063
270	0.0021	53	0.053
325	0.0017	44	0.044
400	0.0015	37	0.037

5. BIN DESIGN

There are a number of factors that determine what type of bin is required. These factors include the cohesiveness of the bulk solid, headroom or footprint constraints, segregation concerns, the likelihood of degradation over time (*e.g.*, caking, spoilage), and discharge rate requirements.

In general, for a given volume, mass flow hoppers, bins, and silos are taller than those designed for funnel flow. If there are headroom restrictions, designing a mass flow bin with the desired capacity may be challenging. If this is the case, an engineer should confirm that the constraints are necessary or consider whether a funnel flow bin will suffice. In some cases, an expanded flow hopper (a mass flow hopper beneath a funnel flow hopper) is a good compromise.

Mass flow hopper angle

The first step in designing a mass flow hopper is to ensure that the hopper walls are steep enough and have friction low enough to allow the bulk material to slide along them. The critical mass flow hopper angle depends on the geometry of the bin (conical or planar), the powder's effective angle of friction, and the angle of wall friction.

By assuming a radial stress field, Jenike [Gravity flow of Bulk Solids, Bulletin 108, University of Utah, 1961] was able to derive equations that described stresses in the region of the hopper outlet as a function of the effective angle of friction δ , hopper angle (from vertical) θ' , and wall friction angle ϕ' . His equations posed a split boundary condition problem,

and he had to integrate the equations numerically by hand. This was back in the 1960's! He didn't have Excel! He didn't even have a PC!

Jenike was not always able to find solutions to the radial stress equations. He reasoned that when combinations of δ , θ' , and ϕ' did not satisfy the boundary condition that described flow along the hopper walls, mass flow was not possible, and a funnel flow pattern would result. Jenike was a freakin' genius! He validated his theoretical mass flow funnel flow boundaries experimentally and presented his results in chart form.

The design charts provide allowable hopper angles for mass flow given values of wall friction angle and effective angle of friction. These charts are summarized in Figures 5.1 and 5.2 for conical (or pyramidal hoppers with square outlets) and planar hoppers (*e.g.*, wedge-shaped hoppers and transition hoppers), respectively. The outlet of a wedge-shaped or transition hopper must be at least two times as long as it is wide for Figure 5.2 to apply if it has vertical end walls and three times as long if its end walls are converging.

Values of the allowable hopper angle for mass flow θ' (measured from vertical) are on the abscissa, and values of the wall friction angle ϕ' are on the ordinate. Any combination of ϕ' and θ' that falls within the mass flow region of the chart (*i.e.*, to the left of the boundaries) will provide mass flow.

Hoppers with round or square outlets should not be designed at the theoretical mass flow hopper angle value. Otherwise, a small change in the bulk material's flow properties may cause the flow pattern inside the hopper to change from mass flow to funnel flow, with its associated risk of flow problems. A 2 to 3° margin of safety with respect to the mass flow hopper angle given in Figure 5.1 is therefore recommended. (Hey, just because it didn't work in the field doesn't mean that it won't work in theory!)

Sloping walls required for mass flow in wedge-shaped hoppers can be 10 to 12° less steep than those required to ensure mass flow in conical or pyramidal hoppers. In fact, hoppers with angles less steep than those given in Figure 5.2 may still allow flow along the walls. Planar-flow hoppers are therefore highly suitable for materials that have high wall friction. (Planar-flow hoppers are like the Clintons. Rules don't apply to them.)

An analytical description of the theoretical boundary between the mass flow and funnel flow regions for conical hoppers is as follows [Jenike Bulletin 108]:

$$\theta' = 90^\circ - \frac{1}{2} \cos^{-1} \left(\frac{1 - \sin \delta}{2 \sin \delta} \right) - \beta \quad (5.1)$$

where β is calculated from

$$2\beta = \phi' + \sin^{-1} \left(\frac{\sin \phi'}{\sin \delta} \right) \quad (5.2)$$

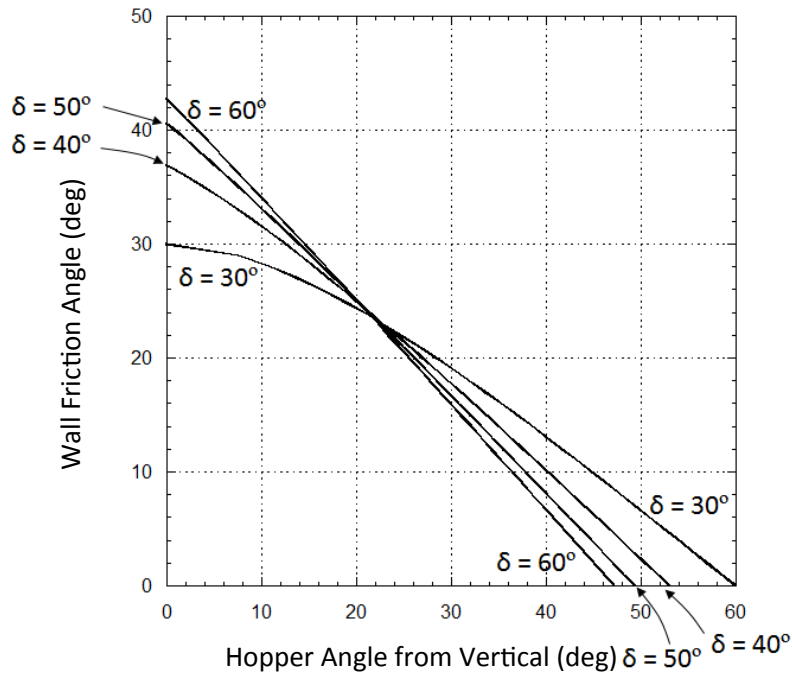


Figure 5.1. Theoretical mass flow hopper angles for hoppers with round or square outlets. Note: a minimum safety factor of 2 to 3° should be used.

In case you are curious, β is the angle formed between the major principal axis and a line normal to the hopper wall. Note that a safety factor of 2 to 3° should be used with Equation 5.1.

For hoppers with slotted outlets, the following equation can be used to calculate the recommended mass flow hopper angle [Arnold *et al.*, Bulk Solids: Storage, Flow, and Handling, TUNRA Publications, 1980]:

$$\theta' = \frac{\exp[3.75(1.01)^{(\delta-30^\circ)/10}] - \phi'}{0.725(\tan \delta)^{1/5}} \quad (5.3)$$

for ϕ' less than $\delta - 3^\circ$.

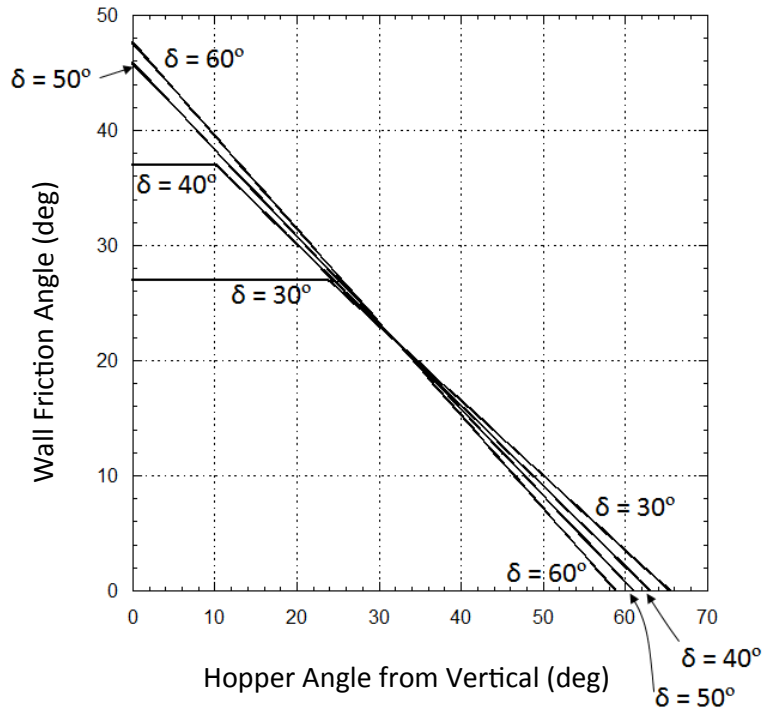


Figure 5.2. Recommended mass flow hopper angles for wedge-shaped hoppers.

Frequently, “off-the-shelf” conical bins have walls that are sloped 30° from vertical. Figure 5.3 illustrates how the hopper section of such a bin is fabricated. A fabricator begins with a square sheet of metal. He or she then cuts two concentric circles and slices the sheet in two. Drawing the straight sides together forms a 30° cone. If a hopper with steeper sides is to be fabricated, a “Pac Man” figure must be cut. Note the greater amount of unused sheet metal. 30° hoppers may be better for the fabricator’s bottom

line, but not for powder flow. Hey, the fabricator might be able to sell the customer a hammer as well.

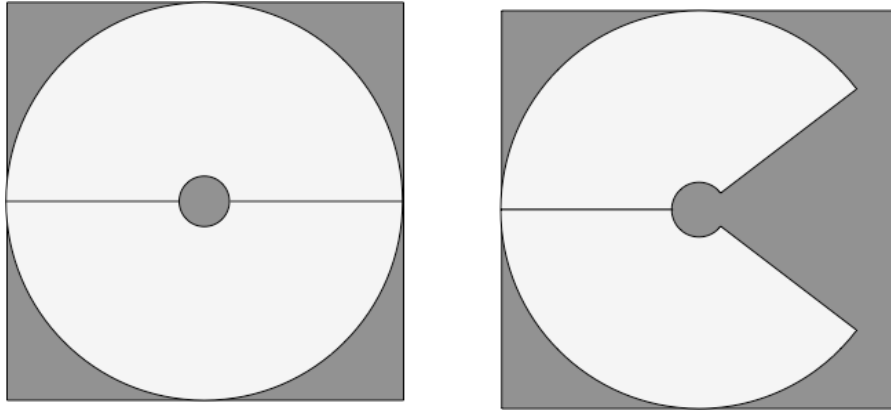


Figure 5.3. Fabrication of 30° (left) and 20° (right) hoppers.

Figure 5.4 shows the percentage of bins that would successfully operate in mass flow as a function of conical hopper wall angle, based on a survey of 500 bulk solids (ter Borg, *German Chem Engr*, 5, 1, 1982, 59). The chart shows that only about 25 percent of installations of 30° hoppers would be expected to allow mass flow. Unfortunately, silo manufacturers often regard this slope as sufficiently steep.

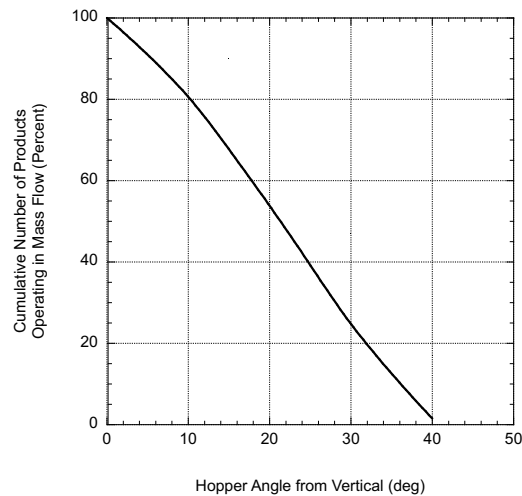


Figure 5.4. Mass flow as a function of hopper angle.

As illustrated in Figure 5.5 transition hoppers have both straight sides (side walls) and round sides (end walls). The appropriate chart or equation must be used in specifying the angles of the end walls (Figure 5.1 or Equation 5.1) and side walls (Figure 5.2 or Equation 5.3) when designing a transition hopper for mass flow.

Additional care must be taken when designing a pyramidal hopper for mass flow. The angles that are formed at the intersections of the sloping walls of pyramidal hoppers are significantly less steep than those of the hopper walls themselves. The valley angle from vertical θ_v can be calculated from

$$\theta_v = \tan^{-1} \sqrt{\tan^2 \theta_{side} + \tan^2 \theta_{end}} \quad (5.4)$$

where θ_{side} and θ_{end} are the side and end wall angles from vertical, respectively. Side, end, and valley angles are defined in Figures 5.5.

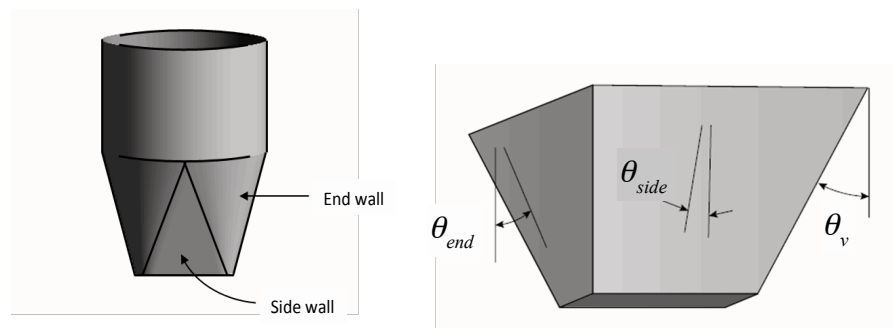


Figure 5.5. Side and end walls of transition hopper (left) and side, end, and valley angles of pyramidal hoppers (right).

Note that if a pyramidal hopper has a square outlet rather than a slotted outlet, design procedures for conical mass flow hoppers should be followed. After all, a pyramid with a square opening is essentially just a crummy cone.

If a bulk material is to be stored at rest for an extended period of time, *e.g.*, overnight or over a weekend, the time wall yield locus should be used.

Jenike's flow - no flow postulate

The outlet of the hopper must be large enough to prevent stable obstructions to flow (arching and stable ratholes) from developing. The required outlet size depends on the solids flow pattern inside the bin and the cohesive strength, the effective angle of friction, and the bulk density of the bulk solid.

An obstruction to flow develops when the magnitude of the stresses on the obstruction is not as great as the bulk solid's cohesive strength. Jenike's flow – no flow postulate is as follows [Jenike, Bulletin 123 (1964)]:

Gravity flow of a solid in a channel will take place provided the yield strength which the solid develops as a result of the action of the consolidating pressure is insufficient to support an obstruction to flow.

Critical mass flow hopper outlet dimensions to prevent arching

In a mass flow bin, as an element of bulk material flows downward, it becomes consolidated under a major principal stress σ_1 and develops an unconfined yield strength f_c . The consolidating stress follows the Janssen equation in the vertical section of the bin, changes dramatically at the cylinder-hopper junction, and then decreases toward the outlet.

Jenike [1961] calculated the stress on the abutment of a cohesive arch over the outlet $\bar{\sigma}$ as

$$\bar{\sigma} = \frac{\rho_b g B}{H(\theta')} \quad (5.5)$$

where B is the diameter of the outlet of a conical hopper or the width of the slotted outlet of a planar hopper, and $H(\theta')$ is a geometry function shown in Figure 5.6.

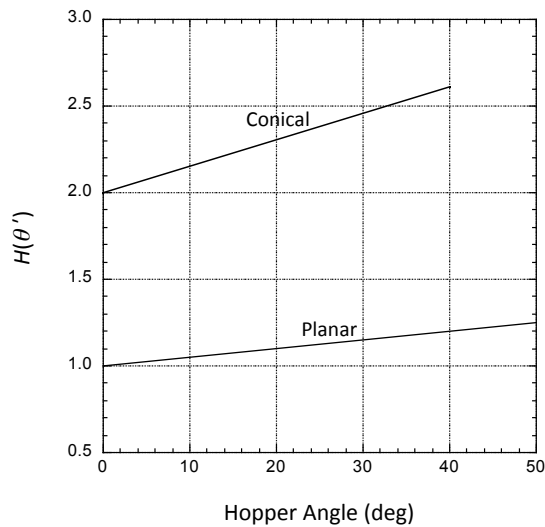


Figure 5.6. Function $H(\theta')$.

$H(\theta')$ can be calculated from [Arnold and McLean, *Powder Techn.*, 13, 255 (1976)]:

$$H(\theta') = \frac{130^\circ + \theta'}{65^\circ} \quad (5.6)$$

for round outlets, and

$$H(\theta') = \frac{200^\circ + \theta'}{200^\circ} \quad (5.7)$$

for slotted outlets.

If the arch had a uniform thickness, the values of $H(\theta')$ would equal exactly 2 and 1 for round and slotted outlets, respectively. Jenike found that the values were slightly higher and depended on the hopper angle, so he came up with the empirical relations plotted in Figure 5.6.

The stress and strength profiles inside a bin are shown in Figure 5.7. Note that there is a critical outlet size where the stress on the abutments of a cohesive arch is equal to the cohesive strength of the bulk solid. This outlet dimension represents the minimum outlet size that will prevent a stable cohesive arch from developing.

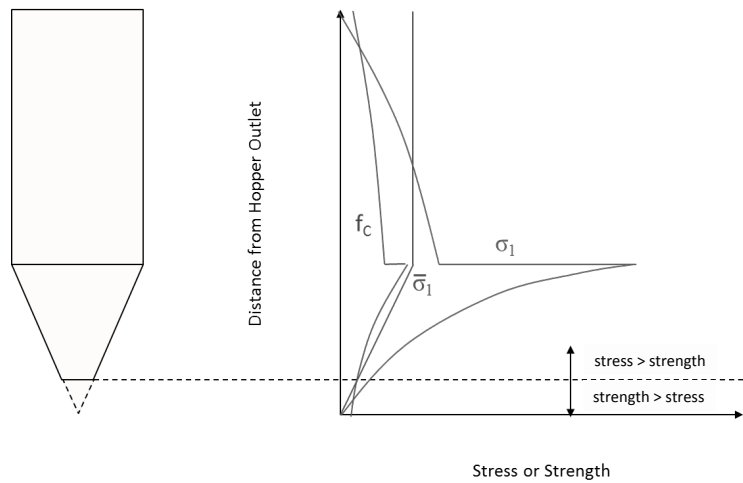


Figure 5.7. Stress and strength profiles of mass flow hopper.

Jenike postulated that near the hopper outlet the stress distribution of the bulk solid could be described by a radial stress field, *i.e.*, the stress distribution could be approximated by a straight line through the hopper vertex. The average stress was modeled as:

$$\sigma_{avg} = r\rho_b g s(\theta') \quad (5.8)$$

where r is the radial coordinate with the origin located at the vertex of the hopper, σ_{avg} is the average stress, and $s(\theta')$ is called the stress function. (The stress function is discussed much later in Chapter 7. It is not for the faint of heart!)

Jenike [1961] developed solutions to the stress function and presented them in doodle form (*i.e.*, chart form – remember that Jenike did not have computers as we have now. We really should admire what he was able to accomplish with a compass, slide rule, straight edge, and a set of trigonometric tables!).

The major principal stress is related to the average stress by

$$\sigma_1 = \sigma_{avg} (1 + \sin \delta) \quad (5.9)$$

At the hopper outlet,

$$\sigma_1 = \frac{B\rho_b g s(\theta')(1 + \sin \delta)}{2 \sin \theta'} \quad (5.10)$$

Jenike [1961] defined the ratio of the major principal stress to the arch support stress as the flow factor ff , that is,

$$ff = \frac{\sigma_1}{\bar{\sigma}} \quad (5.11)$$

Hence, the flow factor is given by

$$ff = \frac{H(\theta')s(\theta')(1 + \sin \delta)}{2 \sin \theta'} \quad (5.12)$$

The flow factor is a function of the hopper angle θ' , angle of wall friction ϕ' , and the effective angle of friction δ . The latter depends on the major principal stress σ_1 at the hopper outlet. The angle of wall friction depends on the stress normal to the hopper wall σ' , which is *not* equal to σ_1 .

Charts that provide flow factors for conical and planar flow hoppers based on Jenike's solutions to the stress function [Jenike, Bulletin 123 (1964)] are given in Figures 5.8 through 5.15.

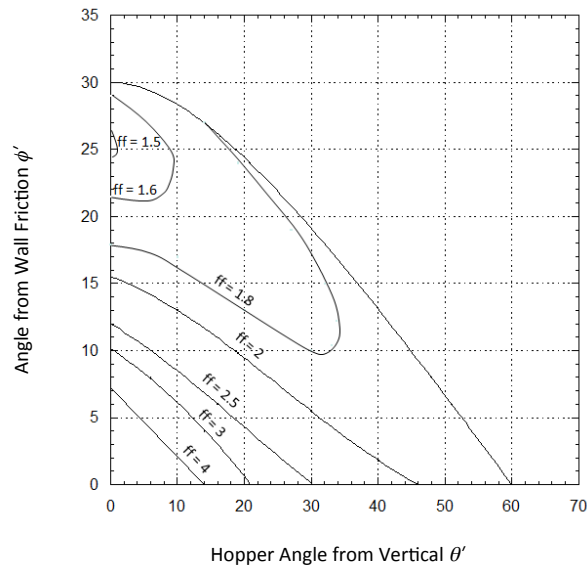


Figure 5.8. Flow factors for conical hoppers, $\delta = 30^\circ$.

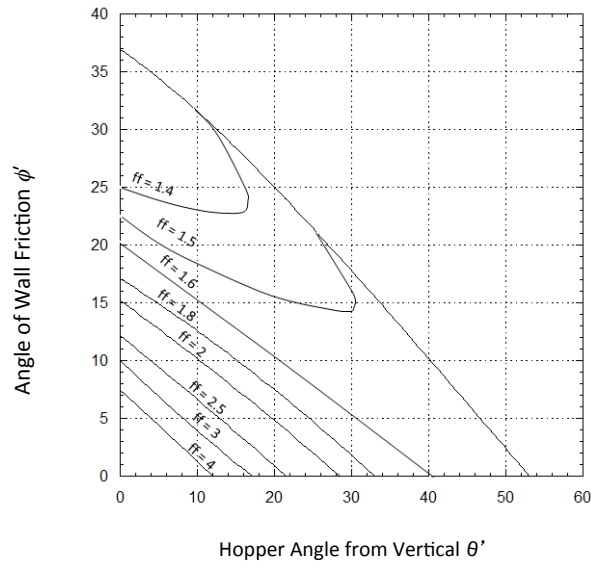


Figure 5.9. Flow factors for conical hoppers, $\delta = 40^\circ$.

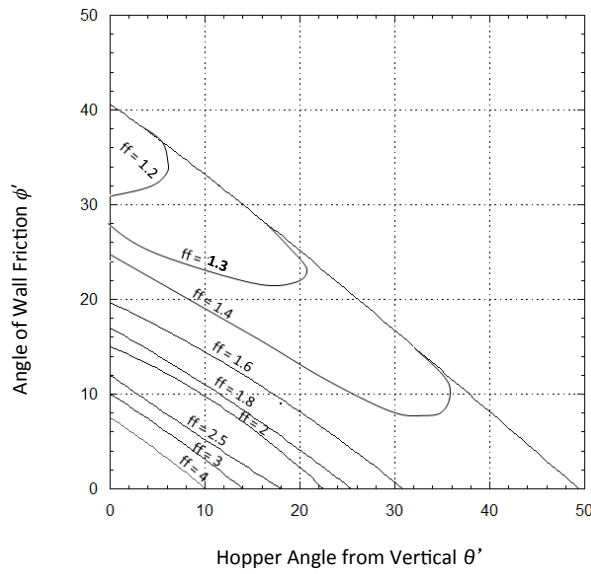


Figure 5.10. Flow factors for conical hoppers, $\delta = 50^\circ$

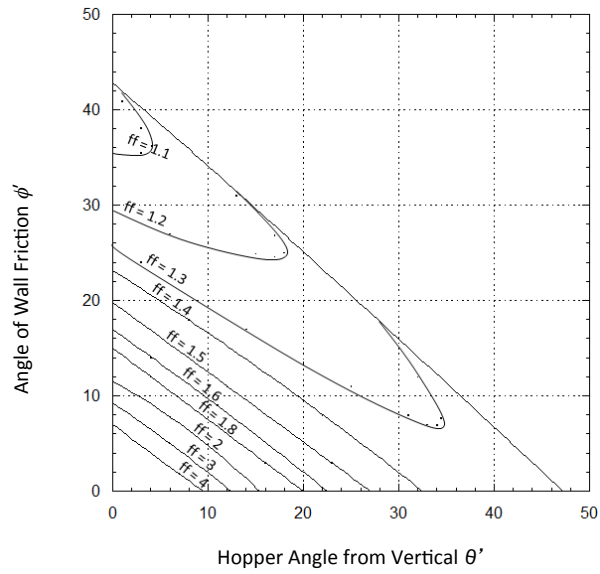


Figure 5.11. Flow factors for conical hoppers, $\delta = 60^\circ$.

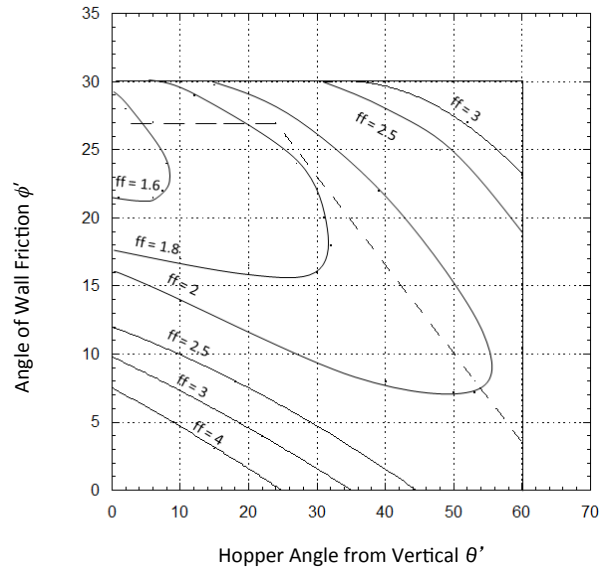


Figure 5.12. Flow factors for planar flow hoppers with slotted outlets, $\delta = 30^\circ$.

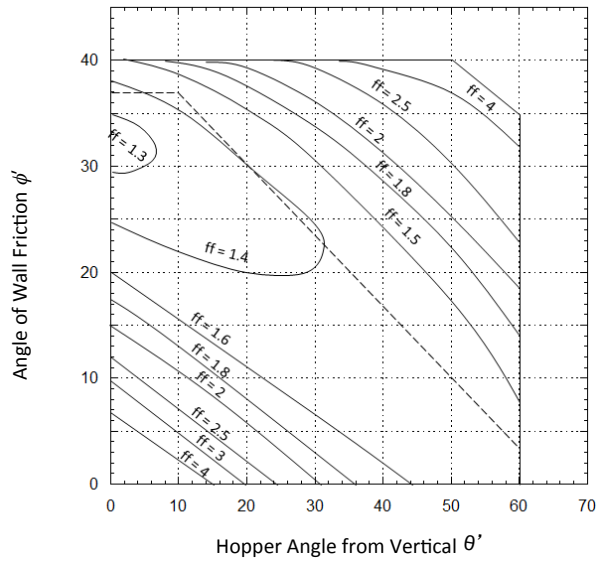


Figure 5.13. Flow factors for planar flow hoppers with slotted outlets, $\delta = 40^\circ$.

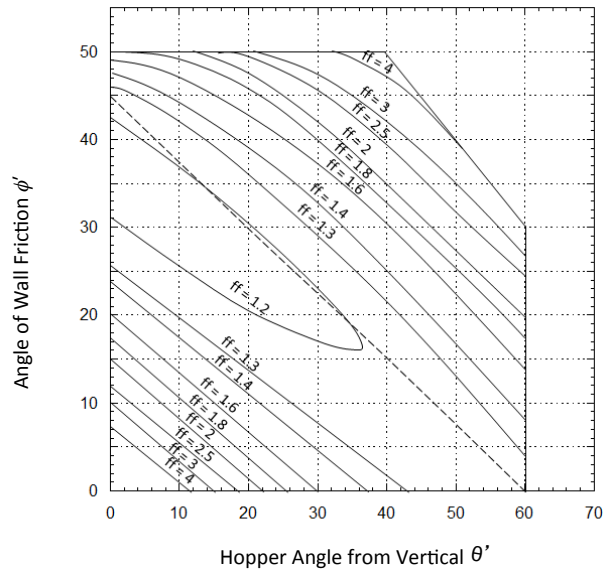


Figure 5.14. Flow factors for planar flow hoppers with slotted outlets, $\delta = 50^\circ$.

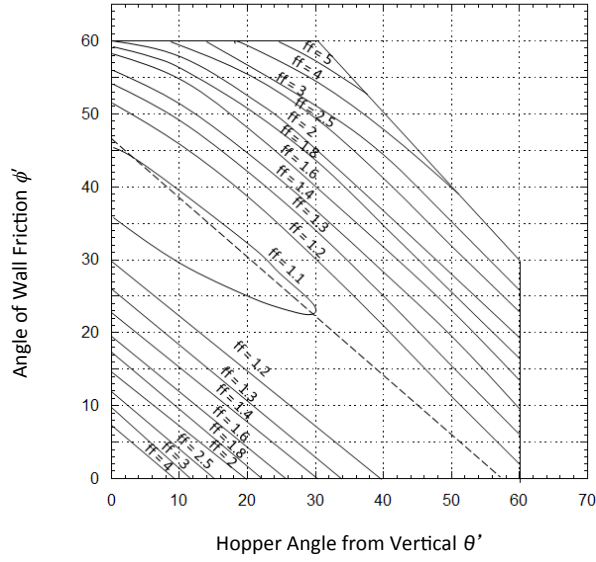


Figure 5.15. Flow factors for planar flow hoppers with slotted outlets, $\delta = 60^\circ$.

Explicit expressions for the flow factor from an analytical form of the stress function were derived by Arnold and McLean [*Powder Techn.*, 13, 255 (1976); *Powder Techn.*, 72, 121 (1992)]. These expressions are as follows:

$$ff = \frac{Y(1 + \sin \delta)H(\theta')}{2(X - 1)(\sin \theta')} \quad (5.13)$$

where

$$X = \frac{2^i \sin \delta}{1 - \sin \delta} \left[\frac{\sin(2\beta + \theta')}{\sin \theta'} + 1 \right] \quad (5.14)$$

$$Y = \frac{[2(1 - \cos(\beta + \theta'))]^i \sin \theta' (\beta + \theta')^{1-i} + \sin \beta \sin^{1+i}(\beta + \theta')}{(1 - \sin \delta) \sin^{2+i}(\beta + \theta')} \quad (5.15)$$

and

$$H(\theta') = \left(\frac{130^\circ + \theta'}{65} \right)^i \left(\frac{200^\circ + \theta'}{200^\circ} \right)^{1-i} \quad (5.16)$$

The value of i in Equations 5.14 - 5.16 is equal to 1 for circular outlets and 0 for slotted outlets. These equations have more Greek letters than an Athens post office, but once they have been entered into Excel or Matlab, calculating a flow factor is just a matter of plugging in values for δ , ϕ' , and θ' .

Superimposing the material's flow function and flow factor on the same graph allows the cohesive strength and arch stress to be compared. The flow factor is constructed by drawing a line having a slope equal to $1/ff$ through the origin. (Recall that ff is the ratio of the major principal stress to the arch stress. The slope is therefore the reciprocal.)

The relationship between the effective angle of friction δ and the major principal stress σ_1 is provided by the effective yield locus. In a converging hopper, the stresses in the bulk solid are represented by a Mohr's circle that is tangent to the material's effective yield locus. The intersections of the Mohr's circle and the horizontal axis give the principal stresses. In mass flow, the material is also slipping along the hopper wall, and therefore, the wall stress σ' is represented by the wall yield locus. The shear and normal stresses at the wall are therefore located at the larger value of the intersections of the wall yield locus and the Mohr's circle. The relationship between σ_1 , δ , σ' , and ϕ' is illustrated in Figure 5.16.

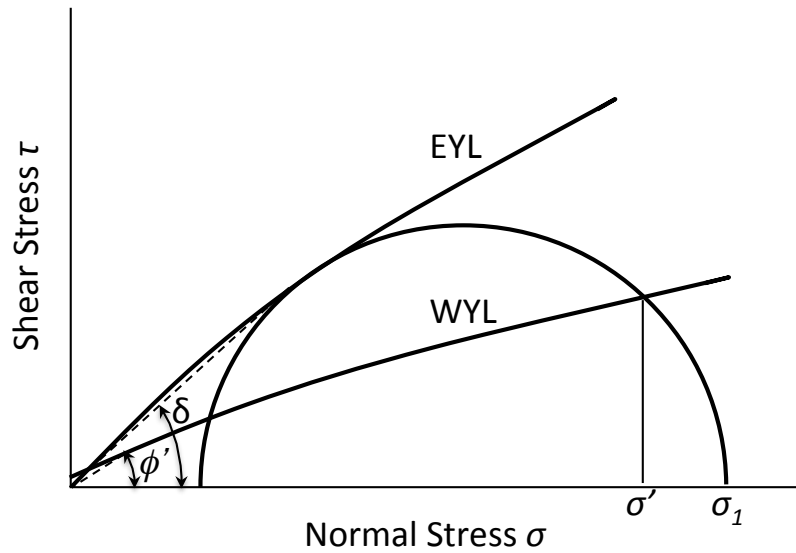


Figure 5.16. Construction of effective yield locus and wall yield locus.

If the wall yield locus is linear, which is often true at low stresses, it can be described by

$$\tau' = a\sigma' + b \quad (5.17)$$

where τ' and σ' are the shear and normal stresses at the wall surface, respectively and a and b are empirical constants determined from regression. The normal stress can then be calculated from

$$\sigma' = \frac{-\beta + \sqrt{\beta^2 - 4\alpha\gamma}}{2\alpha} \quad (5.18)$$

where

$$\alpha = a^2 + 1 \quad (5.19)$$

$$\beta = 2(ab - \sigma_{avg}) \quad (5.20)$$

and

$$\gamma = b^2 + \sigma_{avg}^2 - R^2 \quad (5.21)$$

with

$$\sigma_2 = \sigma_1 \frac{1 - \sin \delta}{1 + \sin \delta} \quad (5.22)$$

$$\sigma_{avg} = \frac{\sigma_1 + \sigma_2}{2} \quad (5.23)$$

and

$$R = \frac{\sigma_1 - \sigma_2}{2} \quad (5.24)$$

The wall friction angle is then calculated from

$$\phi' = \tan^{-1} \left(\frac{\tau'}{\sigma'} \right) \quad (5.25)$$

where the shear stress at the wall τ' is calculated from Equation 5.17.

To determine the size of the outlet required to prevent arching, the flow function and flow factor are compared. The flow factor is dependent on the material's effective angle of friction δ and its angle of wall friction ϕ' , as well as the hopper angle and geometry. The angle of wall friction is a function of the stress normal to the hopper wall σ' . Hence, unless the angle of wall friction and effective angle of friction are constant, calculation of the critical outlet diameter or width is iterative. The procedure is as follows:

1. An estimate of the flow factor ff is made. Because ff is typically in the range of 1.1 to 1.5, a value of 1.3 is a good starting point.
2. The flow factor and flow function are plotted together. As shown in Figure 5.17, there are three possibilities:
 - a. There is no intersection, and the flow function lies below the flow factor. A cohesive arch cannot develop. Instead, B is selected based on other considerations such as discharge rate requirements, choice of feeder, or prevention of particle interlocking. The hopper angle required for mass flow requires the major consolidation stress σ_1 at the outlet to be known. The major principal stress σ_1 is determined from Equation 5.26:

$$\sigma_1 = ff \frac{\rho_b g B}{H(\theta')} \quad (5.26)$$

- b. The flow factor and flow function intersect. This allows determination of the major principal stress at the outlet σ_1 to be calculated from the intersection.
 - c. There is no intersection and the flow function lies above the flow factor. Gravity flow will no longer be possible in a hopper with converging walls. Consideration should be given to using a standpipe or changing the flow properties of the material, such as increasing its particle size, reducing its moisture content, or using a flow aid.
3. If the flow factor and flow function intersect, the effective angle of friction is determined from a plot of δ against σ_1 , and the effective yield locus is drawn by drawing a straight line through the origin at an angle equal to δ . A Mohr's circle is drawn through σ_1 that is tangent to the effective yield locus. The value of ϕ' is then found from the intersection of the Mohr's circle and the wall yield locus, as shown in Figure 5.16.

4. The hopper angle is selected, one that ensures mass flow, by using the appropriate charts (Figure 5.1 or Figure 5.2) or equations (Equation 5.1 or 5.3). Note that if a conical hopper is to be specified, a safety factor of *ca.* 3° should be used with respect to the theoretical mass flow boundary.
5. The flow factor ff is determined from the appropriate chart given by Figures 5.8 through 5.15 or Equation 5.13.
6. The steps are repeated until convergence is reached.
7. The minimum outlet dimension B_{min} is then calculated using Equation 5.27:

$$B_{min} = \frac{H(\theta')\sigma_{crit}}{\rho_b g} \quad (5.27)$$

where σ_{crit} , the critical stress, is the value of the unconfined yield strength where the flow factor and flow function intersect. A flow chart that describes the design procedure is shown in Figure 5.18. Larger outlet diameters or widths of course can be used, and they are generally selected by considering standard feeder sizes or discharge rate requirements.

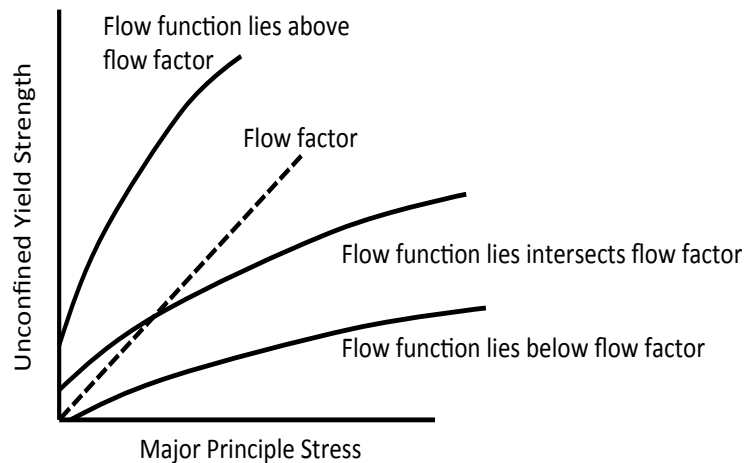


Figure 5.17. Plot showing both flow factor and flow function.

To be über conservative, the unconfined yield strength measured at the lowest stress used to obtain the flow function can be used. If this value lies far to the right of the intersection of the flow factor and flow function, the

hopper outlet dimension will be much larger than necessary, but one will be confident in the design.

A similar procedure is followed to determine recommended mass flow hopper angles for a given hopper outlet dimension, and a flow chart is shown in Figure 5.19. Hopper angles steeper than those recommended can be used.

In the absence of wall friction test results, the following empirical equation can be used to calculate the flow factor¹⁰:

$$ff = \left[1.118 + \frac{0.285}{(\tan \delta)^{1.59}} \right]^i \left[1.125 + \frac{0.176}{(\tan \delta)^{2.90}} \right]^{1-i} \quad (5.28)$$

where $i = 1$ for round outlets and $i = 0$ for slotted outlets. Equation 5.28 provides design values for ff as a function of the effective angle of friction and is based on a plot by Jerry Johanson (Kulwiec, Materials Handling Handbook, John Wiley and Sons, Hoboken, NJ, 1985). Equation 5.28 is plotted in Figure 5.20. The flow factor is approximately the same value that would be calculated for wall friction angles between 15 and 25 degrees and hopper angles in the neighborhood of the mass flow boundary. This flow factor is often referred to as the limiting or critical flow factor. If a powder has exceptionally low wall friction, the rigorous method for determining B_{min} should be followed. See Figure 5.21 for a flow chart that shows the procedure for determining critical outlet dimensions without wall friction test results. For design purposes, $H(\theta')$ can be set equal to 2.3 or 1.1 for round and slotted outlets, respectively.

To prevent mechanical interlocking, the following rules of thumb are used: for a conical hopper, the outlet diameter should be at least 6-8 times the size

¹⁰ Johanson used flow factors provided in Jenike's bulletins that were based on Jenike's hand calculations. A relation equation based on TUNRA's analytical solution to Jenike's stream function, which gives approximately the same result, is:

$$ff = \left[1.081 + \frac{0.269}{(\tan \delta)^{2.06}} \right]^i + \left[0.998 + \frac{0.353}{(\tan \delta)^{2.57}} \right]^{1-i}$$

of the largest particle that will be handled; for hoppers with slotted outlets, the outlet width should be at least 3-4 times the largest particle size.

If a bulk solid is to be stored at rest in a bin, the flow function and wall yield locus must be based on time tests. The intersection of the time flow function and flow factor is used to determine the critical stress and hence the minimum outlet size.

Solids discharge rates

While an outlet diameter greater than the minimum will prevent cohesive arching, it may not necessarily be large enough to allow the desired discharge rate. The steady-state discharge rate of a coarse powder from a hopper can be determined from a force balance.

Consider a hopper with the geometry shown in Figure 5.22. If only inertial and gravitational forces are included, a force balance on a bulk solid in a converging hopper yields

$$a = -g \quad (5.29)$$

where a is the acceleration of the solids. Defining time and spatial coordinates t and z , respectively, and employing some calculus gives

$$a = \frac{dv}{dt} = \frac{dz}{dt} \frac{dv}{dz} = v \frac{dv}{dz} \quad (5.30)$$

Equation 5.29 can then be rewritten as

$$v \frac{dv}{dz} = -g \quad (5.31)$$

From continuity (assuming a constant bulk density),

$$\frac{d}{dz}(Av) = v \frac{dA}{dz} + A \frac{dv}{dz} = 0 \quad (5.32)$$

and therefore,

$$\frac{dv}{dz} = -\frac{v}{A} \frac{dA}{dz} \quad (5.33)$$

Substitution of Equation 5.33 into Equation 5.31 gives

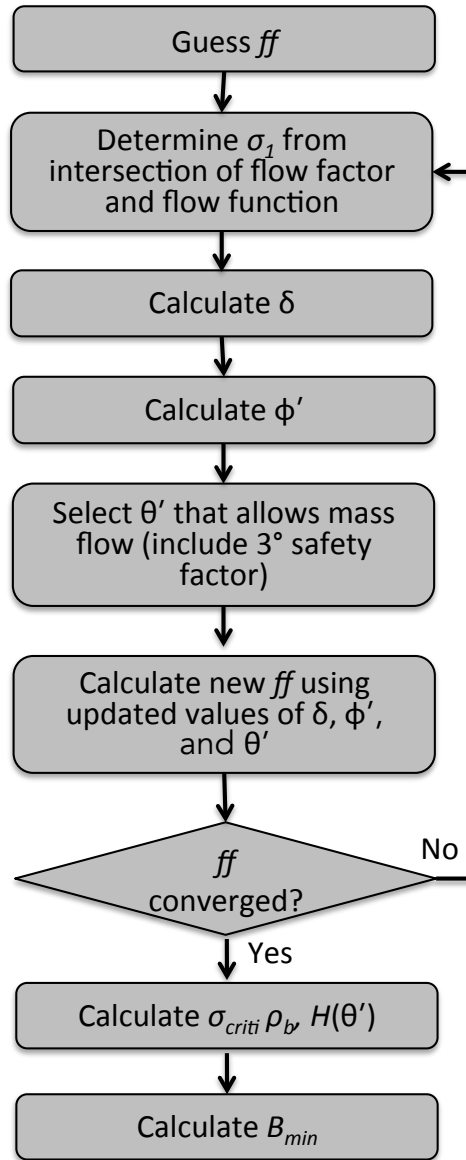


Figure 5.18. Flowchart for determining critical hopper outlet size and mass flow hopper angle.

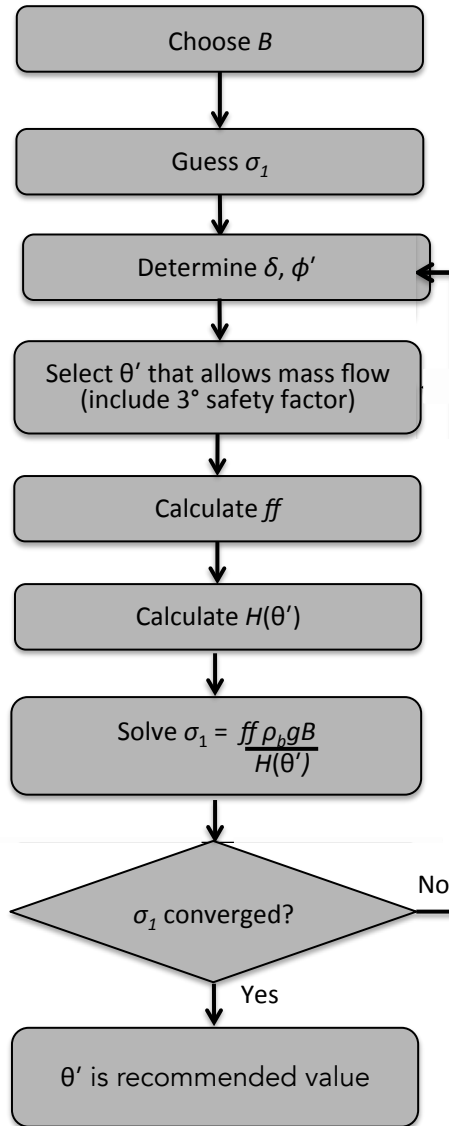


Figure 5.19. Flowchart for determining recommended mass flow hopper angle for a specified outlet dimension.

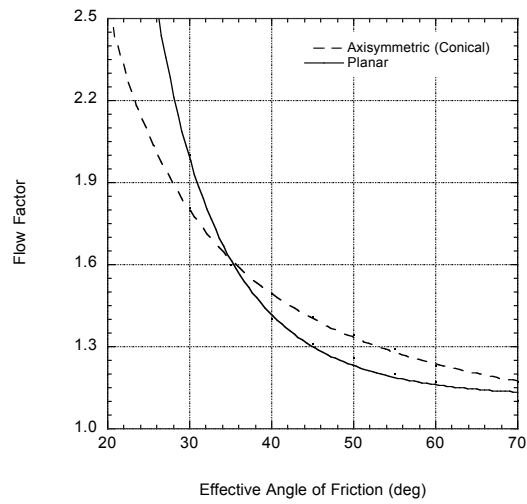


Figure 5.20. Flow factor vs. effective angle of friction.

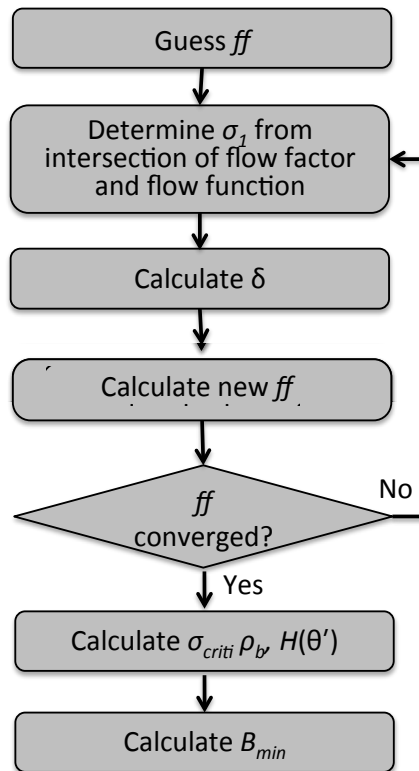


Figure 5.21. Flow chart for determining critical arching dimensions sans wall friction test results.

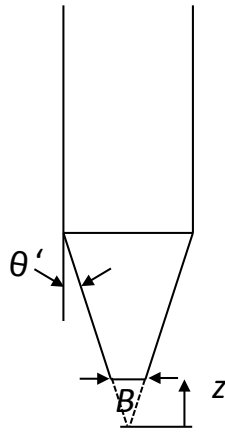


Figure 5.22. Hopper geometry.

$$\frac{v^2}{A} \frac{dA}{dz} = g \quad (5.34)$$

For a conical hopper with a circular outlet,

$$A = \pi(z \tan \theta')^2 \quad (5.35)$$

$$\frac{dA}{dz} = 2\pi z \tan \theta' \quad (5.36)$$

$$A_o = \frac{\pi B^2}{4} \quad (5.37)$$

$$\frac{1}{A_o} \frac{dA}{dz} \Big|_o = \frac{4 \tan \theta'}{B} \quad (5.38)$$

where the subscript o denotes the hopper outlet. Then

$$\frac{4v_o^2 \tan \theta'}{B} = g \quad (5.39)$$

and solving for v_o gives

$$v_o = \sqrt{\frac{Bg}{4 \tan \theta'}} \quad (5.40)$$

The mass discharge rate \dot{m}_s is equal to the product of the velocity, bulk density, and cross-sectional area of the outlet:

$$\dot{m}_s = \rho_{bo} \frac{\pi B^2}{4} \sqrt{\frac{Bg}{4 \tan \theta'}} \quad (5.41)$$

For hoppers with slotted outlets having an outlet width equal to B , a similar analysis gives

$$v_o = \sqrt{\frac{Bg}{2 \tan \theta'}} \quad (5.42)$$

and therefore in general,

$$v_o = \sqrt{\frac{Bg}{2(m+1) \tan \theta'}} \quad (5.43)$$

and

$$\dot{m}_s = \rho_{bo} A_o \sqrt{\frac{Bg}{2(m+1) \tan \theta'}} \quad (5.44)$$

where B is the diameter of a round outlet or the width of a slotted outlet, and m is equal to 1 for a circular opening and 0 for a slotted outlet.

Equations 5.43 and 5.44 do not account for the cohesive strength of the bulk solid. Jerry Johanson (*Trans. Soc. Mining Engr.*, March 1965) included cohesive strength in his force balance:

$$-\frac{a}{g} = 1 - \frac{(m+1)f_c}{\rho_b g B} \quad (5.45)$$

and

$$\frac{2(m+1) \tan \theta'}{Bg} v_o^2 = 1 - \frac{(m+1)f_c}{\rho_b g B} \quad (5.46)$$

which he elegantly recast as

$$\frac{2(m+1) \tan \theta'}{B} v_o^2 = g \left(1 - \frac{ff}{ff_a} \right) \quad (5.47)$$

where ff is the flow factor (the ratio of the major principal stress (σ_1) to the stress on the abutments of an arch) and ff_a is the actual flow function defined by

$$ff_a = \frac{\sigma_{1o}}{f_c} \quad (5.48)$$

where the solids stress of the outlet σ_{1o} is calculated from

$$\sigma_{1o} = ff \frac{\rho_{bo} g B}{m+1} \quad (5.49)$$

Following the same steps as before yields

$$v_o = \sqrt{\frac{Bg}{2(m+1) \tan \theta'} \left(1 - \frac{ff}{ff_a}\right)} \quad (5.50)$$

and

$$\dot{m}_s = \rho_{bo} A_o \sqrt{\frac{Bg}{2(m+1) \tan \theta'} \left(1 - \frac{ff}{ff_a}\right)} \quad (5.51)$$

Equation 5.51 is called the Johanson equation. The Johanson equation can be used to determine the size of a hopper outlet required to provide the desired discharge rate of a coarse, cohesive bulk solid¹¹.

Johanson assumed that the angle of the slope of the failing arch was equal to 45°. In his Bulletin 108, Jenike noted that its angle is equal to $\beta + \theta'$, where

¹¹ Many investigators like to use the Beverloo equation to calculate solids discharge rates from hoppers with round outlets:

$$\dot{m}_s = Cg^{\frac{1}{2}}(B - kd_p)^{\frac{5}{2}}$$

where d_p is the particle diameter and C and k are empirical parameters. Comparison of the Beverloo and Johanson equations suggests that the parameter C is related to the slope of the hopper walls or the flow channel and k is related to the powder's cohesive strength, which is in general inversely proportional to the particle size. Beverloo and Johanson both found that for conical hoppers, the solids discharge rate was roughly proportional to the diameter to the 5/2 power. Beverloo's relation is purely empirical. Johanson's was based on fundamentals.

$$\beta = \frac{1}{2} \left[\phi' + \sin^{-1} \left(\frac{\sin \phi'}{\sin \delta} \right) \right] \quad (5.52)$$

and ϕ' is the wall friction angle. Hence,

$$\frac{ff}{ff_a} = \frac{2(m+1) \cos \theta' \sin(\beta + \theta') f_c}{\rho_{bo} g B} \quad (5.53)$$

In addition, Jenike modified Equation 5.49 to account for the non-uniformity of the arch:

$$\sigma_{1o} = ff \frac{\rho_{bo} g B}{H(\theta')} \quad (5.54)$$

The maximum flow rate of a fine powder can be several orders of magnitude lower than that of coarser materials. Two-phase flow effects are significant due to the movement of interstitial gas as the powder compresses and expands during flow. Figure 5.23 illustrates solids and gas pressure profiles in bins for coarse (high permeability) and fine (low permeability) powders.

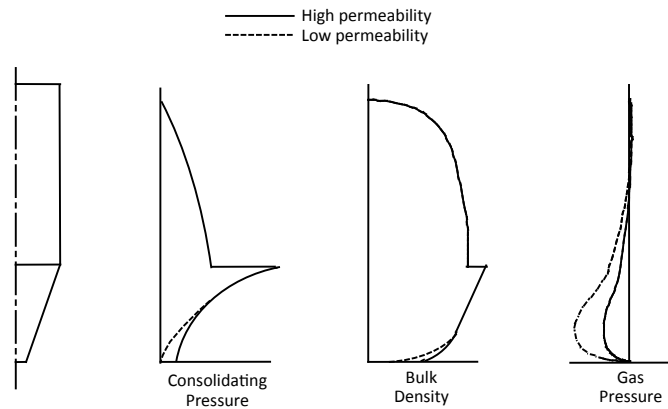


Figure 5.23. Consolidating pressure, bulk density, and gas pressure profiles for coarse (high permeability) and fine (low permeability) powders.

For fine powders, gas-phase effects cannot be neglected, and a pressure gradient term should be included in the force balance:

$$\frac{2(m+1)\tan\theta'}{Bg}v_o^2 = 1 - \frac{ff}{ff_a} + \frac{1}{\rho_{bo}g} \frac{dP}{dz} \Big|_o \quad (5.55)$$

Flow of gas through a bed of material is described by Darcy's Law:

$$u = -\frac{K}{\rho_b g} \frac{dP}{dz} \quad (5.56)$$

where u is the gas slip velocity, P is the interstitial gas pressure and K is the permeability. Applying continuity to the gas phase, Gu *et al.* [*Powder Techn.*, 72, 121 (1992)] derived a relationship between the air and solids flow rates that when combined with Darcy's law gives:

$$u = v_o \rho_{bo} \left(\frac{1}{\rho_{bmp}} - \frac{1}{\rho_{bo}} \right) \quad (5.57)$$

where the subscript mp denotes the location where the interstitial gas pressure is at a minimum and the pressure gradient is zero. The pressure gradient is therefore related to the solids velocity by:

$$\frac{dP}{dz} = \frac{v_o \rho_{bo}^2 g}{K_o} \left(\frac{1}{\rho_{bmp}} - \frac{1}{\rho_{bo}} \right) \quad (5.58)$$

Substitution of Equation 5.58 into Equation 5.57 yields the following quadratic:

$$\left[\frac{2(m+1)\tan\theta'}{Bg} \right] v_o^2 + \left[\frac{1}{K_o} \left(1 - \frac{\rho_{bo}}{\rho_{bmp}} \right) \right] v_o + \frac{ff}{ff_a} - 1 = 0 \quad (5.59)$$

from which the solids discharge rate can be calculated from

$$\dot{m}_s = \rho_{bo} A_o v_o \quad (5.60)$$

The solids stress where the gas pressure is at a minimum is difficult to calculate. Kerry Johanson, ["Powder Flow Properties", Chapter 13, *Encapsulated and Powdered Foods*, Onwulata, C., ed., CRC Press, Boca Raton, FL, 2005.] noted that it is approximately equal to the maximum solids stress in the cylinder section, which can be calculated from the Janssen equation:

$$\sigma_1 = \frac{\rho_b g R_H}{k \tan \phi'} \left[1 - \exp\left(\frac{-k(\tan \phi')h}{R_H}\right) \right] \quad (5.61)$$

If the level of solids in the cylinder section is low, the maximum solids stress can be estimated from

$$\sigma_1 = \frac{\rho_b g D}{(m+1) \tan \theta'} \quad (5.62)$$

where D is the diameter or diagonal of the cylinder. The solids stress at the outlet is determined from

$$\sigma_{1o} = \frac{\int \left(\rho_{bo} g + \frac{dP}{dz} \right) B}{H(\theta')} \quad (5.63)$$

The solids velocity is calculated by first estimating the solids stress at the outlet and then using that value to calculate the bulk density, permeability, and unconfined yield strength at the outlet. The outlet solids velocity v_o is then calculated by solving Equation 5.59. Knowing the velocity allows the pressure gradient to be calculated from Equation 5.58. An updated value of the solids stress at the outlet can then be calculated from Equation 5.63. The calculations are repeated until the correct value of σ_{1o} is found. The solids mass discharge rate is the product of the velocity, cross-sectional area, and bulk density at the solids stress at the outlet.

Funnel flow outlet size to prevent arching and ratholing

For funnel flow hoppers, the outlet must be large enough to prevent both a cohesive arch and stable rathole from developing. The critical rathole diameter is calculated by first determining the maximum major principal stress, σ_1 , on the bulk solid. For hoppers with tall cylinders, the consolidating load can be estimated by the Janssen equation:

$$\sigma_1 = \frac{\rho_b g R_H}{k \tan \phi'} \left[1 - \exp\left(\frac{-k(\tan \phi')h}{R_H}\right) \right] \quad (5.64)$$

where h is the solids level in the cylinder. For short (or no) cylinders, an approximate value of the maximum solids stress is

$$\sigma_1 = 2\rho_b g R_H \quad (5.65)$$

In general, it's good to use the smaller value of σ_1 calculated from Equations 6.64 and 6.65.

Jenike [Bulletin 108 (1961)] calculated the stress on a rathole as

$$\bar{\sigma}_1 = \frac{\rho_b g D}{G(\phi_t)} \quad (5.66)$$

where D is the diameter of a round outlet or the *diagonal* of a slotted outlet and $G(\phi_t)$ is a function given in Jenike's Bulletins 108 and 123, which is plotted in Figure 5.24. The rathole will collapse provided that the flow channel stress is greater than the cohesive strength of the bulk solid that makes up the rathole. The critical rathole diameter D_F can therefore be calculated as:

$$D_F = \frac{G(\phi_t) f_C}{\rho_b g} \quad (5.67)$$

where f_C is the cohesive strength of the bulk solid at the consolidation pressure given by the Janssen equation.

Courtesy of McGlinche, Bulk Solids Characterization, Blackwell Publishing Co., Carlton, Victoria Australia, 2005), a convenient expression for $G(\phi_t)$ is

$$G(\phi_t) = 4.3 \tan \phi_t \quad (5.68)$$

A conical funnel flow hopper with an outlet diameter smaller than D_F or a planar funnel flow hopper with an outlet whose diagonal is less than D_F will not empty completely. This is illustrated in Figure 5.25. Because the major consolidation stress is higher in the lower part of the bin, the cohesive strength of the bulk solid will be correspondingly higher. As material discharges in a funnel flow pattern, ratholes that form in the upper part of the vessel may continually collapse, provided that the stress on the stagnant material is greater than its cohesive strength. However, if the size of the outlet is smaller than the critical rathole diameter, a level will be reached where the ratholes will no longer fail.

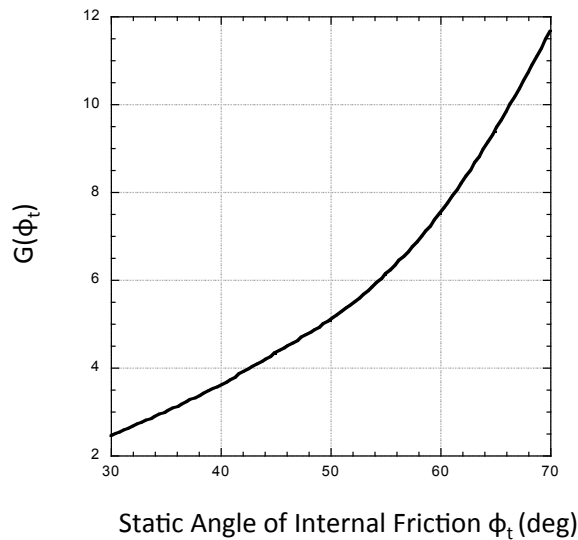


Figure 5.24. Function $G(\phi_t)$.

If a hopper with a square or round outlet is designed with an opening large enough to prevent development of a stable rathole, cohesive arching is unlikely to occur. When funnel flow hoppers with elongated outlets are designed, prevention of arching must also be considered, *i.e.*, the width of the slotted outlet must be large enough to prevent a cohesive arch from developing. The same procedure that is used to determine the minimum outlet width to prevent arching in a planar-flow mass flow hopper is followed, except that a flow factor of 1.7 is used. (A flow factor of 1.2 is sometimes used to determine the critical arching diameter of a conical funnel flow hopper. Keep in mind that this diameter will be smaller than the critical rathole diameter.)

Comparison of Equations 5.66 (critical rathole diameter) and 5.27 (minimum arching dimension) shows that D_F can be much larger than B_{min} if cohesive powders are handled. The cohesive strength of the powder at the hopper cylinder junction is usually significantly higher than the critical stress in a mass flow hopper, and $G(\phi_t)$ is greater than $H(\theta')$. While the diameter of a conical hopper required to prevent arching might be reasonably small, the critical ratholing diameter of a hopper that handles a cohesive powder can be bigger than Donald Trump's rap sheet.

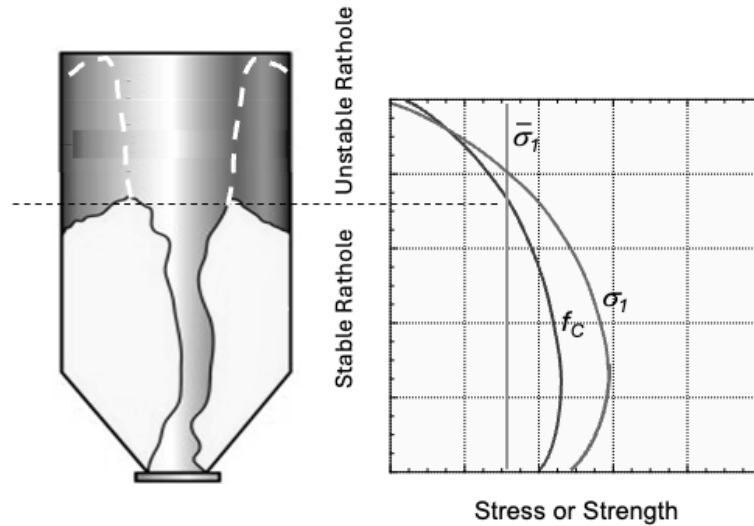


Figure 5.25. Formation of a stable rathole in a funnel flow hopper.

Expanded flow hopper dimensions

An expanded flow hopper is essentially a funnel flow hopper above a mass flow hopper. The upper diameter of the mass flow section must be larger than the critical rathole diameter D_F , while its outlet size must be larger than the critical arching dimension. An example of an expanded flow hopper is shown in Figure 5.26.

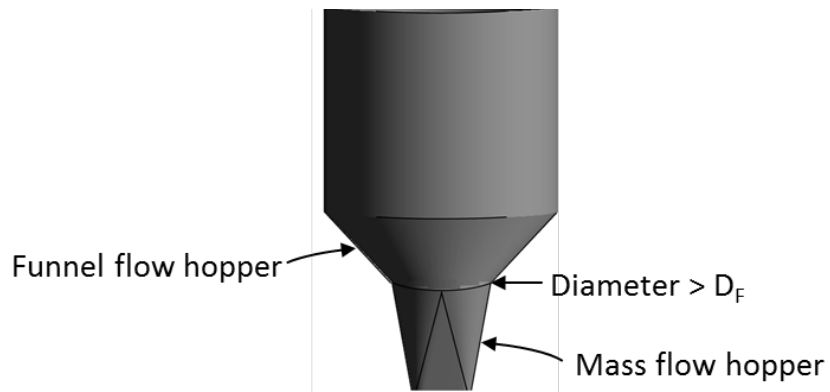


Figure 5.26. Expanded flow hopper.

Inserts

A disadvantage of conical mass flow bins is that relatively steep hopper sections are generally required, and therefore the bins may be too tall for the available space. A planar mass flow bin having flat walls and a slotted outlet can have a reasonably shallow hopper section. However, discharge from a slotted outlet cannot be modulated with a rotary valve, which is often preferred because of its low cost and small footprint.

When properly designed, an insert can be used to allow mass flow in a conical bin with shallow hopper walls that, without modifications, would discharge in a funnel flow pattern. Cone-in-cone and bullet designs are shown in Figure 5.27. A cone-in-cone insert is designed to allow mass flow through the inner cone and also through the annular space between the inner and outer cones. The angle of the inner cone is equal to or steeper than the hopper angle recommended for mass flow in a conical hopper, and the angle of the outer cone is equal to twice that of the inner cone. The cones form an annulus, which allows planar flow to be mimicked. The outlet diameter of the inner cone must be greater than the critical arching diameter. For cohesive materials that would otherwise arch over the outlet of the inner cone of an insert, an inverted cone or “bullet” can be placed above the inner cone.

The position and dimensions of the insert are determined by locating the vertex of the outer hopper and then extending lines with angles equal to the recommended mass flow hopper angle. Arcs constructed as shown in Figure 5.28 locate the inlet and outlet of the inner cone.

To design a cone-in-cone insert, the following inputs are required:

θ_i Inner cone hopper angle (referenced from vertical)

D_C Cylinder diameter or outer cone inlet diameter

D_{oo} Outer cone outlet diameter

From these inputs, the following dimensions and hopper angles can be calculated:

θ_o Outer cone hopper angle (referenced from vertical)

D_{ii} Inner cone inlet diameter

D_{io} Inner cone outlet diameter

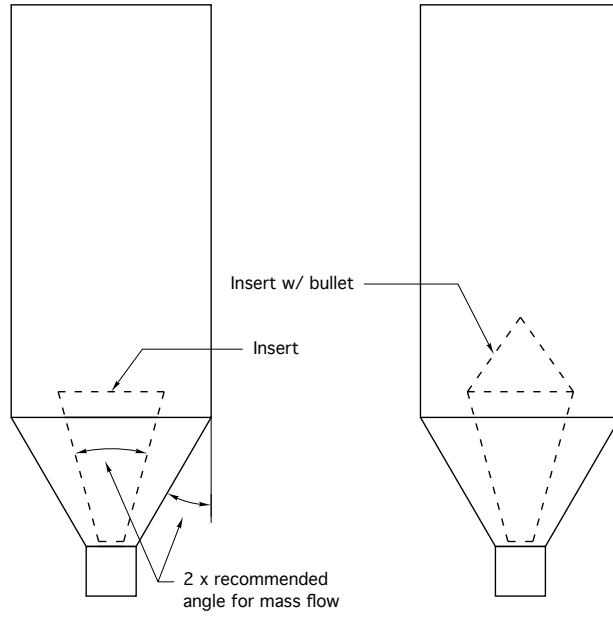


Figure 5.27. Inserts; cone-in-cone, left, and bullet, right.

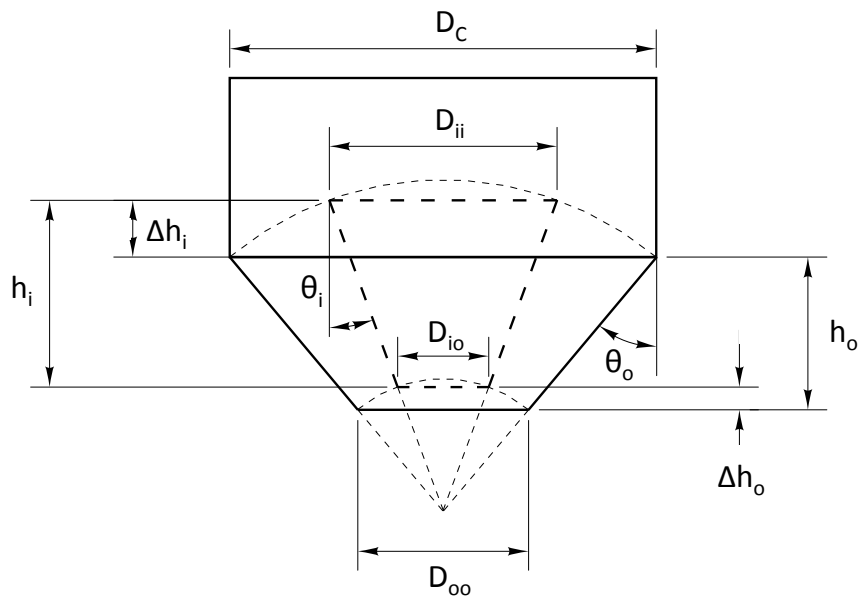


Figure 5.28. Insert geometry.

- Δh_i Distance between inner and outer cone inlets
 Δh_o Distance between inner and outer cone outlets
 h_i Height of inner cone
 h_o Height of inner cone

The hopper angle of the outer cone is twice that of the inner cone:

$$\theta_o = 2\theta_i \quad (5.69)$$

From geometry, trigonometry, and assorted other -ometries, the following dimensions and placements are derived:

$$D_{ii} = D_C \frac{\sin \theta_i}{\sin \theta_o} \quad (5.70)$$

$$\Delta h_i = \frac{D_{ii}}{2 \tan \theta_i} - \frac{D_C}{2 \tan \theta_o} \quad (5.71)$$

$$D_{io} = D_{oo} \frac{\sin \theta_i}{\sin \theta_o} \quad (5.72)$$

$$\Delta h_o = \frac{D_{io}}{2 \tan \theta_i} - \frac{D_{oo}}{2 \tan \theta_o} \quad (5.73)$$

$$h_o = \frac{D_C - D_{oo}}{2 \tan \theta_o} \quad (5.74)$$

$$h_i = \frac{D_{ii} - D_{io}}{2 \tan \theta_i} \quad (5.75)$$

To prevent bridging, the width of the annulus at the bottom of the insert should be equal or greater than the minimum width of the slotted outlet of a planar mass flow hopper. Alternatively, the slope of the walls of the insert can be steepened below this dimension as shown in Figure 5.29. This creates a lower section where the walls do not converge.

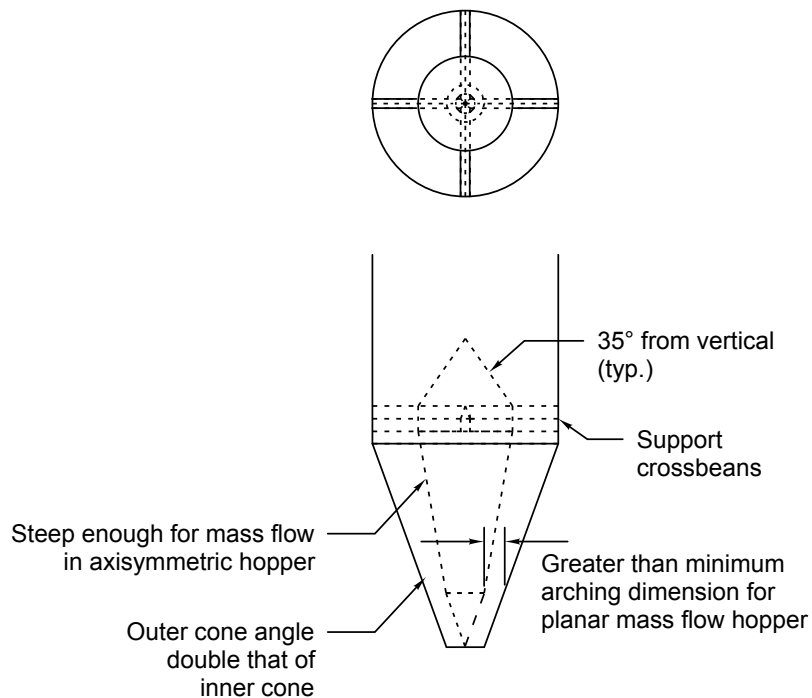


Figure 5.29. Hopper with insert and steepened walls.

In some cases, the outlet of the inner cone may be too small and will cause the powder to arch. When this is the case, the outlet diameter of the outer cone should be increased to allow the required inner cone outlet diameter. A hopper section steep enough to allow mass flow that converges to the desired outlet diameter is then added beneath the bin, as illustrated in Figure 5.30. A spool piece is installed above the lower cone to prevent high solids velocities in the center of the bin.

According to Lyn Bates, the Andrew Jenike of the United Kingdom, the walls of the outer cone can be fairly shallow provided that the angle between the inner and outer cones is less than the recommended conical mass flow hopper angle θ_C , the hopper outlet diameter is greater than the critical arching diameter B_C , and an inverted cone or bullet is in place to prevent powder from entering the inner cone. A disadvantage of any bin with a bullet insert is that its capacity will be decreased. Lyn Bates' design is illustrated in Figure 5.31.

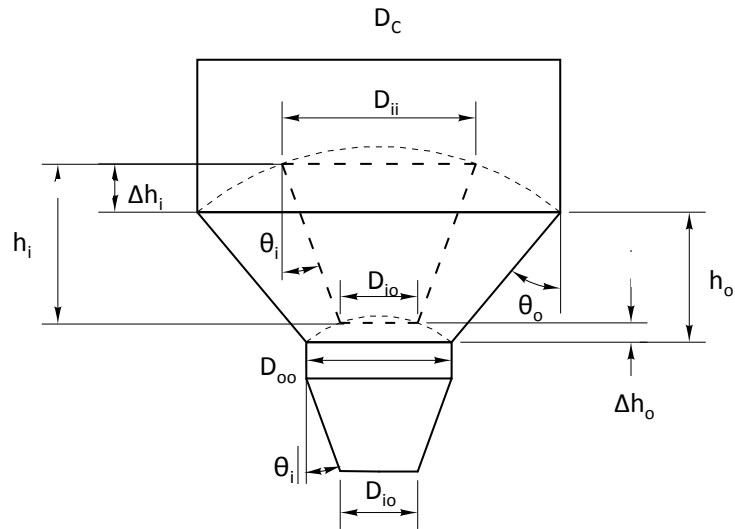


Figure 5.30. Hopper with insert and extended conical section.

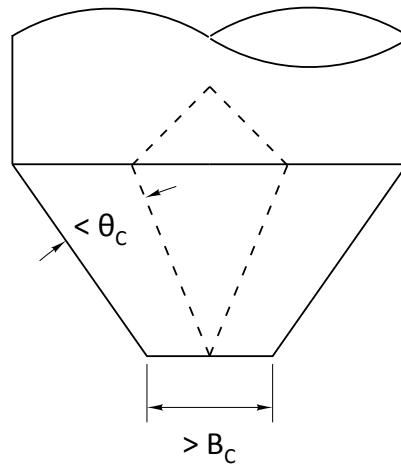


Figure 5.31. Lyn Bates' bullet insert.

While less effective than cone-in-cone inserts, inverted-cone inserts are sometimes used to improve the flow in hoppers, bins, and silos. They are frequently used to retrofit funnel flow vessels that suffer from stable ratholes. An inverted-cone insert is shown in Figure 5.32a.

The design procedure is as follows:

1. Select the slope angle of the insert θ_2 . 30° is typical; steeper slopes should be used for materials with exceptionally high wall friction.
2. Determine the critical ratio W/R from Figure 5.32b and the critical angle α from Figure 5.32c.
3. Select a location for the top of the insert (Point A in Figure 5.32a) and draw a line AF to the hopper wall with a slope equal to $90^\circ - \theta_2 - \alpha$ from horizontal.
4. Draw a line inclined at angle α from the vertex of the hopper. Points on this line represent values of the critical ratio W/R .
5. Draw a line of slope angle θ_2 from Point A . Point E (see Figure 5.32a) locates the bottom of the insert.
6. Confirm that the width of the annulus W is large enough to prevent an arch from forming. The critical arching dimension can be assumed equal to three-quarters of the critical arching diameter of a mass flow cone.
7. Check that the diameter of the hopper at the level aligned with Point A is greater than the critical rathole diameter.

Converging/diverging walls

The angle required for mass flow in hoppers with flat walls can be significantly less steep, typically $10\text{-}12^\circ$ or greater, than for conical hoppers provided that they have slotted outlets. Hoppers with slotted outlets generally cannot be fitted with simple feeders such as rotary valves. For this reason, hoppers with round or square openings are often desired.

Designs with converging and diverging walls allow hoppers with round outlets and hopper angles greater than the minimum recommended for mass flow in conical hoppers to be used. The Diamondback hopper [US Patent No. 4,958,741 (1990)] is shown in Figure 5.33. The outlet diameter must be greater than the minimum arching diameter for a conical hopper, but the slope of the end walls can be $10\text{-}20^\circ$ greater than the recommended conical mass flow hopper angle. When the length:width ratio of the outlet of a section is less than 2, the non-converging walls should diverge slightly. According to the patent, this will allow the minimum outlet dimension to be the critical arching width of a slotted outlet.

Lyn Bates recommends wedge-shaped hoppers with slotted outlets and diverging end walls for handling challenging bulk materials (see Figure

5.34). He refers to such a design as “Sigma2 Relief” as it allows the material to move sideways during flow.

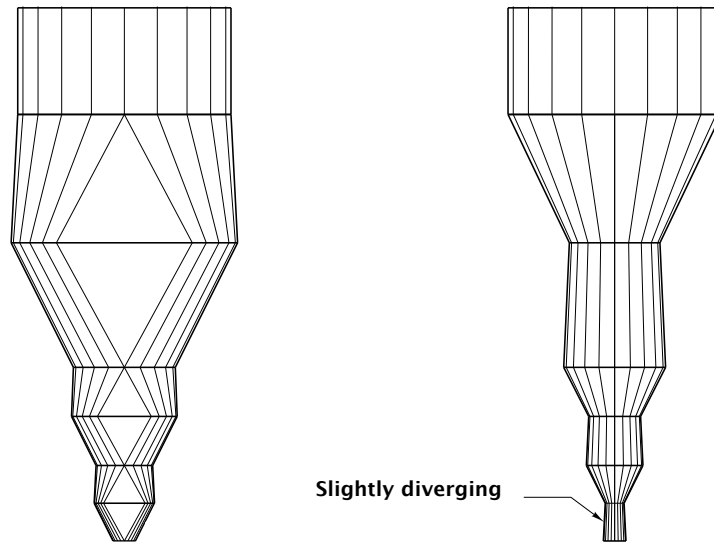


Figure 5.33. Diamondback hopper.



Figure 5.34. Lyn Bates’ Sigma2 Relief bin.

Over-pressurization

For cases in which over-pressurization is anticipated due to, for example, vibration or external forces, the critical outlet diameter or width should be

increased. To calculate the minimum arching dimension, the solids stress at the outlet is multiplied by an appropriate factor when calculating the critical arching diameter ([McLean, *Bulk Solids Handling*, 5, 1 (February 1985)]. When calculating the critical rathole diameter, the stress used to calculate the cohesive strength of the powder at the cylinder-hopper junction is multiplied by the factor. This factor is commonly called the *P-factor*.

Formulas for *P-factors* are summarized at the following site:

<https://www.powderbulksolids.com/instrumentation-control/how-interpret-solids-flow-report>.

Note that an increase in solids stress can lead to both an increase in the material's unconfined yield strength and its bulk density, which have the opposite effects on the bulk solid's likelihood of arching.

Vibration. Vibration has two effects: while it tends to break arches that obstruct flow, it also packs the solid in stagnant regions, thereby giving it greater strength. In order to allow for this packing, a *P-factor* of 1.5 should be used when calculating critical arching dimensions for use with vibrating equipment.

Vibrators are suitable for materials that are free flowing under conditions of continuous flow but cake and gain strength when stored at rest for hours or days. Hoppers for these materials should be equipped with pads for mounting external vibrators. Vibrators should be used only to initiate flow and should be turned off once flow has started. The following equation can be used to estimate *P-factor* due to vibrator use as described here:

$$P\text{-factor} = 1 + \frac{a_z}{g} \quad (5.76)$$

or

$$P\text{-factor} = 1 + \frac{a_y}{g} \quad (5.77)$$

where g is the gravitational constant and a_z and a_y are the vertical and horizontal acceleration components imposed on the solid, respectively. The component that gives the highest *P-factor* should be used.

Fine powders and wet materials tend to pack severely when vibrated; hence, vibrating equipment is generally not recommended for these materials.

Impact pressure from fall into a bin. A coarse material compacts as it is charged into a bin, under the impact of the falling particles. When the material contains fines and the impact area is close to the outlet, the impact *P-factor* should be used in the design:

$$P\text{-factor} = (1 + m) \frac{\dot{m}}{AB\rho_b} \sqrt{\frac{2h}{g}} \quad (5.78)$$

where m is equal to 1 or 0 for a round or elongated outlet, respectively, A is the impact area of the solids, B is the diameter of a round outlet or the width of a slotted outlet, and h is the drop height.

External loading. If the solid has been compacted by an external load F (such as the weight of a tractor passing over an outside stockpile), the overpressure factor at the point of application is given by

$$P\text{-factor} = \frac{(1 + m)F}{AB\rho_b g} \quad (5.79)$$

where A is the area of load application.

Liquid or gas flow loading. If the solid has been subjected during storage to fluid or gas flow such as having been imposed by an air blaster, draining of a saturated solid or the flow of air or gas during drying or chemical processing, the overpressure factor is given by

$$P\text{-factor} = 1 + \frac{1}{\rho_b g} \frac{dP}{dz} \quad (5.80)$$

where dp/dz is the (vertical) liquid or gas pressure gradient at the bin outlet and z is positive upward.

If a *P-factor* calculation yields a value less than one, a *P-factor* equal to one should be used.

The *P-factor* approach is likely very conservative in that it essentially assumes that over-pressurization affects the solids stress and not the external stress (*i.e.*, the stress on the abutment of an arch). As such, *P-factor* can be

considered a safety factor, and it is especially appropriate to use if the slope of the flow function is nearly equal to 1, in which case the value of the critical stress cannot be determined with confidence, or if the flow function is dramatically steep and a small change in solids stress can result in a significant increase in cohesive strength.

Flow channel angle

In funnel flow, flow only occurs in a central channel above the hopper outlet. The channel expands at an angle that depends on the effective angle of friction δ and the geometry (*i.e.*, axisymmetric or planar). If the flow channel is less steep than the hopper walls, the flow channel will reach the hopper walls and will flow along a thin layer that adheres to the wall. The flow behavior will be essentially mass flow on a thin stagnant layer of bulk material.

The flow channel angle θ_{fc} can be estimated using the following equation adapted from Arnold, *Bulk Solids Handling*, 5, 1 (February 1985):

$$\theta_{fc} = \left[45^\circ - 0.5 \cos^{-1} \left(\frac{1 - \sin \delta}{2 \sin \delta} \right) \right]^i \left[65^\circ - 0.5 \cos^{-1} \left(\frac{1 - \sin \delta}{\sin \delta} \right) \right]^{1-i} \quad (5.81)$$

where i is equal to 1 for round outlets and equal to 0 for slotted outlets. The flow angle is referenced from vertical. Note that for conical hoppers, the flow angle can be very steep unless the material's effective angle of friction is very small. Flow channel is plotted against the effective angle of friction in Figure 5.35.

When material is discharged from a funnel flow hopper, the solids will flow only in the central flow channel. As the flow channel empties, the ratholes will collapse and tumble into the falling channel provided that the diameter of the flow channel exceeds the critical rathole diameter D_F . The angle formed when material slides into the channel is called the drawdown angle θ_{ds} , which is referenced from horizontal. If unknown, the drawdown angle can be crudely estimated as the average of the effective angle of friction δ and the kinematic angle of internal friction ϕ . Flow channel and drawdown angles are illustrated in Figure 5.36.

The solids discharge rate equations given in the previous section can be used with funnel flow hoppers by replacing θ' with the flow channel angle.

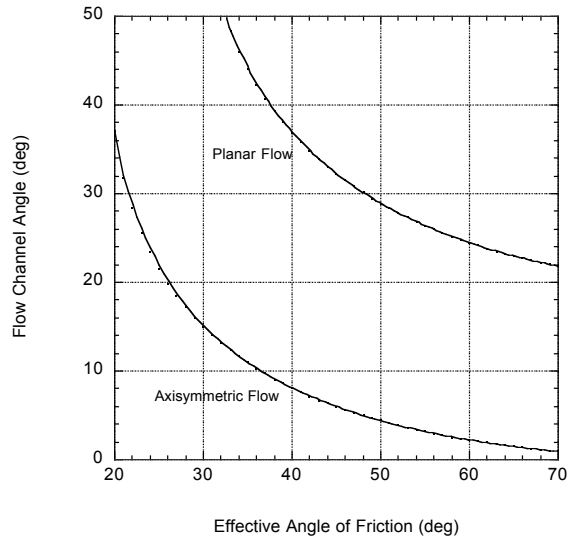


Figure 5.35. Solids flow channel angle in funnel flow hoppers.

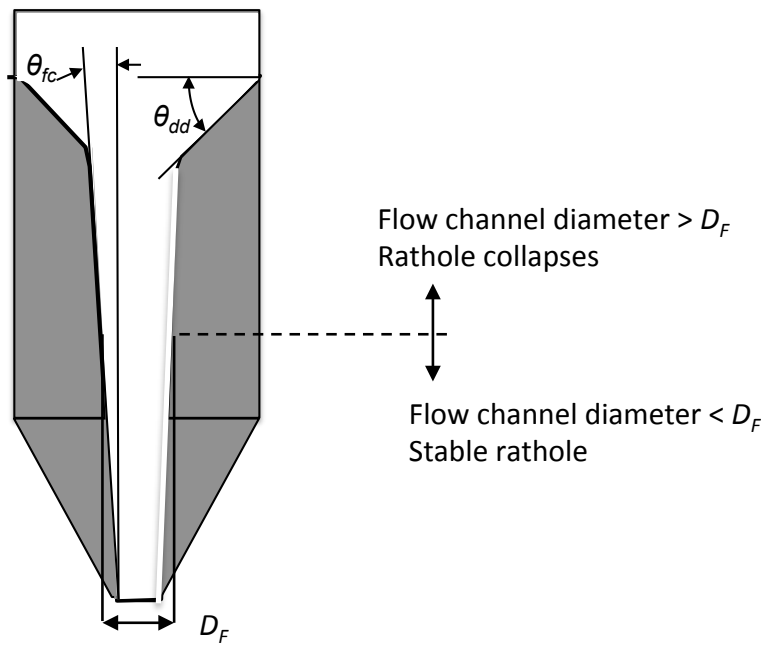


Figure 5.36. Flow channel and drawdown angles.

Capacity

A reasonable height-to-diameter ratio (H/D) of the cylinder section should be used, with ratios between about 1.5 to 4 usually being the most economical. Height may be limited because of building constraints, zoning considerations, or restrictions imposed by other structures or equipment.

The following formulas can be used to calculate the height and volume of common bin geometries shown in Figure 5.37.

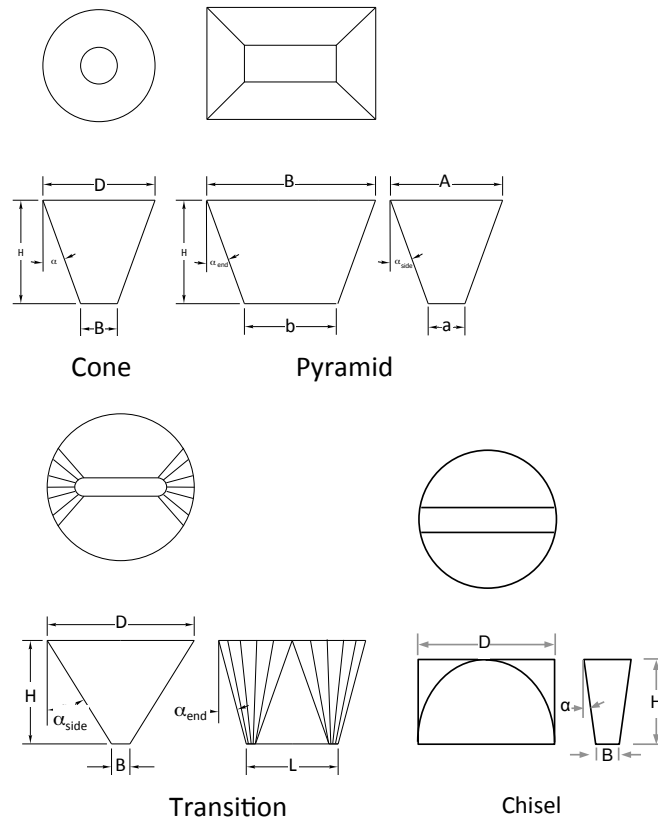


Figure 5.37. Conical, pyramidal, and transition hopper nomenclature.

Cone:

$$H = \frac{D - B}{2 \tan \alpha} \quad (5.82)$$

$$V = \frac{\pi(D^3 - B^3)}{24 \tan \alpha} \quad (5.83)$$

Pyramid:

$$H = \frac{A - a}{2 \tan \alpha_{side}} = \frac{B - b}{2 \tan \alpha_{end}} \quad (5.84)$$

$$V = \frac{H[2(AB + ab) + Ab + aB]}{6} \quad (5.85)$$

For symmetric pyramids with curved walls, the volume can be calculated by solving

$$H = \int_0^H \left[(a + 2z \tan \alpha_{side})(b + 2z \tan \alpha_{end})(\pi - 4) \left(\frac{b}{2} + \frac{B-b}{2H} z \right)^2 \right] dz \quad (5.86)$$

An analytical solution can be found, but numerical integration is straightforward.

To determine the height and volume of a wedge-shaped hopper, note that either $A = a$ or $B = b$ when using Equations 5.84 and 5.85, respectively.

Transition:

$$H = \frac{D - B}{2 \tan \alpha_{side}} = \frac{D - L}{2 \tan \alpha_{end}} \quad (5.87)$$

$$V \approx \left[\frac{\pi D^2}{12} + \frac{BL}{3} + \frac{D(B + 2L)}{12} \right] H \quad (5.88)$$

Chisel:

$$H = \frac{D - B}{2 \tan \alpha} \quad (5.89)$$

$$V \approx 0.452 \frac{HD^3}{D - B} - \frac{HDB^2}{2(D - B)} \quad (5.90)$$

Be careful how you regress the data!

Typically, a yield locus or cohesive strength test is performed three times. Unless you are fortunate enough to have a Schulze ring shear tester, determining the critical stress when calculating the critical hopper outlet arching dimension will require an extrapolation of the test data, which can be risky.

Consider the cohesive strength data shown in Figure 5.38. The data were regressed to fit the following empirical formulas:

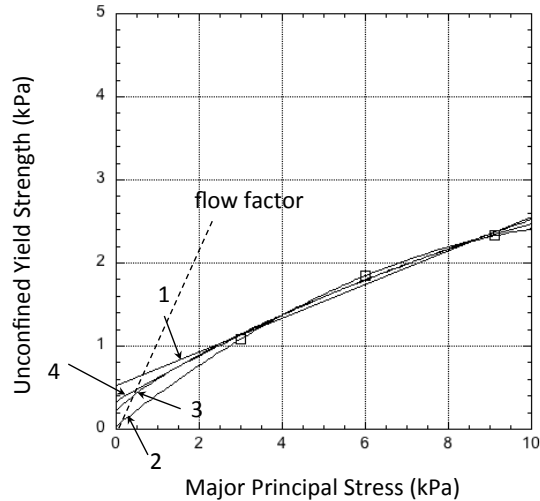
$$f_c = a + b\sigma_1 \quad (5.91)$$

$$f_c = a + b\sigma_1 + c\sigma_1^2 \quad (5.92)$$

$$\left(\frac{f_c}{a}\right)^c = \frac{\sigma_1 + b}{b} \quad (5.93)$$

where a , b , and c are empirical constants. Equation 5.93 is the Warren Spring equation, which is frequently used to fit shear cell data when curvature of the yield locus is dramatic and some investigators believe it can describe a curved flow function as well.

The flow function denoted as No. 1 in Figure 5.36 was determined by linear regression. The correlation coefficient is > 0.98 , which seems impressive but not all that surprising considering that there were three data points and two empirical constants. Inspection of the data suggests that there is curvature, as is frequently the case, so perhaps a quadratic relationship would be more appropriate. The flow function denoted as No. 2 was determined by fitting the data to a second-order polynomial. The correlation coefficient equals 1 as the quadratic passes through every data point – even less a surprise since the number of adjustable parameters (the regression constants a , b , and c) is the same as the number of data points. Note how this choice of a regression model gives a very low value of the critical stress, as determined from the intersection of the flow function and flow factor. As a consequence, the calculated minimum hopper outlet dimension to prevent arching will be correspondingly small, and considering that extrapolation of the data was required to determine the critical stress, specifying such a small outlet can be dicey.



- 1 - Linear fit: $f_c = 0.532 + 0.203\sigma_1$
- 2 - Polynomial: $f_c = 0.039 + 0.399\sigma_1 - 0.0161\sigma_1^2$
- 3 - Warren Spring: $(f_c/0.236)^{1.44} = (\sigma_1 + 0.342)/0.342$
- 4 - Polynomial with fixed intercept: $f_c = 0.340 + 0.289\sigma_1 - 0.00751\sigma_1^2$

Figure 5.38. Regression of cohesive strength data.

The flow function represented by curve No. 3 was constructed by fitting the data to the Warren Spring equation. The flow function fits the data nicely, and the calculated critical stress seems more truthful. The flow function denoted as No. 4 is a quadratic. However, this time, a linear regression was first performed using only the two data points obtained at the two lowest consolidation stresses; then, all the data were fit to a quadratic while fixing the intercept equal to the value obtained by the linear regression. This regression method is easier to execute, and it allows calculation of a critical arching dimension that is slightly less conservative than if a linear regression were used.

Software that is supplied with various automated shear cell testers sometimes includes modules for hopper design. The software should be used with caution, especially if the user is unable to choose the appropriate description of the flow function (and also the wall yield locus and compressibility). An engineer should use judgment when extrapolation of

the data is required to derive an equation for the flow function. Some useful regression formulas are given in Table 5-1.

Bin selection

When designing a bin, keep in mind that mass flow is not always necessary. Funnel flow and expanded flow bins are advantageous because they allow greater capacity if there are height restrictions. A flow chart that illustrates the bin design procedure is shown in Figure 5.39.

The engineer typically begins with a basis (*e.g.*, capacity and throughput, materials handled) and constraints (*e.g.*, available height, allowable footprint, acceptable wall materials). The volume occupied by the pile of bulk material in the cylinder that is defined by its angle of repose is roughly equal to that of the hopper section. Hence, a reasonable starting point for sizing the cylinder section is to choose a diameter or width such that a height equal to 1.5 to 4 times the diameter or width gives the desired capacity. Ratios in this range are economical, and the required height can be determined once the hopper section has been designed.

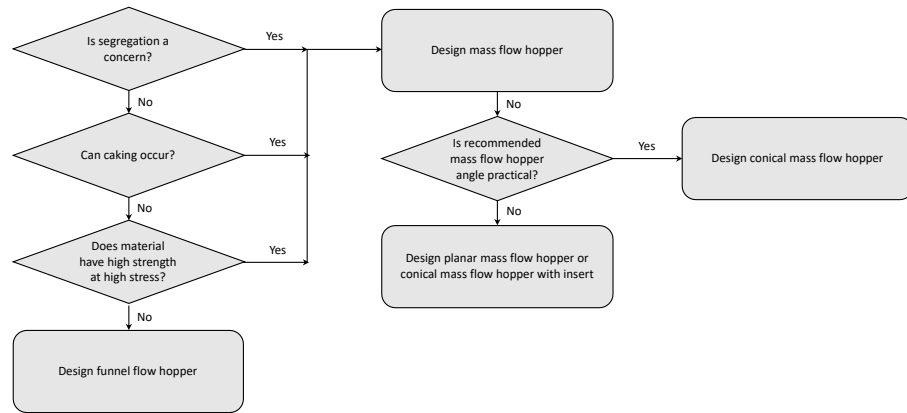


Figure 5.39. Bin design procedure.

Example bin design

Consider a powder having the flow properties shown in Figures 5.40a through 5.38d. Determine the critical outlet dimensions and recommended mass flow hopper angle that can reliably handle the powder.

Table 5-1 Least Squares Regression Formulas	
Equation	Regression Constants
$y = ax + b$	$a = \frac{n \sum_{i=1}^n x_i y_i - \sum_{i=1}^n x_i \sum_{i=1}^n y_i}{n \sum_{i=1}^n x_i^2 - \left(\sum_{i=1}^n x_i \right)^2}$ $b = \frac{\sum_{i=1}^n y_i - a \sum_{i=1}^n x_i}{n}$
$y = ax$	$a = \frac{\sum_{i=1}^n x_i y_i}{\sum_{i=1}^n x_i^2}$
$y = ax^2 + bx + c$	$\bar{x} = \frac{\sum_{i=1}^n x_i}{n} \quad \bar{y} = \frac{\sum_{i=1}^n y_i}{n} \quad (x^2)_{avg} = \frac{\sum_{i=1}^n x_i^2}{n}$ $a = \bar{y} - b\bar{x} - c[(x^2)_{avg}]^2$ $b = \frac{S_{xy} S_{x^2 x^2} - S_{x^2 y} S_{xx^2}}{S_{xx} S_{x^2 x^2} - (S_{xx^2})^2}$ $c = \frac{S_{x^2 y} S_{xx} - S_{xy} S_{xx^2}}{S_{xx} S_{x^2 x^2} - (S_{xx^2})^2}$ $S_{xx} = \sum_{i=1}^n (x_i - \bar{x})^2 \quad S_{xy} = \sum_{i=1}^n (x_i - \bar{x})(y_i - \bar{y})$ $S_{x^2 y} = \sum_{i=1}^n [(x_i^2 - (x^2)_{avg})(y_i - \bar{y})]$
$y = ax^2 + bx + c$ <i>c is known</i>	$b = \frac{\left(\sum_{i=1}^n x_i^2 y - c \sum_{i=1}^n x_i^2 \right) \sum_{i=1}^n x_i^3 - \left(\sum_{i=1}^n x_i y_i - c \sum_{i=1}^n x_i \right) \sum_{i=1}^n x_i^4}{\left(\sum_{i=1}^n x_i^3 \right)^2 - \sum_{i=1}^n x_i^2 \sum_{i=1}^n x_i^4}$ $a = \frac{\sum_{i=1}^n x_i^2 y - c \sum_{i=1}^n x_i^2 - b \sum_{i=1}^n x_i^3}{\sum_{i=1}^n x_i^4}$

First, design a mass flow hopper. Following the procedure described in Figure 5.21:

Step 1. Estimate ff . Choose $ff = 1.3$.

Step 2. Determine σ_l from the intersection of the flow function and a line through the origin with a slope equal to $1/1.3$. By setting $f_c = \bar{\sigma}$, the

solution to the simultaneous equations Equation E.1 and $\bar{\sigma} = \sigma_1/1.3$ gives $\sigma_1 = 0.26$ kPa.

Step 3. Calculate δ . Substitution of $\sigma_1 = 0.26$ kPa into Equation E.2 gives $\delta = 42.9^\circ$.

Step 4. Update flow factor. Solving Equation 5.28 with $\delta = 42.9^\circ$ and $i = 1$ gives $ff = 1.44$.

Step 5. Update σ_1 from intersection of the flow function and the updated flow factor gives 0.29 kPa.

Step 6. Update δ . Solving Equation E.3 with updated value of σ_1 gives $\delta = 41.7^\circ$.

Step 7. Solving Equation 5.28 gives $ff = 1.44$. The solution has converged.

Step 8. Calculate σ_{crit} . $\sigma_{crit} = \sigma_1/ff = 0.29/1.44 = 0.20$ kPa.

Regression of the data gives the relationships in the accompanying Table 5-2.

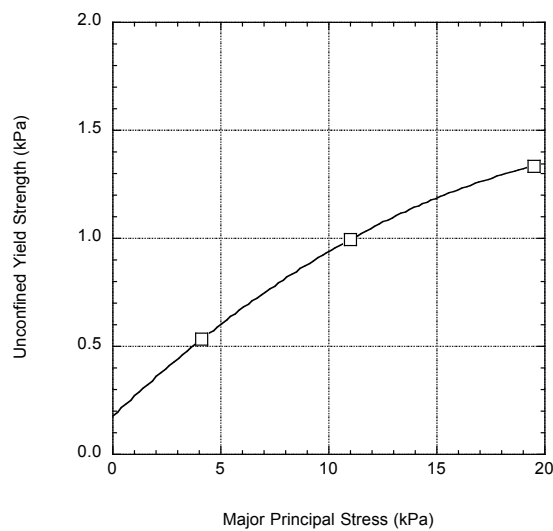


Figure 5.40a. Flow function.

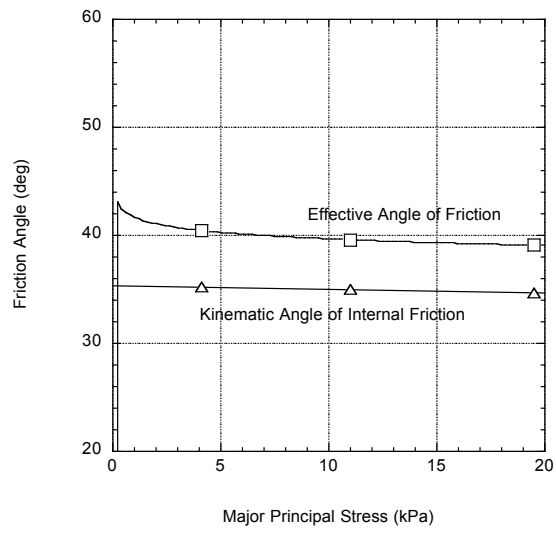


Figure 5.40b. Internal friction.

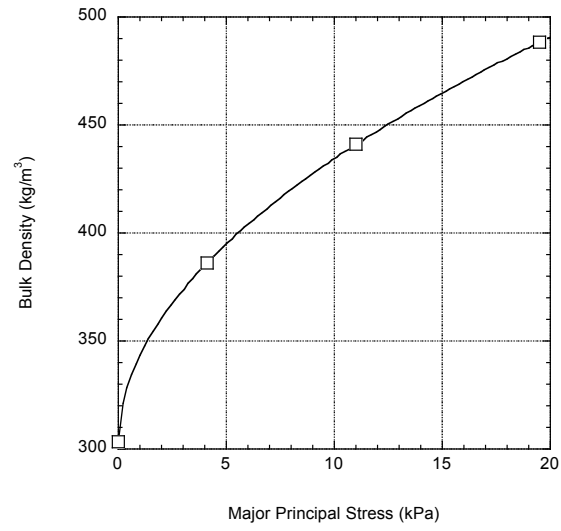


Figure 5.40c. Compressibility.

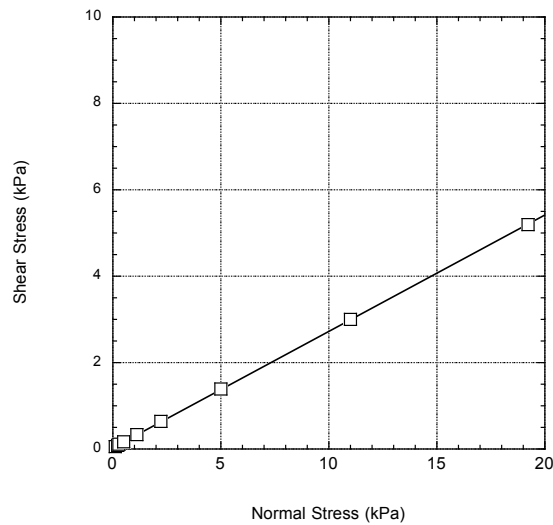


Figure 5.40d. Wall yield locus.

Step 9. Find B_{min} . From Equation E.4, $\rho_b = 325 \text{ kg/m}^3$. Setting $H(\theta') = 2.3$ and solving Equation 5.27 gives $B_{min} = 0.15 \text{ m}$ (5.8 in.).

Step 10. Specify the outlet diameter. For this example, choose $B = 0.25 \text{ m}$ = 10 in.

Step 11. Estimate σ_l . From Equation 5.26 after setting $H(\theta') = 2.3$, $ff = 1.3$, and $\rho_b = 304 \text{ kg/m}^3$, $\sigma_l = 0.46 \text{ kPa}$.

Step 12. Update δ and ϕ' . From Equation E.2, $\delta = 42.4^\circ$. Solving Equations 5.17 – 5.25 gives $\phi' = 20.4^\circ$.

Step 13. Estimate recommended mass flow hopper angle. From Equation 5.1 after subtracting a 3° safety factor, $\theta' = 23.3^\circ$.

Step 14. Update ff . Solution of Equations 5.16 – 5.28 gives $ff = 1.40$.

Step 15. Update σ_l . Solution of Equation 5.26 using $H(23.3^\circ) = 2.36$ gives $\sigma_l = 0.48 \text{ kPa}$.

Step 16. Update δ and ϕ' . From Equation E.2, $\delta = 42.3^\circ$. Solving Equations 5.17 – 5.25 gives $\phi' = 20.1^\circ$.

Table 5-2
Regression Results

Flow function:

$$f_C = 0.177 + 0.0939 \sigma_I - 0.00177 \sigma_I^2 \quad (\text{E.1})$$

Effective angle of friction:

$$\delta = 41.7 - 0.88 \ln \sigma_I \quad (\text{E.2})$$

Kinematic angle of internal friction:

$$\phi = 35.3 - 0.0312 \sigma_I \quad (\text{E.3})$$

Bulk density:

$$\rho_b = 303.6 + 39.77 \sigma_I^{0.517} \quad (\text{E.4})$$

Wall yield locus:

$$\tau' = 0.0395 + 0.269 \sigma' \quad (\text{E.5})$$

Permeability:

$$K = 0.022 (\rho_b/303.6)^{2.2} \quad (\text{E.6})$$

Units: stress: kPa; bulk density: kg/m³; internal friction: deg; permeability: m/s

The flow function empirical relationship was found by fitting the data to a quadratic, fixing the intercept equal to a value obtained by linear extrapolation of the two lowest data points.

Step 17. Update recommended mass flow hopper angle. From Equation 5.1 after subtracting a 3° safety factor, $\theta' = 23.7^\circ$.

Step 18. Calculate ff . Updated flow factor equals 1.40.

Step 19. Update σ_I . Solution of Equation 5.26 with $H(23.7^\circ) = 2.33$ gives $\sigma_I = 0.48$ kPa. Solution has converged.

Our recommended mass flow conical hopper has a 10-in. diameter outlet (minimum arching diameter is 5.8 in.) and walls sloped 24° walls from vertical if fabricated using the same material used in the wall friction test.

To confirm that the recommended mass flow hopper will allow the desired steady discharge rate, solve Equation 5.60. The discharge rate depends on the dimensions of the cylinder section of the storage vessel. For this example, specify a 4 ft (1.2 m) diameter, 15 ft (4.6 m) tall cylinder, which together with the hopper section can store about 200 cu ft of bulk material. Solving Equations 5.59, 5.60, and 5.63 gives $\sigma_{10} = 0.31$ kPa, $dP/dz = -1300$ N/m³, and $v_o = 0.044$ m/s. At this stress, $\rho_b = 330$ kg/m³. The solids discharge rate is then equal to $(0.044\text{m/s}) (0.25^2\pi/4 \text{ m}^2)(330 \text{ kg/m}^3)(3600 \text{ s/hr}) = 2,600$ kg/hr (2.6 ton/hr). It is best to multiply this number by 0.8 to be conservative.

Now consider a funnel flow hopper. The critical rathole diameter depends on the dimensions of the cylinder. From Equations E.1 and E.3, at $\sigma_l = 8.3$ kPa, $f_C = 0.83$ kPa and $\phi = 35^\circ$, respectively. From Equation 5.67, $G(\phi) = 3.0$. Solving Equation 5.66 for D_F gives a critical rathole diameter of 0.60 m (24 in.).

A funnel flow conical hopper may not be practical due to the large outlet diameter required to prevent stable ratholes from developing. However, a hopper section that transitions from the cylinder to a slotted outlet may be an option provided that the *diagonal* of the outlet is greater than 0.61 m. The width of the outlet must be large enough to prevent bridging. Jenike recommends using a flow factor of 1.7 to determine the critical arching dimension. For a transition hopper beneath a 1.2-m diameter, 4.5-m cylinder and filled with bulk material, the outlet width should be greater than or equal to 0.18 m (6.9 in.)

There is always more than one answer (another example design problem)

So how 'bout another example? This time, the results of shear cell tests conducted on a bulk material are given in Figure 5.41a through 5.41d. In addition, discharge rate is assumed not to be an issue since the permeability of the material high.

Our task is to design a silo that will reliably handle the material. The silo has the following requirements:

- Capacity: 50 metric tonne
- Throughput: 5 metric tonne/hr
- Maximum diameter: 4.88 m (limited by floor space)

Material will be continuously discharged (no time tests are required)

The first step is to determine critical arching and ratholing diameters. Using Equation 5.28 or Figure 5.20 to calculate the flow factor gives a critical arching diameter of 390 mm for a conical mass flow hopper and a critical arching width of 180 mm for a planar mass flow hopper with a slotted outlet. Using a value of $ff = 1.7$, the critical arching width of a slotted outlet for a planar funnel flow hopper is 210 mm.

The critical rathole diameter depends on the maximum stress in the cylinder section of the silo. Using Equation 5.66 with $G(30^\circ) = 2.47$ gives the relationship between the critical rathole diameter and the major principal stress at the hopper-cylinder junction given in Figure 5.42.

The procedure outlined in Figure 5.19 is used to determine the recommended hopper angle for conical and planar mass flow hoppers. The results are shown in Figures 5.43 and 5.44.

Inspection of the analysis shows that a conical funnel flow silo is unlikely to be practical because the diameter of a large silo required to prevent a stable rathole from developing is larger than Al Gore's carbon footprint. However, an expanded silo consisting of a funnel flow hopper section above a mass flow hopper is feasible. A planar funnel flow hopper with a slotted outlet is feasible provided that the width of the outlet is at least 210 mm (8¼ in.) and the *diagonal* of the slotted outlet is greater than D_F , which may be achievable. Mass flow can be achieved in conical silos with reasonably shallow hopper walls if 304 stainless steel with a #2B finish is used. A conical mass flow hopper fabricated using carbon steel must be very steep unless it has a large outlet. Mass flow planar hoppers can be fabricated with 304 #2B stainless steel or carbon steel.

Three possible designs are shown in Figures 5.43 through 5.45. Figure 5.43 is a conical mass flow silo. As designed, its hopper section must be fabricated or lined with 304 #2B stainless steel. Although the critical arching diameter for a mass flow hopper handling this material is 390 mm, a 690-mm diameter outlet is specified to allow the desired solids discharge rate. A 24-in. rotary valve operated at *ca.* 8 rpm can provide the required throughput. (Feeders are discussed in Chapter 6.)

The silo drawn in Figure 5.44 has both a transition hopper section and a cone. All sloping surfaces can be fabricated using carbon steel. Note that

the required hopper angle for mass flow in the cone is reasonably shallow because it has a large outlet. (The wall friction angle is highly dependent on the wall stress, which increases with hopper diameter.) Beneath the hopper is a 305-mm mass flow screw feeder, which can be operated at approximately 25 rpm to allow the desired discharge rate.

The final design, shown in Figure 5.47, is an expanded flow silo that includes a shallow cone above a steep cone. Both cones are fabricated using carbon steel. The lower cone is steep enough to allow mass flow, and the outlet of the upper cone is large enough to prevent a stable rathole from developing.

least costly wall material and the simplest feeder (*i.e.*, rotary valve). It is also taller due to its steep mass flow hopper section.

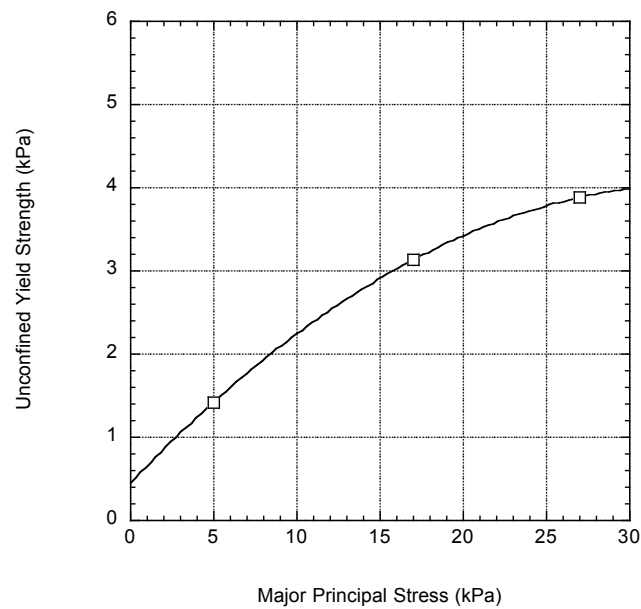


Figure 5.41a. Cohesive strength.

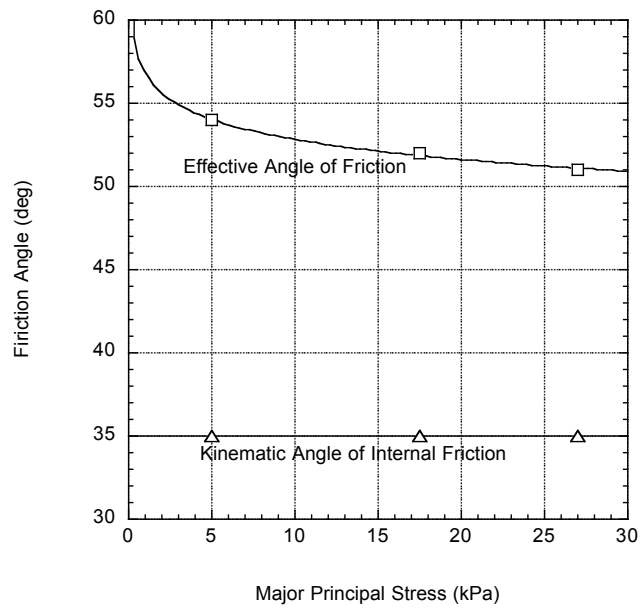


Figure 5.41b. Internal friction.

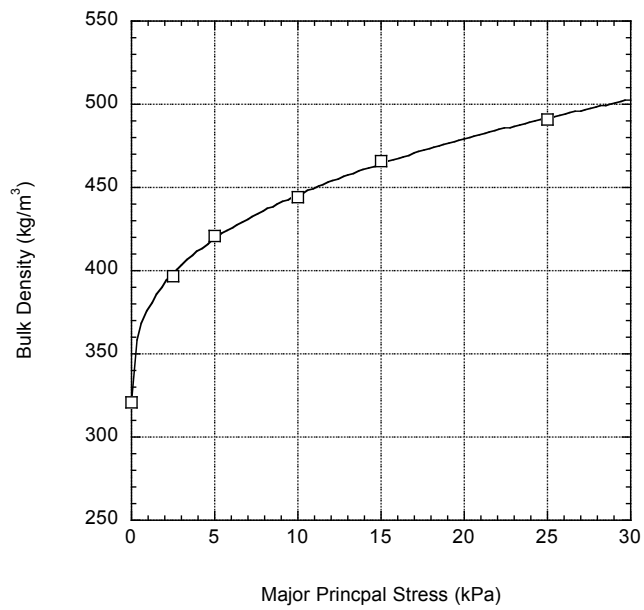


Figure 5.41c. Compressibility.

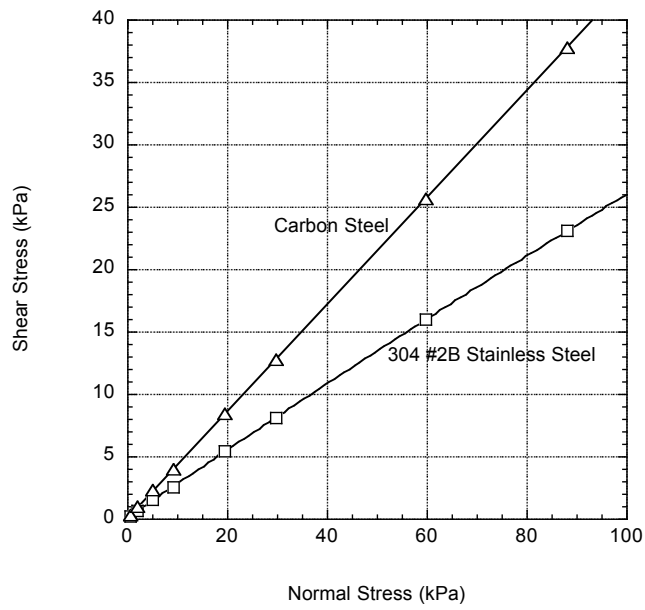


Figure 5.41d. Wall friction.

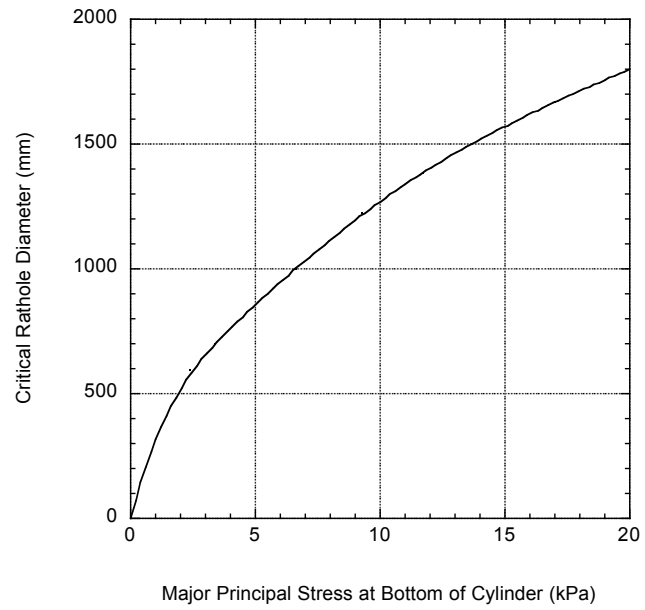


Figure 5.42. Critical rathole diameter.

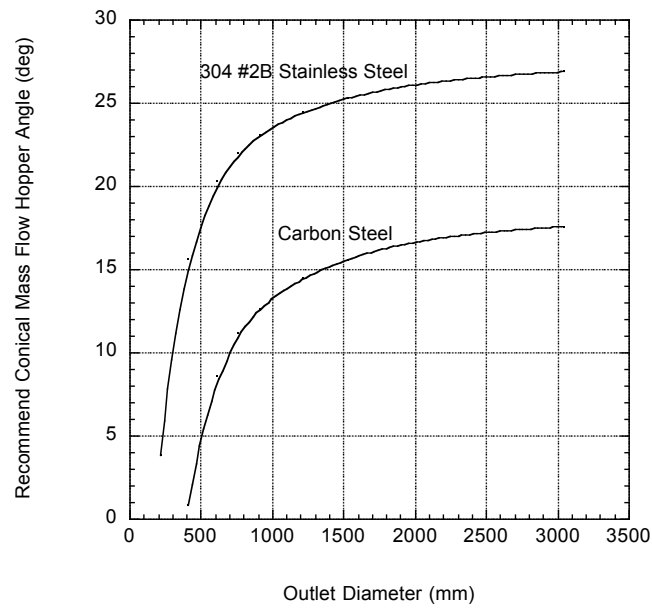


Figure 5.43. Recommended mass flow hopper angles for conical hopper.

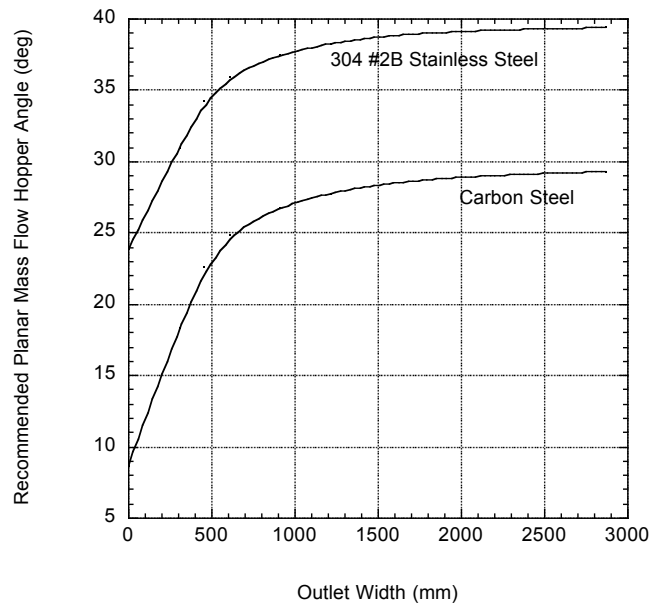


Figure 5.44. Recommended mass flow hopper angles for planar hopper.

That's all very nice, but what is the best choice? The mass flow cone is the simplest, but it requires a relatively expensive stainless steel liner. The transition hopper can be fabricated using inexpensive carbon steel; however, it cannot accommodate a rotary valve and instead a more expensive mass flow screw feeder (or belt feeder) must be installed beneath the outlet. It is also the shortest of the three choices. The expanded flow option uses the

The design engineer must consider the advantages and disadvantages of alternative designs. In some cases, constraints can be relaxed. For example, if segregation is not a problem and tight control of the discharge rate is not required, a funnel flow hopper, which can be shorter, that is equipped with a bin activator may be a more economical option.

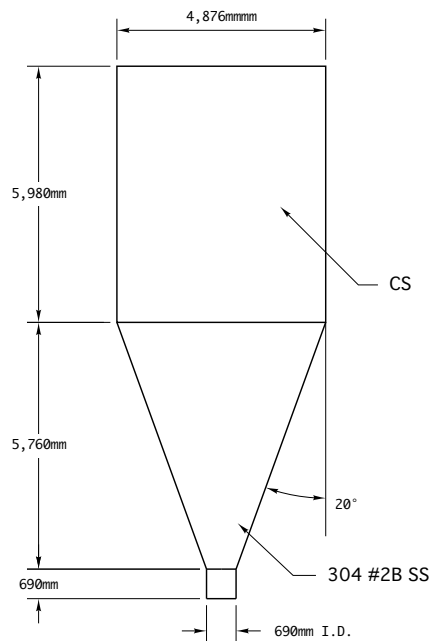


Figure 5.45. Conical mass flow silo.

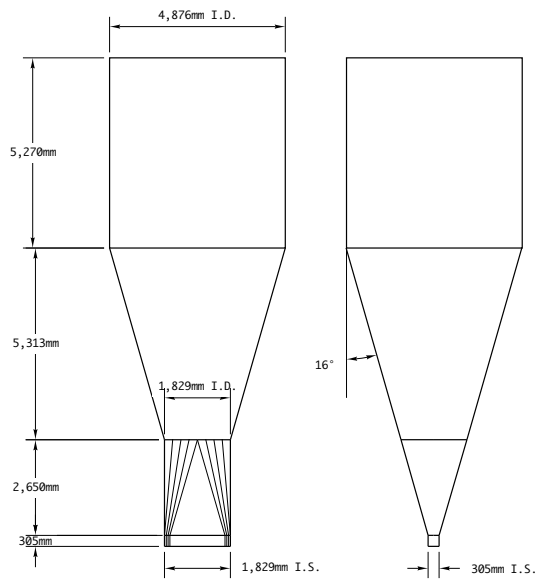


Figure 5.46. Silo with transition hopper and cone sections.

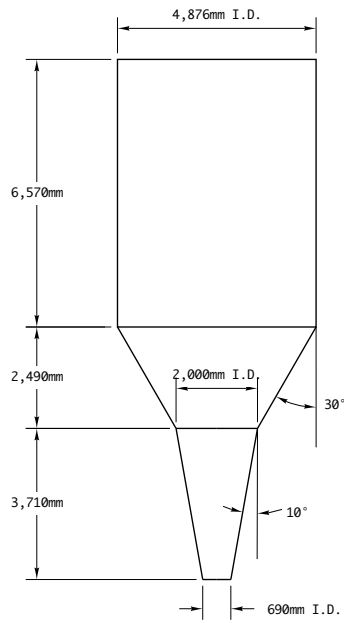


Figure 5.47. Expanded flow hopper.

6. FEEDERS AND FLOW AIDS

Feeders can be a source of hopper flow problems if improperly used or if they are improperly designed. This is especially true for hoppers with slotted outlets, where feeders should be designed to draw uniformly from the entire cross-section of the outlet in order for mass flow to occur. However, even hoppers with round outlets can have uneven flow if a proper interface is not utilized.

There are two primary categories of feeders available to handle bulk solids: volumetric and gravimetric. A volumetric feeder discharges a particular volume of powder over a period of time. This type of feeder is adequate for many applications, especially for mass flow hoppers, in which the bulk density of the powder at the hopper outlet is nearly independent of level inside the vessel.

A gravimetric feeder relies on a control system that adjusts the speed of the feeder based on loss-in-weight measurements. Because the controller cannot determine a discharge rate when its hopper is being filled with material, typically two hoppers are used in series. The upstream system is designed so that it can feed the downstream vessel very quickly. During the fill cycle, the downstream feeder is operated in a volumetric mode (*i.e.*, at a constant speed), and then in gravimetric mode (*i.e.*, its speed is controlled by measuring the loss in weight of material inside the hopper) once the downstream hopper is filled. The hopper on the gravimetric feeder, which is sometimes called the extension hopper, should be designed for mass flow to

reduce variability of the discharge rate when it is operated in volumetric mode. Gravimetric feeders are usually much more expensive than volumetric feeders.

An advantage of mass flow bins is that the bulk density at the bin outlet is independent of the height of material inside the vessel and does not change even when a vertical stress is imparted when the hopper is refilled. If precise measurement of the discharge rate from a bin is not critical, volumetric feeders are often adequate and a less expensive alternative to gravimetric feeders.

Rotary valves

Rotary valves are often used beneath hoppers with round or square outlets. They are particularly useful for applications in which a seal must be provided to prevent air from flowing out of or into the hopper outlet. A schematic of a rotary valve is shown in Figure 6.1.

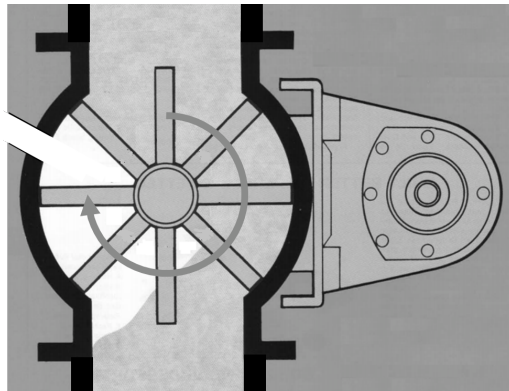


Figure 6.1. Rotary valve feeder.

If a rotary valve is used, a short vertical spool section (length equal to or greater than its diameter) should be installed between the hopper outlet and valve inlet. Otherwise, material may flow preferentially from the upside of the valve and affect the flow pattern inside the vessel as shown in Figure 6.2.

When the powder is dropped from a pocket, the air or gas that replaces it can be pumped back into the bin. A vent line should be considered, especially if the rotary valve discharges material into a high-pressure line.

Typically, the vent line directs air either into a dust collector or into the top of the hopper.

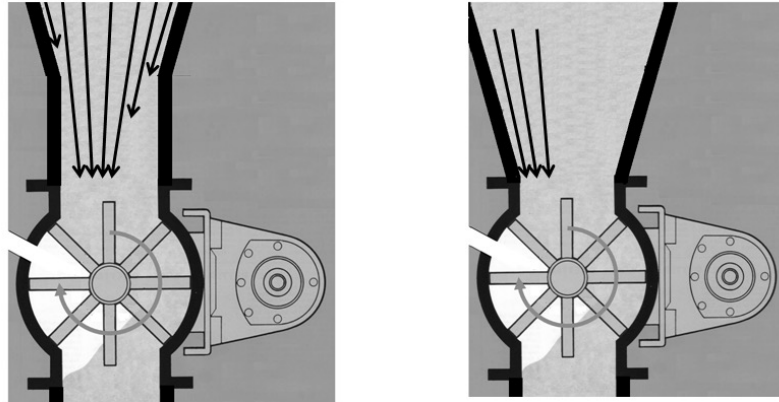


Figure 6.2. Flow of powder through rotary valve with (left) and without (right) spool section.

The capacity of a rotary valve can be calculated from

$$q = \frac{N\pi(D^2 - d^2)W}{4} \quad (6.1)$$

where q is the volumetric discharge rate, N is the rotary valve speed, D and d are the vane and shaft diameters, respectively, and W is the width of the vane. The result is often multiplied by a factor of about 0.8 to account for incomplete filling of the pockets. Rotary valve speeds of 15 - 45 rpm are preferable. For valves with scalloped pockets, capacities from the supplier should be used. Young Industries' website has a nice app for sizing rotary valves that can be downloaded.

Screw feeders

Screw feeders are primarily used to control the discharge of powders from hoppers with slotted outlets. A screw is comprised of a series of flights wound around one or more shafts.

A screw that has a constant pitch and constant shaft diameter will cause the formation of a flow channel at the back of the hopper over the first pitch of the screw. As illustrated in Figure 6.3, this channel will draw material from the top surface into the flow channel until a stable rathole forms and the

channel empties. The rathole will then periodically fail as the base of the material fails above the screw. This will continue to broaden the flow channel, and this cyclic fail-flow-empty cycle will continue until the hopper empties. If the powder is cohesive, an arch or stable rathole may develop, causing a disruption in flow.

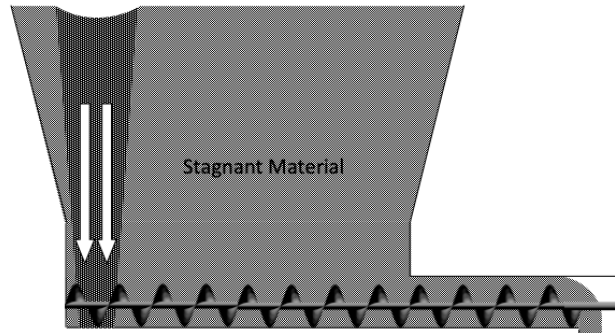


Figure 6.3. Screw feeder with constant pitch, constant diameter screw.

A mass flow screw feeder, comprised of a tapered section followed by an increasing pitch section, ensures that the capacity of the feeder increases in the direction of flow (see Figure 6.4). The length of the cone and the pitch schedule are chosen such that the capacity of the screw increases linearly along the hopper length. The screw flight diameter should equal the width of the hopper outlet, and the trough should be about an inch wider than the screw. Fabrication tolerances limit the length-to-width ratio of the hopper to ≤ 6 .

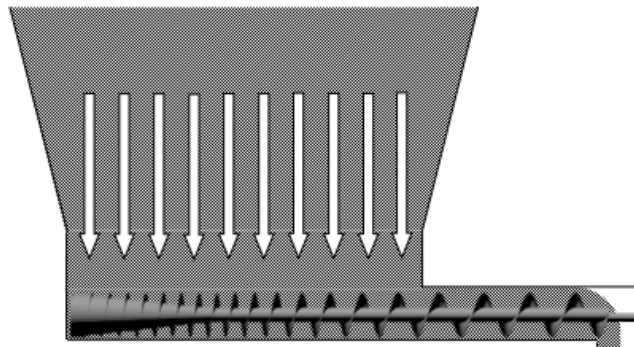


Figure 6.4. Mass flow screw feeder.

The capacity of the screw C is the volume between adjacent screw flights. In the tapered shaft section, the volume of screw segment is given by

$$C = \frac{\pi}{12}(3D^2 - d_{start}^2 - d_{start}d_{end} - d_{end}^2)(P - t) \quad (6.2)$$

where

$$d_{end} = d_{start} - \frac{P(d_0 - d_s)}{L_C} \quad (6.3)$$

In Equations 6.2 and 6.3, D and d are the screw and shaft diameters, respectively, L_C is the length of the cone, *start* and *end* of course denote the start and end of the screw section, respectively, 0 and s denote the diameter of the large end of the tapered section and the diameter of the constant-shaft-diameter section, respectively, P is the screw pitch, and t is the flight thickness. For the constant shaft diameter section, the capacity of each screw segment is given by

$$C = \frac{\pi}{4}(D^2 - d_s^2)(P - t) \quad (6.4)$$

A mass flow screw feeder is designed such that its capacity increases linearly in the direction of discharge. Usually the capacity of the screw at the discharge end of the hopper outlet is around 75-85 percent of that of the constant-diameter conveying section, which extends past the hopper outlet. Such a design reduces the power requirements of the screw feeder. A shroud is often installed immediately past the hopper wall to ensure that the conveying section does not completely fill.

To prevent logging, the pitch should be greater than one half the height of the flight, that is,

$$\frac{P}{(D - d) / 2} \geq \frac{1}{2} \quad (6.5)$$

The final pitch determines the throughput of the screw feeder, that is,

$$v = NC_f f \quad (6.6)$$

where v is the volumetric discharge rate, C_f is the capacity of the screw in the constant-pitch conveying section (typically equal to the flight diameter), N is the screw speed, and f is the fill fraction. Generally, screw feeders are best operated between 3 and 40 rpm.

The trough should be U-shaped rather than V-shaped to prevent material from stagnating. Screw flights should have lower friction than the trough; otherwise, material will only be spun about the shaft and will not be conveyed. The conveying section should be long enough to prevent material from falling into the outlet when the feeder has been stopped. This length can be determined from the material's angle of repose. The flights should terminate 1-2 in. from the start of the screw feeder outlet to prevent compaction of the solids.

The power requirements depend on the solids stress at the feeder inlet, the wall friction between the solids and the trough wall, the screw diameter, and the screw speed. The running torque T can be estimated from

$$T \approx \frac{\sigma_v \tan \phi' \pi D^2 L}{2} \quad (6.7)$$

where σ_v is the average vertical solids stress at the feeder inlet and L is the length of the screw (both the feed section and the conveying section). The solids stress is calculated from

$$\sigma_v = q \rho_b g B \left(\frac{4}{\pi} \right)^m \quad (6.8)$$

where B is the outlet width, m equals 0 or 1 for a slotted or round outlet, respectively, and q is Jenike's non-dimensional surcharge factor that can be determined using charts in his Bulletin 123. McLean and Arnold [*Powder Techn.*, 19, 279 (1978)], obviously having too much time on their hands, derived an analytical expression for q :

$$q = \frac{1}{4 \tan \theta'} \left[2 \left(\frac{\sigma'}{\rho_b g B} \right) (\tan \theta' + \tan \phi') - 1 \right] \quad (6.9)$$

where

$$\frac{\sigma'}{\rho_b g B} = \frac{Y}{X-1} \left(\frac{1 + \sin \delta \cos 2\beta}{2 \sin \theta'} \right) \quad (6.10)$$

and θ' is the hopper angle (referenced from vertical), ϕ' is the wall friction angle, δ is the effective angle of friction, σ' is the wall stress, ρ_b is the bulk density, and g is acceleration due to gravity. The terms β , X , and Y , and were given in Equations 5.2, 5.14, and 5.15, respectively.

If a vertical section exists between the hopper outlet and feeder inlet (often to allow installation of a slide gate), Equation 3.11 is used. Since the vertical section is usually short, the additional stress can be approximated as $\rho_b g h$, where h is the height of the vertical section.

The running power requirement W_s is equal to the product of the torque and the rotational speed of the screw:

$$W_s = 2\pi NT \quad (6.11)$$

For applications where cohesive powders must be discharged at low rates, feeders with agitators are often used. Frequently, the screws are shaft-less so that they can be operated at a higher speed, which improves their ability to handle particularly cohesive powders. A ribbon-like agitator or other device is located in a bowl above the augers to ensure a live bottom at the outlet of the extension hopper. Figure 6.5 is a schematic of an auger feeder equipped with an agitator.

Instead of an agitator, some feeders employ flexible walls. If cohesive powders are handled, the flexing can compact the powder and increase its strength, preventing it from entering the screws. Such screw feeders should be used with caution.

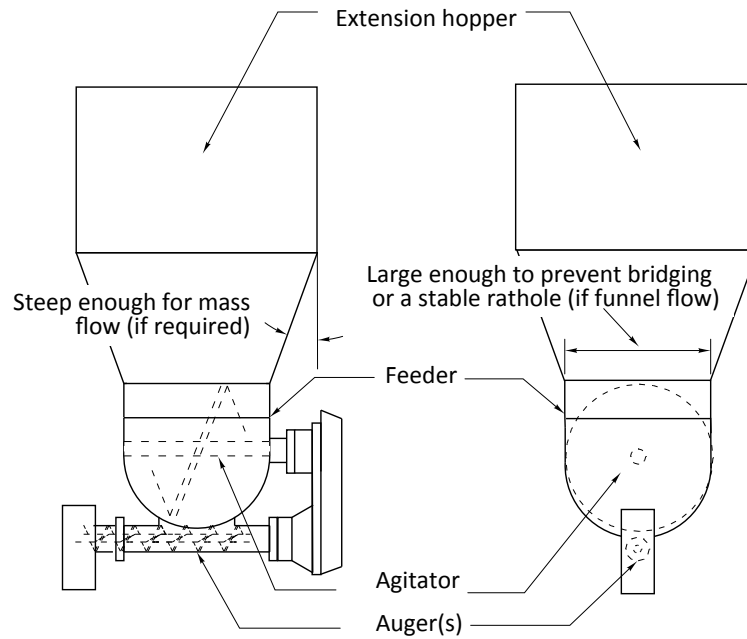


Figure 6.5. Low-throughput screw feeder.

The outlet to the extension hopper should be large enough to prevent a cohesive arch or a stable rathole from developing. A mass flow hopper is generally preferred since the critical arching diameter is significantly smaller than the critical rathole diameter. In addition, the stress at the hopper outlet will remain nearly constant both as it empties and when additional powder is added during refill (see Figure 6.6) due to the radial stress field that develops inside the hopper. This allows a more constant bulk density in the feeder and a steadier discharge rate, even while the hopper is refilled. If the extension hopper is a funnel flow hopper or a short cylinder with vertical walls, the solids stress and hence the bulk density will decrease as the hopper empties. A gravimetric feeder can change the screw speed to adjust for the reduction in bulk density; however, it is not always able to compensate during the refill stage when the addition of fresh powder compacts the powder and increases its bulk density because the feeder is operated volumetrically.

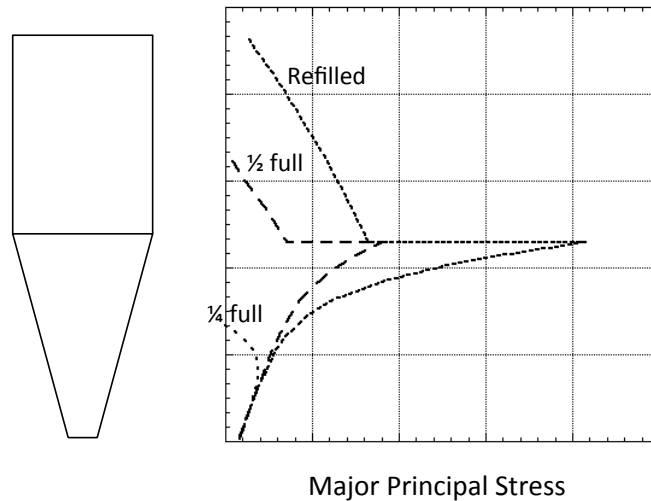


Figure 6.6. Major principal stress on solids when hopper is refilled and emptied.

Other feeders

Belt feeders consist of a moving belt, idlers that support the belt, and a motor to power the belt. Like screw feeders, a belt feeder is useful for hoppers with slotted outlets. To ensure that all the contents of the hopper are in motion when the belt is in motion, a feeder-hopper interface must be carefully designed so that its capacity will increase in the direction of flow. A belt interface is shown in Figure 6.7.

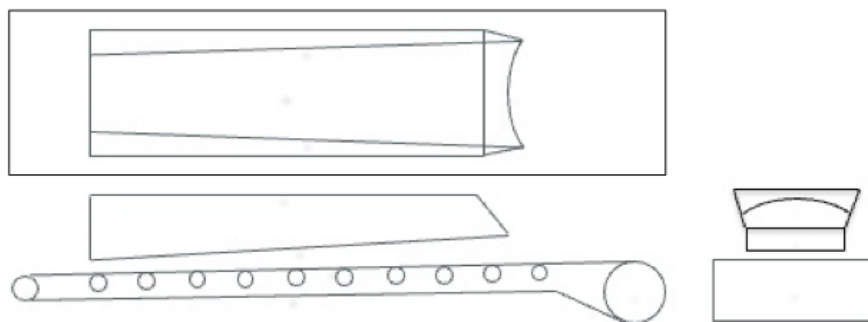


Figure 6.7. Belt feeder interface.

Both the width of the interface and its distance from the belt surface increase in the direction of discharge. A good rule of thumb is that the increase in

elevation and width should be approximately $\frac{1}{4}$ inch per foot (20 mm/m in third-world units). Experts such as Thayer Scale should be contacted for design and supply of belt feeders and interfaces.

Pan feeders, also known as vibratory feeders, use vibration to modulate the flow of powder from a hopper. As the pan of the feeder vibrates, material is thrown upward and forward. Eriez (Erie, Pennsylvania) manufactures vibratory feeders with a wide range of capacities. A vibratory feeder is shown in Figure 6.8.



Figure 6.8. Eriez vibratory feeder.

Vibratory feeders should not be used with funnel flow hoppers that handle fine powders. If aerated material reaches the feeder, *e.g.*, the result of a collapsed rathole, the feeder will not be able to stop its discharge.

Siletta feeders use an array of louvers and a vibratory drive to control the discharge rate of a bulk material from a hopper. The angle and spacing of the louvers are set such that the material will find its angle of repose and will not discharge unless the feeder is vibrating. Figure 6.9 is a photograph of a siletta feeder.

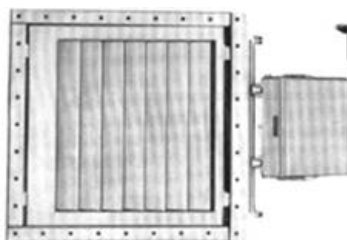


Figure 6.9. Siletta louvered feeder.

Belt, vibrating pan, and siletta feeders should be used with caution if fine powders are discharged. Fine powders may fluidize and flood the feeder if operated at too high a rate or if ratholes in a funnel flow hopper collapse and

the powder remains aerated, resulting in uncontrollable discharge of the material. The angle of repose of a fluidized powder is zero.

The Kamengo feeder is equipped with openings that move laterally along the slotted outlet of a planar hopper, which prevents preferential flow during discharge. Figure 6.10 is a schematic of a Kamengo feeder.

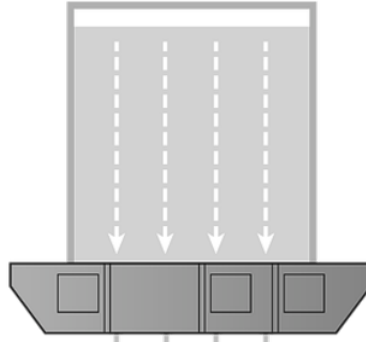
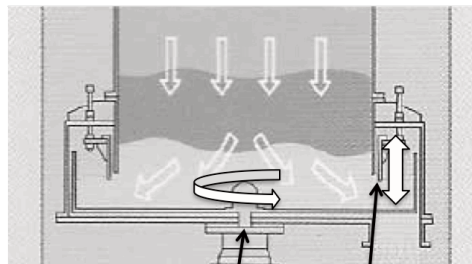


Figure 6.10. Kamengo feeder.

Table feeders, a.k.a. circle feeders, are useful for handling materials that require large hopper outlets to prevent bridging or the formation of stable ratholes. Flat, slowly-rotating blades convey material radially toward an outer ring and into one or more discharge ports. Figure 6.11 is a schematic of LCI Corporation's circle feeder.



Controls: rotor speed, weir height

Figure 6.11. LCI Circle feeder.

Often, circle feeders are used beneath bins with straight, non-converging walls, which ensures mass flow. However, this can lead to high power requirements due to high solids stresses on the feeder. Installing vertical,

flat plates in the cylinder so that more of the load can be supported by wall friction can reduce these stresses.

Crammer feeders (or Kramer feeders if you are a Seinfeld enthusiast) are frequently used to feed powders into extruders. Figure 6.12 is a drawing of a crammer feeder.

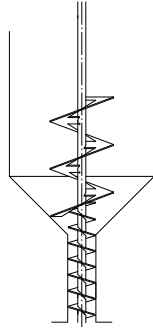


Figure 6.12. Crammer feeder.

The pitch is generally equal to the hopper outlet diameter, *i.e.*, the screw diameter. The diameter of the reverse pitch ribbon in the hopper should be greater than the critical rathole diameter. High power requirements are often required due to wall friction.

Flow aids

Flow aids are pneumatic or mechanical devices or chemical additives used to induce bulk solids to flow more readily. Examples of mechanical and pneumatic flow aids are vibrators and air cannons, respectively. Common chemical additives include silicates and stearates.

Vibrators impart forces to the bulk solid through the hopper walls of the bin. Some vibrators produce high-frequency, low-amplitude forces, while others deliver low-frequency, high-amplitude forces. Their effectiveness is mixed. In some cases, they may be an effective means of restoring flow when a bin becomes plugged. In other cases, however, their effect is marginal or can even exacerbate flow problems. Applying sufficient but not excessive force where it is required is difficult, particularly in the case of ratholing where the forces often must be transmitted through a significant amount of material to reach it.

The force required to overcome a cohesive arch depends on the bulk solid's cohesive strength and the size of the outlet. If the hopper outlet is slightly undersized, *i.e.*, the size of the outlet is only marginally smaller than its critical arching dimension after storage at rest, a vibrator may be able to provide enough force to restart flow. Because ratholes are inherently stable, the outlet diameter required to prevent a stable rathole from developing can be several times the outlet size of a bin; therefore, vibrators generally cannot be used to overcome ratholing.

A steeply sloped flow function is evidence of a bulk solid that is pressure sensitive, *i.e.*, its strength increases substantially when additional stresses are applied. Vibrating pressure-sensitive bulk materials often will exacerbate flow problems. Another challenge is that a Google search for vibrators will likely direct you to an adult website.

A bin activator or vibrating discharger utilizes an inverted cone or dish that moves in a gyratory, horizontal, or vertical motion. The bulk solid then flows around the cone or dish into a conical section beneath it, which essentially operates as a chute. Vibratory dischargers can be effective in overcoming flow problems if they are used appropriately. When used at the outlet of a funnel flow bin, the flow channel above the discharger will be approximately the size of its top diameter. If this diameter is smaller than the bulk material's critical rathole diameter, a stable rathole will form, and the discharger will be ineffective in collapsing it. The width of the annulus formed by installation of the bin activator should be smaller than the critical arching dimension to ensure that flow halts when the discharger is stopped.

A cone valve is similar to a bin activator in that it uses a vibrating inverted cone inside the bin. The position of the cone can be adjusted vertically and opened and shut for short intervals to control the discharge rate or stop flow completely. Cone valve assemblies include a discharge station equipped with a probe that controls the height of the insert.

Air or nitrogen cannons operate differently in that they rely on a pressure wave to provide the stress required to break an arch. Cannons work by releasing a small volume of high-pressure gas into the bin. The required size, number, and location of the cannons depend on the cohesive strength of the bulk material and the dimensions of the bin.

Air cannons are best used for reinitiating flow after a cohesive arch develops when the material is stored at rest. Air cannons are usually not effective in preventing flow problems in funnel flow bins since ratholes are inherently stable. Contact Martin Engineering for size, number, and placement.

Air sweeps, in which nozzles inject a high-pressure, high-volume, 360-degree burst of compressed gas to lift and sweep stagnant material back into the flow stream, can be effective. Contact Control Concepts for sizing and location.

Chemical flow aids are often used to prevent arching or the formation of a stable rathole. Parting agents such as silicon dioxide (preferably CAB-O-SIL[®], a shameless plug for my old employer Cabot Corporation) and calcium stearate are effective as they increase the distance between adjacent particles, thereby reducing the magnitude of their cohesive forces. Note that while a flow aid may be effective in reducing a bulk solid's cohesive strength, the additive may increase wall friction, potentially resulting in flow problems associated with funnel flow. In addition, only a small amount should be added. High additive levels can increase a bulk material's cohesive strength rather than reduce it. To reduce wall friction, small amounts of magnesium stearate are frequently added.

Air assist and fluidization

Air pads are sometimes used to inject low-pressure air into a bin. They are sometimes effective in correcting solids flow problems caused by arching or ratholing. Air pads may be effective in increasing the discharge rate of fine powders by reducing or eliminating the adverse pressure gradient that develops above a hopper outlet that causes counter flow of air.

A better means to increase the discharge rate of fine powders is to use an air permeation system, which consists of a sloping shelf or insert through which air is introduced at a low rate. The air reduces or eliminates the vacuum that naturally develops when a bulk solid dilates in the hopper section and increases its void fraction. The air does not fluidize the bulk material. Rather, its flow rate should be low enough to prevent fluidization, the air should be distributed evenly, and the permeation system should not impede solids flow in the hopper.

Air-assist dischargers are designed to reduce the wall friction angle to nearly zero, thereby allowing powders to glide along hopper walls. The hopper

section is either lined with air panels or is fabricated using a permeable membrane through which air is injected at a low rate. Jenike [Bulletin 123 (1964)] recommends conical hopper angles between 40° and 50° from vertical as steeper hoppers may require large outlet diameters to prevent arching. (Note that the flow factors in Figures 5.8 - 5.15 have large values for combinations of steep hopper angles and low wall friction angles.) Steep hopper angles can be used provided that a fully open, unrestricted on/off valve is used or if enough gas is added to completely fluidize the bulk material at the outlet.

A fluidized discharger can be used when the bulk material is fluidizable and a low bulk density of the discharged material is acceptable. A schematic of a fluidized discharger is shown in Figure 6.13.

Fluidized dischargers can generally be used for Geldart Group A, B, and C materials [*Powder technology*, 7, 5 285 (1973)], although Group C materials may require mechanical agitation. Discharge from a bin equipped with a fluidized discharger is typically controlled through use of a rotary valve. A Geldart powder classification chart is shown in Figure 6.14.

Young Industries offers a patented design (US Patent No. US11325776B1) where two cones having gas-permeable walls are used (see Figure 6.15). The lower cone is a conventional, shallow fluidizing discharger through which enough gas is injected to fluidize the powder. The upper cone is steeper, and gas-permeable walls allow a relatively small amount of gas to be introduced, *i.e.*, just enough to reduce wall friction and ensure mass flow. Think of it as a conical air hockey table. The design is advantageous in that compared to conventional fluidizing dischargers, significantly less gas is required.

Reclaim systems

Reclaim systems have screws that draw material into the centered outlet of a conical or flat-bottomed hopper. The screw turns about its own axis conveying material toward the center while rotating along the hopper walls or floor sweeping the material. Material conveyed to the outlet then flows into a discharge auger or conveyor. A schematic of a Laidig reclaimer is shown in Figure 6.16.

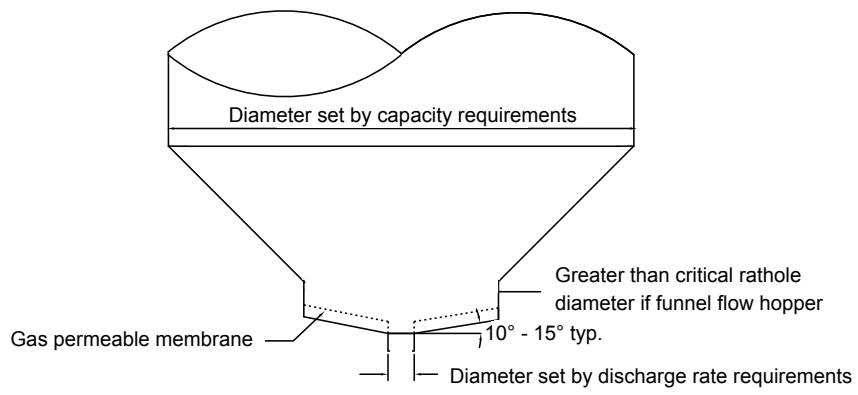


Figure 6.13. Fluidized discharger.

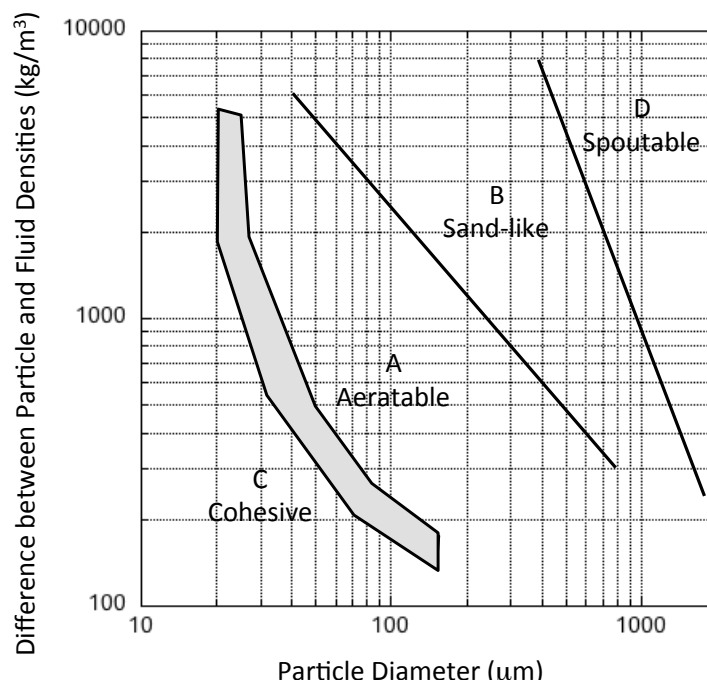


Figure 6.14. Geldart powder classification chart.

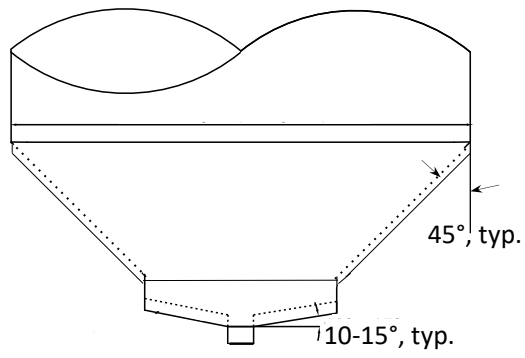


Figure 6.15. Young Industries mass flow fluidizer.



Figure 6.16. Laidig reclaim system.

7. OTHER STUFF

Segregation

Some materials, when transferred into a bin, will segregate, that is, particles of different size, shape, density, *etc.* will separate. Segregation can occur by a number of different mechanisms, depending on the physical characteristics of the particles and the method of handling. The three most common mechanisms are *fluidization* (air entrainment), *dusting* (particle entrainment), and *sifting*. These segregation methods are illustrated in Figure 7.1.

Fluidization, or air entrainment, can cause vertical segregation, *i.e.*, horizontal layers of fines and coarse material. Fine powders generally have a lower permeability than coarse materials and therefore retain air longer. Thus, when a bin is being filled, the coarse particles are driven into the bed while the fine particles remain fluidized near the surface. Air entrainment often develops in materials that contain a significant percentage of particles below 100 μm in size. Fluidization segregation is also likely to occur when a bin is filled or discharged at high rates or if gas counter-flow is present. Segregation by the fluidization segregation mechanism is illustrated in Figure 7.1a.

Dusting, a.k.a particle entrainment or impact segregation, involves airborne particles, differences in settling velocities between particles, and air currents to cause movement of suspended particles. Dusting can occur when powder is dropped and impacts onto a pile surface, causing the release of finer particles into the air. Particles can also be re-entrained in air if large pockets of air bubble up through a stationary bed of material from below. These particles will tend to remain suspended in the air and be carried by air currents to the least active portion of the receiving vessel's area, generally the lowest part of the pile surface that is furthest away from the impact point. Generally, powders that are susceptible to this mechanism contain a portion of finer particles below 50 μm that do not readily adhere to larger particles. Dusting is illustrated in Figure 7.1b.

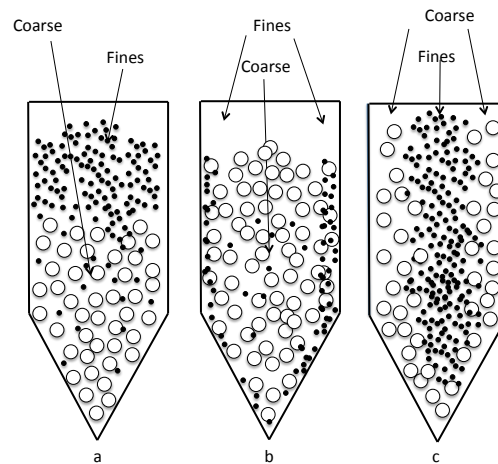


Figure 7.1. Segregation by fluidization (left), dusting (center), and sifting (right).

Sifting, which is illustrated in Figure 7.1c, occurs when smaller particles move through a matrix of larger ones. Four conditions must exist for sifting to occur:

- A difference in particle size between the individual components, typically a minimum ratio of 2:1 or greater.
- A sufficiently large mean particle size, typically one greater than approximately 500 μm .
- Free flowing material.
- Inter-particle motion.

All four of these conditions must exist for sifting segregation to occur. If any one of these conditions does not exist, the mix will not segregate by this mechanism.

Sifting segregation is also illustrated in Figure 7.2, which is a photograph of a typical pile that forms when a vessel is filled. Because coarser particles tend to be more mobile, they roll downward towards the periphery of the pile. Fines percolate through the bed as they fall from the center and accumulate in the middle. The result is side-to-side separation of particles by size.



Figure 7.2. Sifting segregation after formation of a pile.

Segregation can be controlled by changing the material or by changing the process. For example, fines can be extracted by sieving and perhaps be introduced later in the manufacturing process, granulated, or recycled. Impact and sifting segregation can be mitigated by adjusting the particle size such that the proportion of fines to coarse is approximately equal to the void fraction of the larger particles. Sometimes moisture or a weak binding agent can be added to reduce inter-particle motion, being careful not to increase the material's cohesive strength significantly enough to cause flow problems.

Changes to the manufacturing process include altering procedures and modifying or replacing equipment. The likelihood of segregation is frequently related to the rate at which the bulk material is handled. Increasing the discharge rate from a bin will often reduce the degree of segregation by allowing less time for segregation methods to progress. Smaller and more frequent batches reduce the scale at which segregation

mechanisms can progress. Altering the sequence of processing steps such as deferring mixing until a later stage of production can reduce segregation.

Segregation caused by fluidization can be reduced by eliminating long drops of material or by introducing the solids tangentially into a bin so that they contact the walls. Air entrainment can be reduced by proper venting. A telescoping chute that rises as a bin is filled will reduce fluidization segregation.

Sifting segregation is more common in funnel flow hoppers. Segregation can be reduced by keeping them nearly full (at the expense of surge or storage capacity) or continuously feeding and discharging from them at approximately the same rate. For the latter case, the bin will be acting as a standpipe.

In some cases, funnel flow can be changed to mass flow by installing a low-friction liner inside the hopper, replacing the hopper section with one designed for mass flow, or installing an insert. Sifting segregation is mitigated when the powder is handled in a mass flow bin because all the material is in motion during discharge.

There will be a solids velocity profile in the hopper section of a mass flow bin, however, as particles at the center will move at a faster velocity than those along the wall. To mitigate sifting segregation, having as uniform a velocity as possible is desirable.

Jenike realized that a radial velocity field was compatible with the radial stress field function that he solved when calculating flow factors. In his Bulletin 108¹², he solved the following equations to determine the velocity profile:

$$\frac{d\psi}{d\theta} = -1 - [ms \sin \delta (1 + \sin \delta) (\cot \theta \sin 2\psi + \cos 2\psi - 1) + \cos \theta - \sin \delta \cos(\theta + 2\psi) + s \cos^2 \delta] / [2s \sin \delta (\cos 2\psi - \sin \delta)] \quad (7.1)$$

$$\frac{ds}{d\theta} = \frac{s \sin 2\psi + \sin(\theta + 2\psi) + ms \sin \delta [\cot \theta (1 + \cos 2\psi) - \sin 2\psi]}{\cos 2\psi - \sin \delta} \quad (7.2)$$

¹² He also presents the equations in his Bulletin 123, but there's a typo. It happens to the best of us!

$$\psi(\theta') = \frac{1}{2} \left[\phi' + \sin^{-1} \left(\frac{\sin \phi'}{\sin \delta} \right) \right] + 90^\circ \quad (7.3)$$

$$\psi(90^\circ) = 90^\circ \quad (7.4)$$

$$\frac{V}{V_0} = \exp \left[-(2+m) \int_0^{\theta'} \tan(2\psi) d\theta \right] \quad (7.5)$$

where δ is the effective angle of friction, θ is the radial coordinate, ϕ' is the wall friction angle, ψ is the angle between the direction of the major principal stress and the radial coordinate ray, m is equal to 0 or 1 for planar flow and axisymmetric flow, respectively, s is the radial stress function, V is the radial velocity, and V_0 is the centerline velocity. Equations 7.3 and 7.4 describe the boundary conditions for Equation 7.1, which means that the set of equations present a split boundary problem. Can you imagine attempting to solve these equations without a computer? Jenike did! In his Bulletin 108, he gave the solution in graph form for δ equal to 50° , which is shown in Figure 7.3. It must have taken him months, which is probably why he only provided a solution for one value of the effective angle of friction.

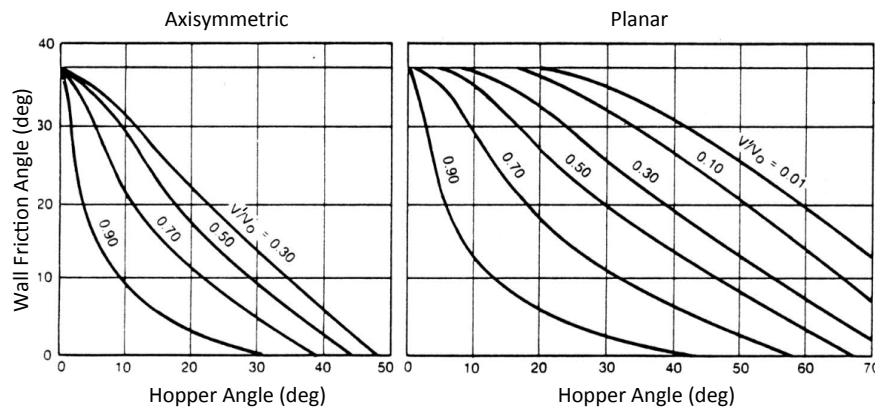


Figure 7.3. Wall-centerline velocity ratio, $\delta = 50^\circ$.

Even with computers, solving the equations is still a pain in the ass, but it can be done. Velocity profiles are plotted against dimensionless distance r/R , *i.e.*, the normalized distance from the hopper wall in Figures 7.4 and 7.5

for conical hoppers with angles of 20° and 30° from vertical, respectively and a bulk material with an effective angle of 50° .

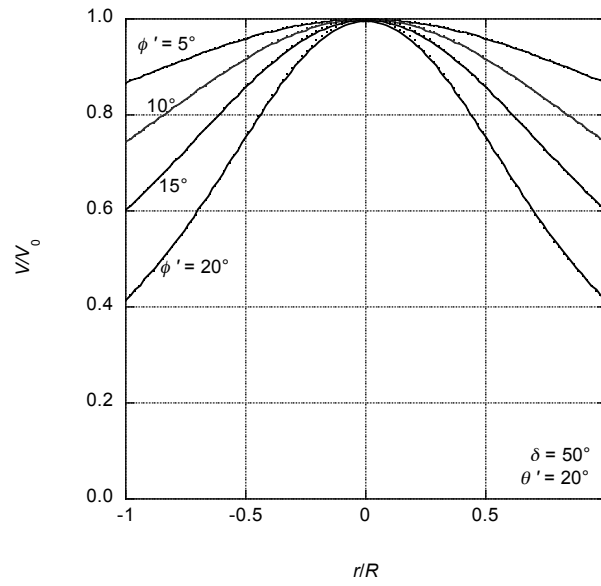


Figure 7.4. Velocity profiles for $\delta = 50^\circ$, $\theta = 20^\circ$, axisymmetric flow.

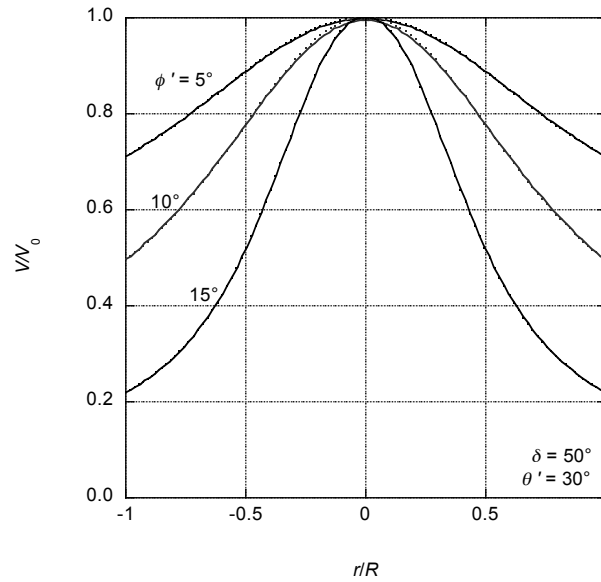


Figure 7.5. Velocity profiles for $\delta = 50^\circ$, $\theta = 30^\circ$, axisymmetric flow.

The ratio of the radial velocity at the wall V' to the centerline velocity V_0 is a good metric for the uniformity of the solids velocity. It can be considered the span of the solids velocity. Figures 7.6 through 7.13 are plots of V'/V_0 vs. hopper angle θ' for different values of the wall friction angle ϕ' .

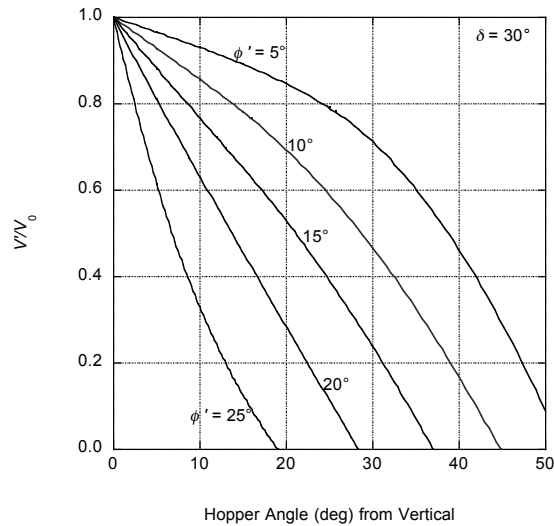


Figure 7.6. Wall-centerline velocity ratio, $\delta = 30^\circ$, axisymmetric flow.

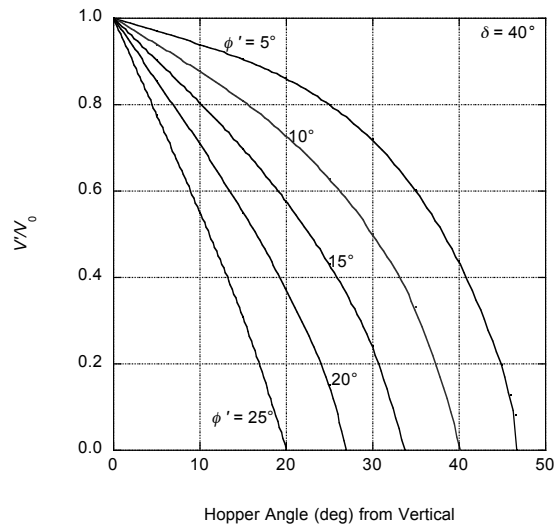


Figure 7.7. Wall-centerline velocity ratio, $\delta = 40^\circ$, axisymmetric flow.

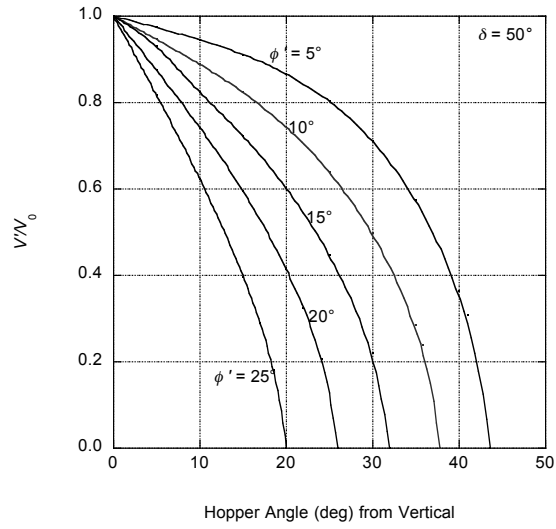


Figure 7.8. Wall-centerline velocity ratio, $\delta = 50^\circ$, axisymmetric flow.

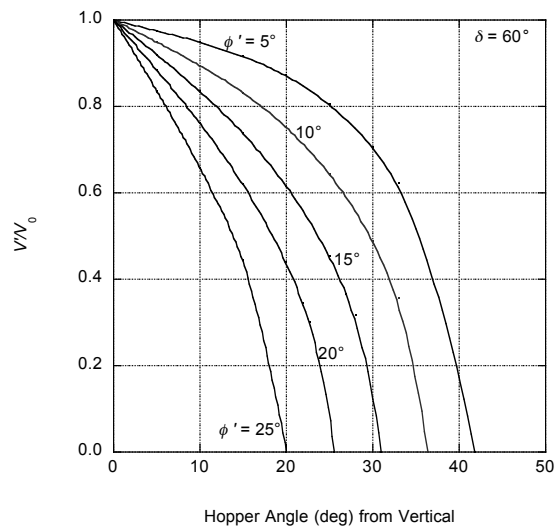


Figure 7.9. Wall-centerline velocity ratio, $\delta = 60^\circ$, axisymmetric flow.

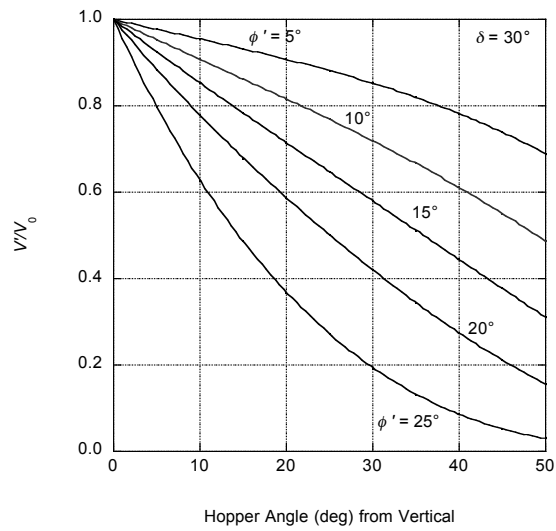


Figure 7.10. Wall-centerline velocity ratio, $\delta = 30^\circ$, planar flow.

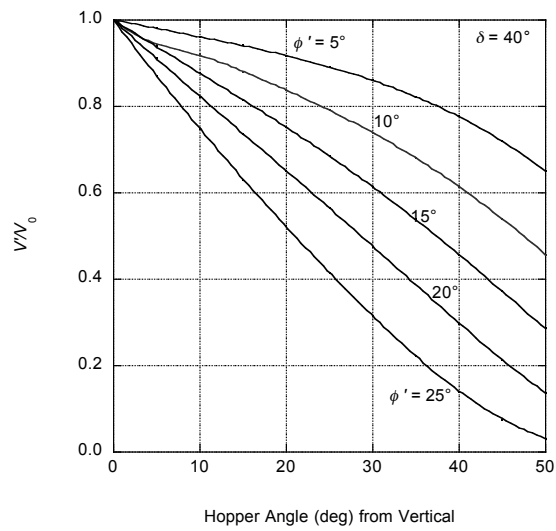


Figure 7.11. Wall-centerline velocity ratio, $\delta = 40^\circ$, planar flow.

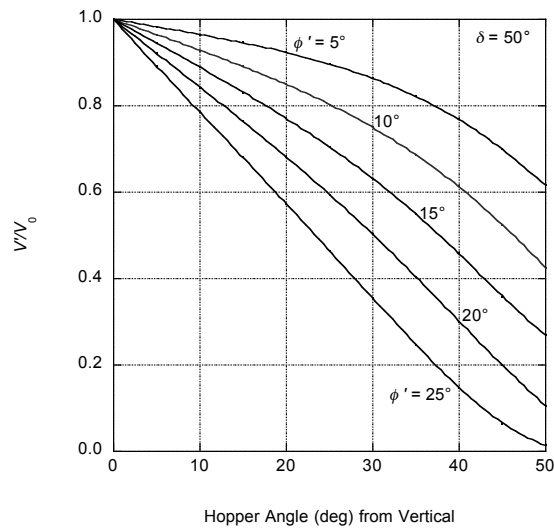


Figure 7.12. Wall-centerline velocity ratio, $\delta = 50^\circ$, planar flow.

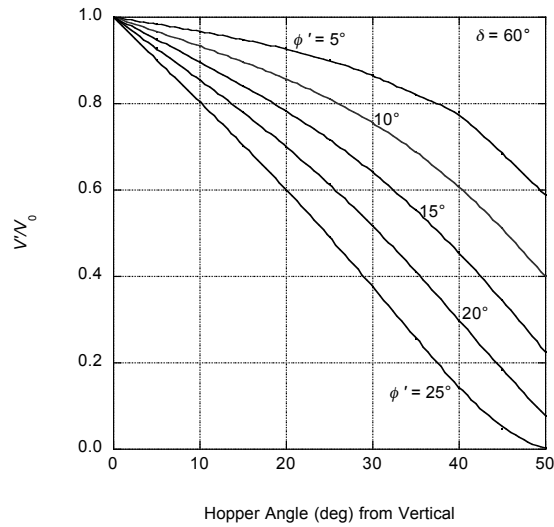


Figure 7.13. Wall-centerline velocity ratio, $\delta = 60^\circ$, planar flow.

Figures 7.14 – 7.21 plot the ratio of the average solids velocity to the centerline velocity. To minimize sifting segregation that occurs during filling of a hopper, it is best to design a mass flow hopper that allows a high average solids velocity to centerline velocity ratio.

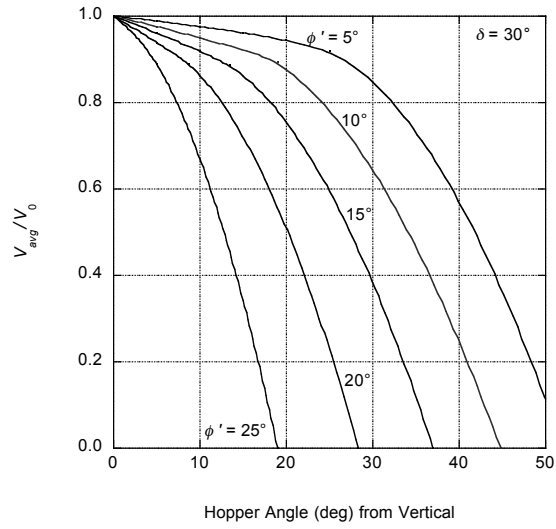


Figure 7.14. Average-centerline velocity ratio, $\delta = 30^\circ$, axisymmetric flow.

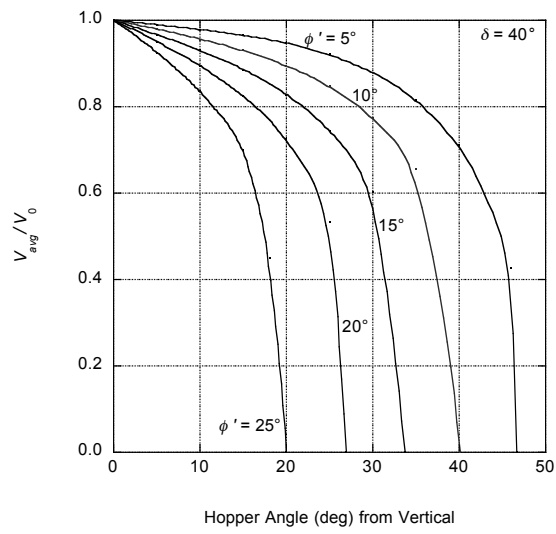


Figure 7.15. Average-centerline velocity ratio, $\delta = 40^\circ$, axisymmetric flow.

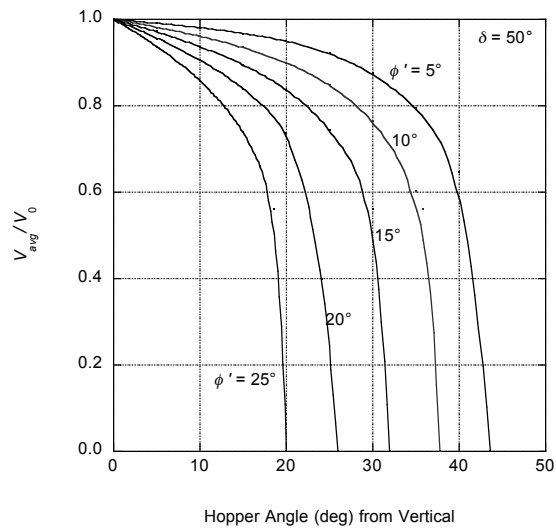


Figure 7.16 Average-centerline velocity ratio, $\delta = 50^\circ$, axisymmetric flow.

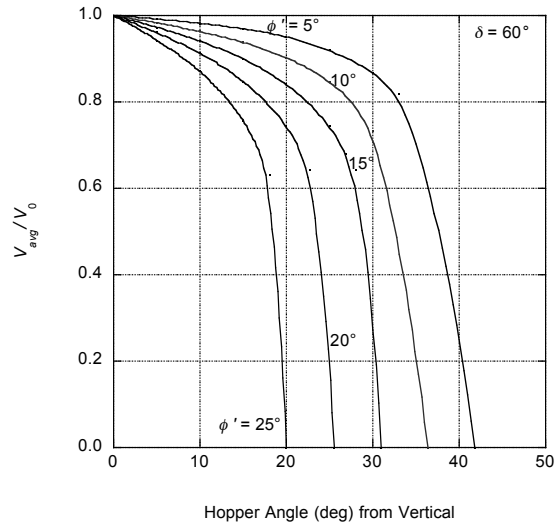


Figure 7.17 Average-centerline velocity ratio, $\delta = 60^\circ$, axisymmetric flow.

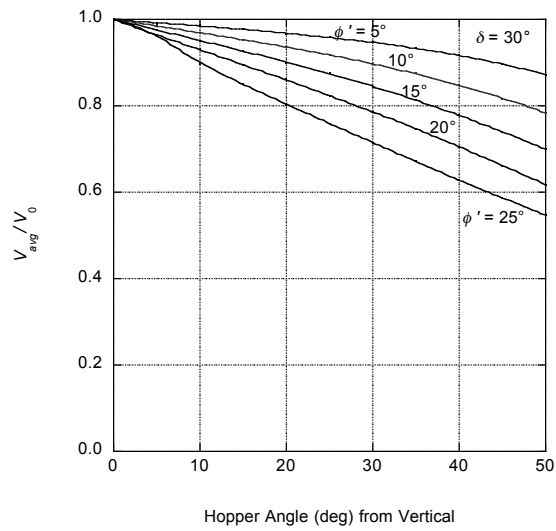


Figure 7.18. Average-centerline velocity ratio, $\delta = 30^\circ$, planar flow.

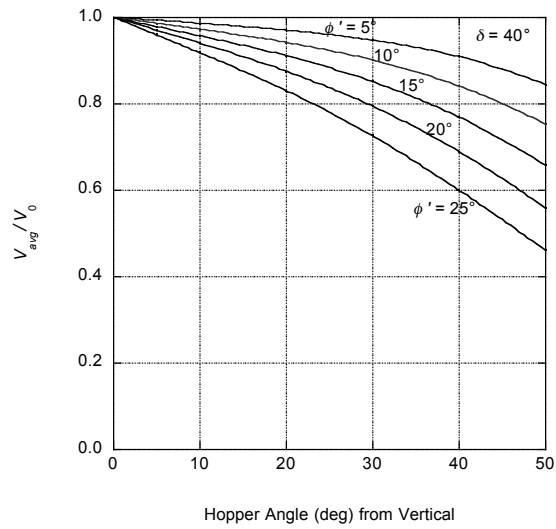


Figure 7.19. Average-centerline velocity ratio, $\delta = 40^\circ$, planar flow.

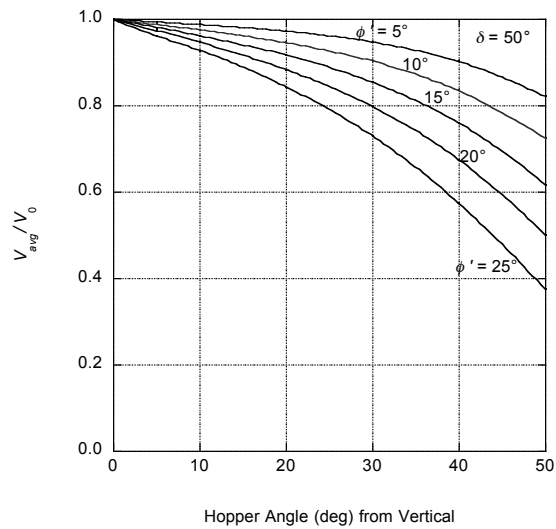


Figure 7.20. Average-centerline velocity ratio, $\delta = 50^\circ$, planar flow.

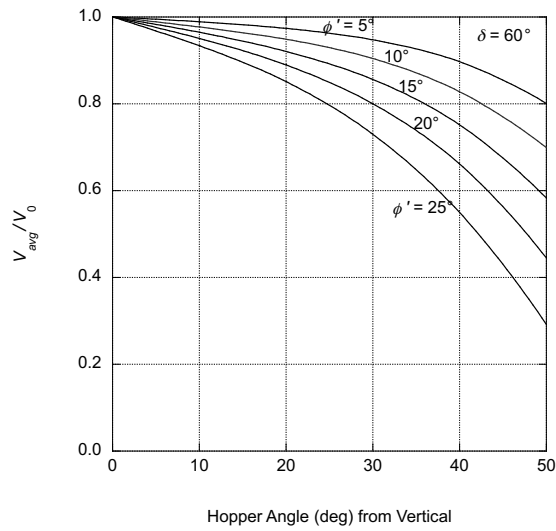


Figure 7.21. Average-centerline velocity ratio, $\delta = 60^\circ$, planar flow.

Devices such as inflow dispersion cones or plates can be used to avoid creating a surcharge upon filling, which can lead to sifting segregation. Figure 7.22 is a schematic of such a device. The disperser is comprised of

an inverted cone above a ring that has equally spaced extensions that redirect approximately one half of the particles when they travel past the cone. This results in mixing of the particles as they fall inside the silo.

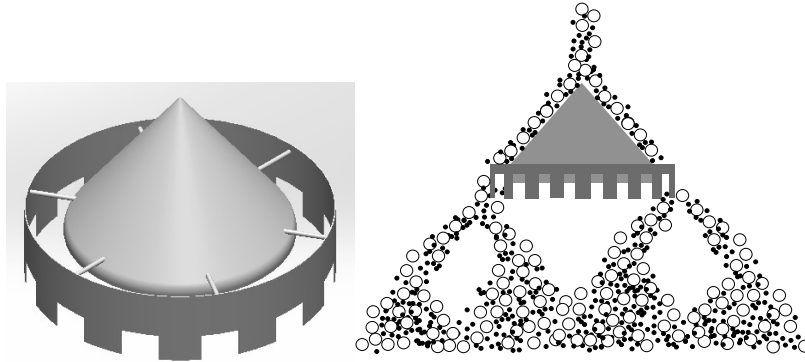


Figure 7.22. Dispersion cone schematic.

If the particles fall freely when they are dropped onto the chute, their velocity before impact V_0 is its free-fall velocity:

$$V_0 = \sqrt{2gh} \quad (7.6)$$

where g is the acceleration due to gravity and h is the drop height (see Figure 7.23).

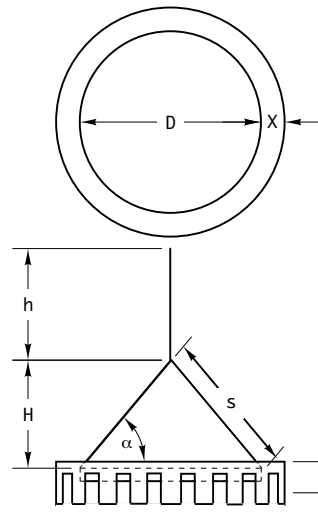


Figure 7.23. Dispersion cone and ring dimensions.

From a momentum balance, V_1 , the velocity of the particles after impact (see Figure 7.24), is given by:

$$V_1 = V_0(\cos\theta - \sin\theta \tan\phi') \quad (7.7)$$

where θ is the impact angle and ϕ' is the angle of wall friction.

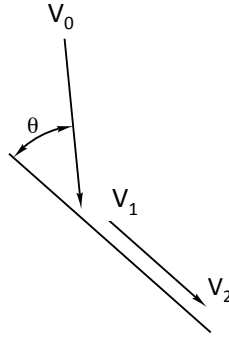


Figure 7.24. Velocity after impact and sliding.

While sliding on a straight surface, the particles accelerate or decelerate, depending on the relative magnitudes of the cone angle α (measured from horizontal) and the wall friction angle:

$$a = g(\sin\alpha - \cos\alpha \tan\phi') \quad (7.8)$$

where a is the acceleration. The particles continue to accelerate (provided that $\alpha > \phi'$), and its velocity V_2 reaches at the end of the cone:

$$V_2 = \sqrt{V_1^2 + 2aS} \quad (7.9)$$

where S is the distance traveled and is calculated from

$$S^2 = \left(\frac{D}{2}\right)^2 + H^2 \quad (7.10)$$

where D is the diameter of the cone and H is its height. Typically, D is approximately one third the diameter of the bin. The height can be calculated from the diameter and cone angle from

$$H = \frac{D \tan\alpha}{2} \quad (7.11)$$

The particles continue to accelerate after leaving the cone; the distance X and Y traveled over time t can be calculated from:

$$X = (V_2 \cos \alpha)t \quad (7.12)$$

and

$$Y = (V_2 \sin \alpha)t + \frac{g}{2}t^2 \quad (7.13)$$

respectively. Referring to Figure 7.23, X is equal to the difference between the radii of the cone and the ring, and Y should be chosen such that the particles impact the extensions from the ring. Combining Equations 7.12 and 7.13 and simplifying yields

$$Y = X \tan \alpha + \frac{g}{2} \left(\frac{X}{V_2 \cos \alpha} \right)^2 \quad (7.14)$$

Surcharge and subsequent segregation due to sifting can be reduced filling the bin from multiple locations. For smaller bins, a screw conveyor with an opening that widens linearly and extends over the full length of the bin can be used.

There are testers available for determining the “propensity” of a powder to segregate by particle size by aggressively handling it in a way that segregation is most probable. Much simpler methods exist. A test that will determine if sifting segregation is a potential problem is to pour a well-mixed sample of powder onto a flat surface to form a pile and then compare the particle size of a subsample taken from the center to that taken from the periphery. To determine if fluidization segregation is a concern, a sample can be poured into, say, a 3-ft tall, 1-in. diameter or similarly dimensioned cylinder. Then, the particle size of a subsample taken from the bottom of the cylinder is compared to that from the top surface. Of course, careful handling, such as ensuring that a mass flow hopper is used and that long vertical drops are avoided, can prevent segregation problems from occurring in the first place.

Caking

Caking occurs when an easy-flowing powder becomes cohesive after storage or transport, forming agglomerates comprised of individual particles that are bonded together. As a consequence, a powder that flowed freely during packaging may contain lumps when the package is opened by a customer; a silo that readily discharges a bulk material when in continuous operation may become constipated after a shutdown. A bulk solid from one production lot may meet performance requirements, but one taken from another lot may be deficient. In extreme cases, dealing with problems created by caked materials can subject personnel to dangerous situations. For example, the sudden collapse of the caked material has caused silos to collapse.

Caking is frequently moisture-induced. When the moisture content of a bulk material reaches a critical value, moisture will condense primarily at the contact points between adjacent particles, causing liquid bridges. If local drying occurs due to temperature swings during storage or transit, solid bridges may form when soluble components in the liquid precipitate. Water is also a plasticizer for many materials, and its presence can cause particles to deform and increase inter-particle contact area. Elevated temperature and impurities also frequently increase the likelihood of a material to cake.

Caking occurs when the magnitude of inter-particle forces increases significantly over time. These cohesive forces are primarily van der Waals forces, polar interactions, and forces associated with plastic creep or liquid bridges (when moisture is present). van der Waals forces include all intermolecular forces that act between electrically neutral molecules. Polar interactions occur when adjacent particles contain regions that are permanently electron-rich or electron-poor. van der Waals forces and polar interactions increase as the distance between particles decreases. Although these forces are proportional to particle size, the likelihood of caking generally decreases with increasing particle size since the number of inter-particle contacts is inversely proportional to the square of the particle diameter.

With some bulk materials, plastic creep, which is the tendency of a material to deform when under consolidation, may occur. Plastic creep can be severe if impurities that behave as plasticizers are present or if the bulk solid is subjected to high temperatures for long periods of time, especially when above its glass transition temperature (T_g). Differential scanning calorimetry (DSC), thermal mechanical analysis (TMA), and inverse gas chromatography (IGC) are frequently used to measure T_g . IGC is preferable over the other methods if moisture is known to act as a plasticizer since tests can be conducted at a constant relative humidity.

Liquid bridging occurs when moisture accumulates at the contact points between adjacent particles. The likelihood of liquid bridging can often be inferred from a powder's moisture sorption isotherm, which relates relative humidity (RH) or activity, which is RH expressed as a fraction, and equilibrium moisture content. Examples of moisture isotherms that are characteristic of bulk materials prone to caking are shown in Figure 7.25.

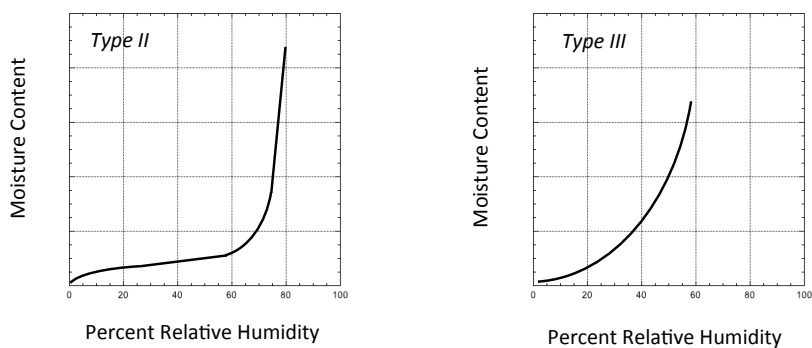


Figure 7.25. Example isotherms.

The Type II moisture isotherm is typical when moisture adsorbs onto the surface of a solid particle. It is initially linear as water molecules are adsorbed until a monolayer is formed. The effect of moisture on caking is generally negligible in this region. As relative humidity increases, multilayer adsorption takes place as a consequence of hydrogen bonding. In this region, the slope of the isotherm is initially shallow but steepens with increasing relative humidity. As moisture uptake increases, the particles become surrounded by moisture. If the solids are water soluble, the layer of moisture can be viscous, and the bulk material may become cohesive.

The third region occurs at high relative humidity, where the equilibrium moisture content increases dramatically. In this region, most of the

incremental condensation takes place at the contact points between particles. This phenomenon is known as capillary condensation. The moisture content at this inflection point on the isotherm is sometimes called the *critical moisture content* or CMC, and its corresponding equilibrium relative humidity is the *critical relative humidity* or CRH. The CRH is also the ratio of the water vapor pressure over a saturated solution of the solid to the vapor pressure of pure water, times 100. Exceeding the critical moisture content or CRH likely will result in caking, and *über* caking if the solid is at least partially soluble in water and solid bridges form if the moisture evaporates.

The Type III isotherm shown on the right is concave upward from the get go and is characteristic of powders that are readily soluble in water. Moisture not only adsorbs onto the surface; it also readily penetrates inside. The moisture content or RH at which caking can be expected may not be obvious.

Water is a universal plasticizer. An increase in a powder's moisture content or activity or an increase in the relative humidity of the interstitial and surrounding air can lower the material's glass transition temperature. The glass transition temperature as a function of relative humidity can be determined by inverse gas chromatography (IGC).

There are other types of isotherms. The Type II is frequently modeled by the Guggenheim, Anderson, and de Boer equation and Type III is often described by Flory-Huggins. Other models, such as one derived by Valdez, Paredes, Vargas-López, and Hernández [*Food and Nutrition Sciences*, 5, 153 (2014)], can be used to describe complex isotherms. I haven't run the statistics, but I'm fairly certain that there is a correlation between the number of authors of a model and the number of its empirical parameters.

Conditions that can lead to moisture-induced caking can frequently be gleaned from moisture sorption tests and glass transition temperature measurements. The critical relative humidity or the relative humidity that causes the glass transition temperature of a powder to fall below its storage temperature can be correlated with the powder's moisture content through its moisture sorption isotherm. This moisture level can serve as a spec that should not be exceeded.

Any moisture limits to avoid caking that are based on equilibrium moisture content should account for the possibility of moisture migration. This occurs when a temperature gradient exists during packaging, storage, or

transit of powders. The mechanism of caking due to moisture migration is as follows:

- The relative humidity of the interstitial air at the warm boundary decreases.
- As a consequence, moisture desorbs from the warmer solids, as the solids and interstitial air are no longer in equilibrium.
- The *absolute* humidity of the interstitial air increases.
- The driving force in the gas phase leads to moisture migration toward the interior, which has a lower absolute humidity.
- The relative humidity of the cooler interstitial air increases.
- Moisture adsorbs onto solids in the interior in an effort to re-establish equilibrium.

Moisture migration is illustrated in Figure 7.26.

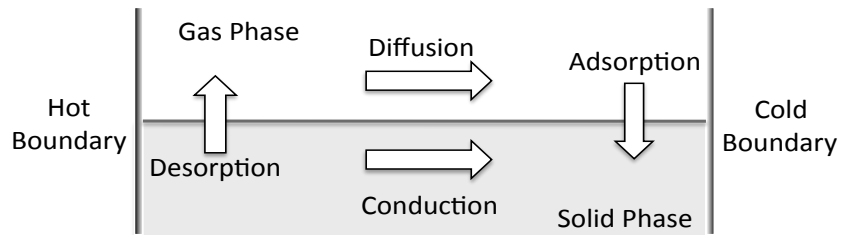


Figure 7.26. Schematic describing moisture migration.

An analysis can be performed to determine the moisture distribution in a bulk solid that will result if a temperature gradient (*e.g.*, if product pack-out temperatures exceed storage temperatures or if storage temperatures vary) is imposed. One assumes that the temperature gradient remains constant. Since this is not true, the analysis results in a conservative view of possible conditions that can exist if temperature differences were to remain for an extended time.

The analysis is as follows. If a bulk solid were exposed to a warm surface (temperature = T_H) on one side and a cool surface (temperature = T_C) on the other, the temperature profile at steady state would be given by:

$$T = T_C + (T_H - T_C)z \quad (7.15)$$

where z is the ratio of the distance from the cold surface to the distance between the hot and cold surfaces.

At steady state, the concentration of water in the interstitial air C_w , is constant. The vapor phase moisture concentration (C_{wv}) is the product of the absolute humidity H and the dry air density ρ_a :

$$C_w = \rho_a H \quad (7.16)$$

The relative humidity RH is related to absolute humidity by

$$\frac{RH}{100} = \frac{29HP_t}{(18 + 29H)P_w^{sat}} \quad (7.17)$$

where P_t and P_w^{sat} are the total pressure and saturation pressure of pure water, respectively. Due to the temperature gradient, the relative humidity of the interstitial air will vary. As a result, the amount of condensed moisture that is in equilibrium with the interstitial air will also vary. The relationship between the solid's equilibrium moisture content X and the relative humidity of the interstitial air RH is given by the material's isotherm. Since the amount of moisture in the gas phase is negligible compared to that in the solid, the total amount of moisture in the solid after migration can be assumed to be equal to the initial solid moisture content X_0 , *i.e.*,

$$\bar{X} = \int_z X(z)dz = X_0 \quad (7.18)$$

A specification for a bulk material's moisture content that, if exceeded, causes caking (as determined from unconfined yield strength measurements) can be determined by finding the value of C_w that satisfies Equations 7.17 and 7.18 and the material's moisture isotherm.

Pneumatic conveying

Facilities that handle bulk solids invariably need to transport material from one location to another. It is usually advantageous to have various storage vessels and equipment at different elevations so that gravity can do the job. In many cases, however, powders must be transported horizontally or vertically upward, which requires the use of conveyors such as screw, belt, and tubular conveyors, hoists and bucket elevators, or pneumatic conveying lines.

Pneumatic conveying is the transfer of particulate solids in a gas stream. Compared to other conveying technologies, pneumatic conveying offers a number of advantages, including:

- Flexibility in layout.
- Discharge to and pick-up from multiple locations.
- Dust-free operation.

Pneumatic conveying systems do have some disadvantages, however, such as:

- High power requirements.
- Abrasive wear, especially in elbows.
- Attrition of particles.

Systems operating above atmospheric pressure are known as *pressure systems* or sometimes *push systems* since material is “pushed” from a pick-up point to a destination point. Conversely, systems operating below

atmospheric pressure suck. They are known as *vacuum systems* or *pull systems*. Pull systems can have multiple feed points, but their overall pressure drop is limited to 1 atm. Push systems allow a greater overall pressure drop, are able to accommodate multiple destination points, and can provide higher capacities at longer distances. Push and pull pneumatic conveying systems are shown in Figures 7.36 and 7.37, respectively.

Pneumatic conveying systems can be classified into two divisions: *dense-phase* and *dilute-phase*. The divisions are sometimes ambiguous, but often they can be inferred from a state diagram. A state diagram, also known as a Zenz diagram, plots pressure gradient against superficial gas velocity when solids are conveyed in a horizontal pipe. Figure 7.38 is an illustration of a state diagram.

At high gas velocities, the system is operating in dilute phase. As the gas velocity is decreased, the pressure gradient decreases until a minimum is reached. This critical velocity corresponds to the system's saltation velocity, the velocity that must be exceeded to keep the solids moving. Past this point, any reduction in gas velocity will result in an increased pressure drop due to a dramatic deposition of solids. With some solids, but not all, material can still be conveyed at low gas velocities in dense phase as slugs or dunes.

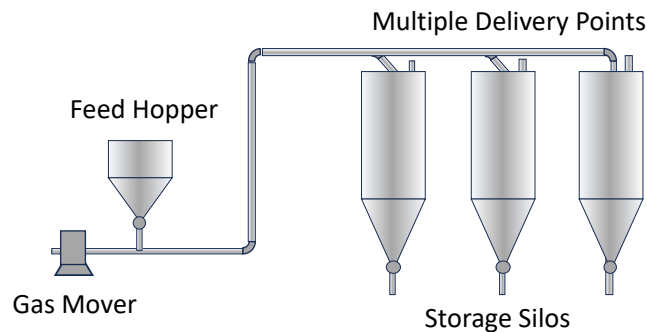


Figure 7.36. Pressure system.

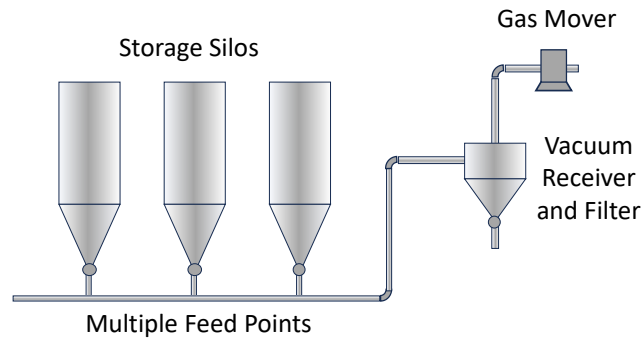


Figure 7.37. Vacuum system.

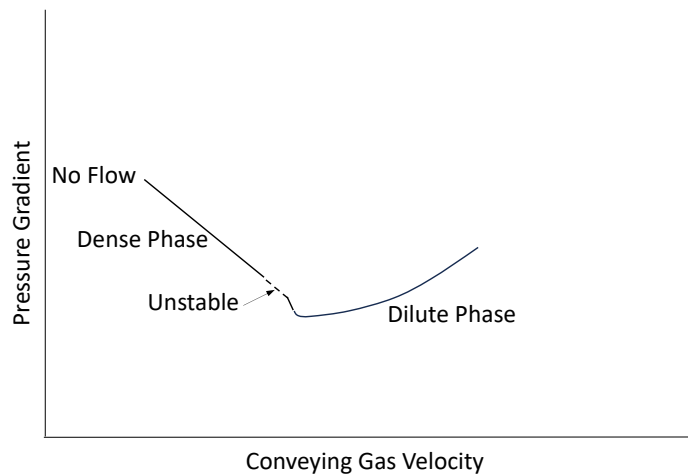


Figure 7.38. State diagram.

The state diagram can be expanded to give the relationship between the pressure gradient, superficial gas velocity, and solids feed rate. Consider the system described in Figure 7.39 operating with solids mass flow rates of $W_{s1} < W_{s2} < W_{s3}$. You would think that increasing the gas velocity would allow a greater solids feed rate. However, the maximum permissible pressure drop is limited by the gas mover. If the system gas velocity is instead *reduced* from point A to point B, you'll be able to increase the solids mass flow rate from W_{s1} to W_{s3} . By lowering the gas velocity, additional solids can be conveyed, which is somewhat counterintuitive. Unfortunately, many engineers wanting to stretch conveying capacity will buy a bigger blower, only to find that the maximum possible solids feed rate is now lower. Sad!

Each of the curves of the state diagram has a minimum. Constructing a line through the minima gives a pressure minimum curve, from which the minimum conveying velocity can be inferred. When coarse particles are conveyed, saltation usually occurs at the pressure minimum. With fine particles, saltation often occurs before the minimum pressure point. The pressure minimum curve also gives the optimal operating condition from an energy consumption perspective. Note that as the solids become dilute, the shape of the curves of the state diagram resemble that of the curve representing gas flow with no solids.

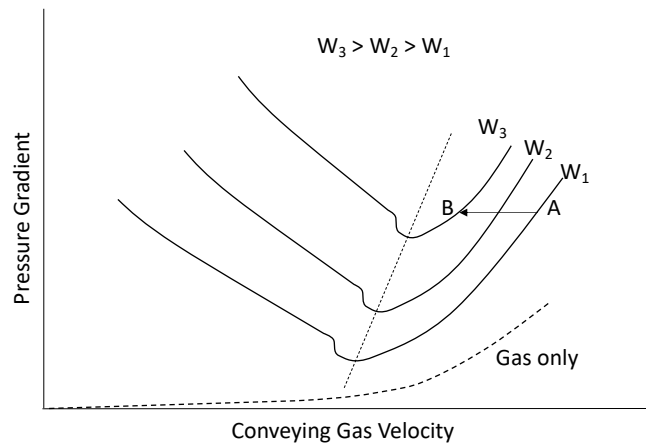


Figure 7.39. Optimization of conveying system.

Saltation velocity

The saltation velocity is the superficial gas velocity that must be exceeded to ensure that the solids will be conveyed. It is best determined by testing on a pilot pneumatic conveying system. Design equations exist, but they are best used for developing a preliminary design or troubleshooting existing systems.

The Rizk equation is frequently used:

$$v_s = \left[\frac{W_s (\sqrt{gD})^k 10^\delta}{\rho_g A} \right]^{\frac{1}{k+1}} \quad (7.53)$$

where v_s is the saltation velocity, W_s is the solids mass flow rate, g is acceleration due to gravity, D is the pipe diameter, ρ_g is the density of the drying gas, A is the pipe cross-sectional area, and δ and κ are parameters given by the following equations:

$$\delta = 1.44d_p + 1.96 \quad (7.54)$$

$$\kappa = 1.1d_p + 2.5 \quad (7.55)$$

where d_p is the particle diameter. Equations 7.54 and 7.55 are dimensional with d_p in millimeters. The accuracy of the Rizk equation is approximately ± 50 percent, so using the Rizk equation can be “Rizky”.

For fine particles, Matsumoto’s method is used to calculate solids loading ratio at saltation ϕ_s , *i.e.*, the ratio of the solids mass flow rate W_s to the gas mass flow rate W_g . The solids loading ratio is also called the phase ratio. The saltation velocity depends on the value of a critical particle diameter d_p^* , which is calculated from

$$\frac{d_p^*}{D} = 1.39 \left(\frac{\rho_s}{\rho_g} \right)^{-0.74} \quad (7.56)$$

where ρ_s is the particle density.

For $d_p \geq d_p^*$,

$$\phi_s = 0.373 \left(\frac{\rho_s}{\rho_g} \right)^{1.06} \left(\frac{u_t}{10\sqrt{gd_p}} \right)^{-3.7} \left(\frac{v_s}{10\sqrt{gD}} \right)^{3.61} \quad (7.57)$$

where the terminal velocity u_t can be estimated from

$$u_t = 1.74 \sqrt{\frac{gd_p(\rho_s - \rho_g)}{\rho_g}} \quad (7.58)$$

For $d_p < d_p^*$,

$$\phi_s = 0.556 \left(\frac{d_p}{D} \right)^{1.43} \left(\frac{v_s}{\sqrt{gD}} \right)^4 \quad (7.59)$$

The saltation velocity v_s is related to ϕ_s by

$$v_s = \frac{W_s}{\phi_s \rho_g A} \quad (7.60)$$

In general, the recommended minimum conveying velocity is at least twenty percent greater than v_s to avoid plugging or unstable conveying. Representative minimum conveying velocities are listed in Table 7-1 (Glinzing *et al.*, Pneumatic Conveying of Solids – A Theoretical and Practical Approach, Springer, New York, 2010). Note that the velocities given in the vacuum conveying column are probably greater than necessary.

In some applications, there can be a maximum allowable conveying velocity, since high velocities can result in excessive abrasive wear, particle attrition, or the formation of streamers or angel hair (see Figure 7.40).

For vertical lines, choking, which occurs when solids cannot be carried upward, must be avoided. The choking velocity can be calculated from

$$v_c = 32 \sqrt{gd_p} \text{Re}_p^{-0.06} \phi^{0.28} \quad (7.61)$$

The particle Reynolds number Re_p is given by

$$\text{Re}_p = \frac{\rho_g u_t d_p}{\eta} \quad (7.62)$$

Other equations exist, but because the choking velocity is usually lower than the saltation velocity, the saltation velocity v_s is generally used in the design of dilute-phase pneumatic conveying systems.

Table 7-1				
Representative Minimum Conveying Velocities				
Material	Bulk Density (kg/m³)	Particle Size (μm)	Min. u_p Push Systems (m/s)	Min. u_p Pull Systems (m/s)
Coal	720	13000	15	-
Coal	720	6000	12	-
Wheat	750	5000	12	-
Polyethylene	480	3000	12	-
Cement	1400	90	7.6	-
Flour	560	150	4.6	-
Pulverized Coal	720	75	4.6	-
Pulverized Coal	720	150	4.6	-
Salt	1400	150	9.1	-
Alumina	930	110	7.6	-
Magnesite	1600	75	9.0	-
Uranium Dioxide	3500	75	18	-
Sodium Sulfate	1400	110	12	-
Alumina	800	-	20	34
Calcium Carbonate	440	-	20	34
Coffee Beans	670	-	14	23
Hydrated Lime	480	-	12	27
Malt	450	-	17	30
Oats	400	-	17	30
Salt	1400	-	25	37
Starch	640	-	17	27
Sugar	800	-	18	34
Wheat	770	-	17	32

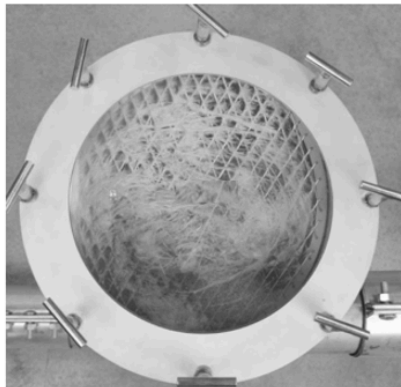


Figure 7.40. Angel hair from pneumatic conveying line (left) and my local grocery store (right).

Pressure drop

The procedure for designing a pneumatic conveying system is similar to that used to analyze compressible flow through a pipe. Contributions to the overall pressure drop ΔP_{total} include that of the conveying gas ΔP_{gas} , acceleration of the solids ΔP_{acc} , lifting the solids ΔP_{lift} , deceleration and reacceleration around elbows ΔP_{bend} , solids friction ΔP_{solids} , and the gas-solids separator $\Delta P_{separation}$:

$$\Delta P_{total} = \Delta P_{gas} + \Delta P_{acc} + \Delta P_{lift} + \Delta P_{bend} + \Delta P_{solids} + \Delta P_{separation} \quad (7.63)$$

The greater the total pressure drop, of course, the greater the power requirements of the gas mover. For low overall pressure drops, a radial-blade centrifugal fan can be used. For greater pressure drops, Roots-type blowers are commonly used. Compressors must be used when pressure differentials exceed *ca.* 1.2 bar.

Gas pressure drop

The gas-only pressure drop is calculated using customary methods based on the friction factor f and the velocity head $u_g^2/2g$:

$$\Delta P_{gas} = f \frac{\rho_g u_g^2}{2} \frac{L}{D} \quad (7.65)$$

where L is the length of the pipe. A handy equation explicit in f is the Sacham equation:

$$f = \left(-2 \log \left[\frac{\frac{\varepsilon}{D}}{3.7} - \frac{5.02}{\mathbf{Re}} \log \left(\left[\frac{\frac{\varepsilon}{D}}{3.7} + \frac{14.5}{\mathbf{Re}} \right] \right) \right] \right)^{-2} \quad (7.66)$$

where \mathbf{Re} is the Reynolds number and ε/D is the relative roughness of the pipe. The Reynolds number is

$$\mathbf{Re} = \frac{\rho_g u_g D}{\eta} \quad (7.67)$$

where η is the viscosity of the conveying gas.

Acceleration pressure drop

The pressure drop that results from acceleration of the gas and solids can be calculated using a method given by Glinzing *et al.*:

$$\Delta P_{acc} = \frac{\rho_g u_g^2}{2} \left[1 + 2\phi \frac{u_p}{u_g} \right] \quad (7.68)$$

where u_p is the particle velocity and the phase ratio ϕ is given by

$$\phi = \frac{W_s}{\rho_g A u_g} \quad (7.69)$$

The particle-to-gas-velocity ratio can be calculated by a relation given in Barton Hinkle's Georgia Tech PhD dissertation:

$$\frac{u_p}{u_g} = 1 - 0.044 d_p^{0.3} \rho_s^{0.5} \quad (7.70)$$

or the IGT correlation

$$\frac{u_p}{u_g} = 1 - 0.68 d_p^{0.92} \rho_s^{0.5} D^{-0.54} \rho_g^{-0.2} \quad (7.71)$$

Equations 7.70 and 7.71 are dimensional. The units for d_p are meters and the units for density are kg/m³. The units of velocity are m/s.

Lift pressure drop

The pressure drop due to lift is given by

$$\Delta P_{lift} = [\varepsilon \rho_g + (1 - \varepsilon) \rho_s] g \Delta z \quad (7.72)$$

where

$$\varepsilon = 1 - \frac{W_s}{\rho_s A u_p} \quad (7.73)$$

Equation 7.70 or 7.71 is used to calculate the particle velocity u_p .

Bend pressure drop

Instead of using equivalent lengths, which is frequently done in the analysis of fluid flow in pipes, the pressure drop in elbows in pneumatic conveying systems is calculated separately for each elbow. As solids enter a bend, they tend to form a rope of material that slides along the outer wall of the elbow. This causes the solids to decelerate, but then they reaccelerate when leaving the bend.

The bend pressure drop can be calculated from

$$\Delta P_{bend} = B(1 + \phi) \frac{\rho_g u_g^2}{2} \quad (7.74)$$

where B is the bend factor. The bend factor depends on R/D , the ratio of the bend radius to the pipe diameter, as given in Table 7-2.

Table 7-2	
Bend Factors	
R/D	B
2	1.50
4	0.75
≥ 6	0.50

Solids friction pressure loss

The equation used to calculate the pressure drop due to friction is similar to the equation for calculating the gas pressure drop except that the phase ratio ϕ is included:

$$\Delta P_{solids} = \phi f_s \frac{\rho_g u_g^2}{2} \frac{L}{D} \quad (7.75)$$

where f_s is the solids friction factor. For horizontal conveying, the solids friction factor is given by

$$f_s = K \phi^a \mathbf{Fr}^b \mathbf{Fr}_s^c \left(\frac{D}{d_p} \right)^d \quad (7.76)$$

where the Froude numbers \mathbf{Fr} and \mathbf{Fr}_s are given by¹³

$$\mathbf{Fr} = \frac{u_g^2}{gD} \quad (7.77)$$

and

$$\mathbf{Fr}_s = \frac{u_t^2}{gd_p} \quad (7.78)$$

and K , a , b , c , and d are parameters given in Table 7-3.

Table 7-3		
Solids Friction Factor Parameters		
Constant	> 500 μm	< 500 μm
K	0.082	2.1
a	-0.3	-0.3
b	-0.86	-1
c	0.25	0.25
d	0.1	0.1

For vertical conveying,

$$f_s = \frac{u_g}{1200u_p} + \frac{2u_g}{u_p \mathbf{Fr}} \quad (7.79)$$

In most cases, the relationship between the differential pressure of the separator and the volumetric flow rate of the gas is provided by the equipment vendor. Bag filters are the most common, and the differential pressure in most units range ranges between 2 and 8 in. H₂O (500 - 2000 Pa). Bag filter suppliers generally shoot for an air-to-cloth ratio based on the gas volumetric flow rate and the particle size of the solids that gives an acceptably low pressure drop. In most cases, solids loading does not come into play.

¹³ Not a typo! The Froude number is typically defined as the velocity divided by the square root of the product of g and the diameter, but not in this case.

Some things to consider

If a positive displacement blower is to be used, blow the dust off your thermodynamics book and look up the adiabatic temperature rise formula. The gas density is inversely proportional to the absolute temperature and coolers may be necessary to prevent problems that stem from high temperatures such as the creation of angel hair.

The terms SCFM (standard cubic feet per minute) and Nm³/hr (normal cubic meters per hour) can be confusing. A standard cubic foot is the volume of a gas at 1 atm pressure and 60°F, while a normal cubic meter is its volume at 1 bar and 0°C. Chemists, bless their hearts, prefer to use STP (standard temperature and pressure) where the temperature is equal to 0°C and the pressure equals 1 atm. Always be sure that you are using actual volumes in your calculations.

The gas mass density can be calculated from the ideal gas law:

$$\rho_g = M_g \frac{P}{RT} \quad (7.80)$$

where M_g is the molecular weight of the gas (29 kg/kmol for air), P is the pressure, R is the ideal gas constant, and T is the *absolute* temperature. (Don't forget to add 460 if your temperature is in degrees Fahrenheit or 273 if it is in degrees Canadian.)

The recommended radius of a bend is 4 to 6 times the pipe diameter. Abrasive wear of pneumatic conveying lines and attrition of particles are more likely at elbows. Products such as Hamertek's Smart Elbow deflect solids away from the curved walls. Blind tees are simpler but suffer from high pressure drops.

A horizontal pipe section should follow the solids feed point. The distance between the feed point and the first bend should be 25 to 50 times the pipe diameter to allow acceleration of the solids.

The end of the line has the lowest pressure and therefore the highest velocity. Some systems are stepped, that is, the pipe diameter of downstream sections are higher to lower the gas velocity and reduce wear and attrition and to reduce the overall pressure drop and gas mover power requirements.

Sloping sections are not recommended as they can cause instabilities, especially at low gas velocities. Instead, horizontal and vertical runs should be used. The number of bends should be kept at a minimum to prevent too great of a pressure drop, and bends should not be placed close to each other.

Example

Design a dilute-phase pneumatic conveying system that can handle a coarse powder made up of 2-mm diameter particles having a particle density of 950 kg/m³. The proposed layout is drawn in Figure 7.41. The solids feed rate is 5,000 kg/hr. The gas temperature is 20°C.

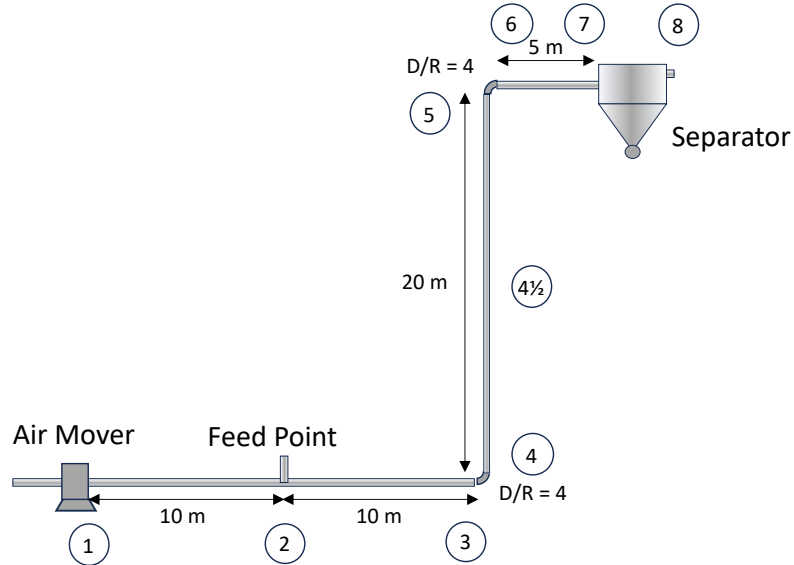


Figure 7.41. Proposed dilute-phase conveying system.

Step 1. Calculate saltation and conveying velocity. Since the particles are large, use the Rizk equation with $\delta = (1.44)(2) + 1.96 = 4.84$, and $\kappa = (1.1)(2) + 2.5 = 4.7$. We need the gas pressure, but for now, let's use the ideal gas law to calculate the density at 1 bar, 20°C. We'll check our result later.

We need to specify a pipe diameter. Let's choose a 4-in. diameter Schedule 40 pipe. We'll see if it gives us a reasonable pressure drop.

$$v_s = \{1.39[(9.81)(0.102)]^{1/2} 4.7 (10^{4.84}) / [(1.2)(0.00214)]\}^{1/5.7} = 16.8 \text{ m/s}$$

$$\text{Conveying velocity } u_g = (1.2)(16.8) = 20.2 \text{ m/s}$$

Step 2. Confirm with bag filter supplier that $\Delta P_{\text{separation}} = 1000$ Pa (4 in. H₂O), *i.e.*, $\Delta P_{7-8} = 1000$ kPa. (Refer to Figure 7.41 from here on out.)

Step 3. Calculate pressure drop in horizontal line feeding separator.

$$\mathbf{Re} = (1.2)(19.4)(0.102)/1.84\text{E-}5 = 1.3\text{E}4$$

Using $\varepsilon/D = 0.0002$ in the Sacham equation gives $f = 0.018$.

$$\Delta P_{\text{gas6-7}} = (0.018)(1.2)(20.2)^2(5)/[(2)(0.102)] = 440 \text{ Pa}$$

$$\text{Solids loading ratio } \phi = W_s/W_g = 1.39/[(1.2)(20.2)(0.00214)] = 1.39/0.198 = 7.0. \quad \mathbf{Fr} = (20.2)^2/[(9.81)(0.102)] = 407$$

$$u_t = (1.74)[(9.81)(0.002)(950-1.2)/1.2]^{1/2} = 6.85 \text{ m/s}$$

$$\mathbf{Fr}_s = (6.85)^2/[(9.81)(0.002)] = 2390$$

$$f_s = (0.082)(7)^{-0.3}(407)^{-0.86}(2390)^{0.25}(0.102/0.002)^{0.1} = 0.0027$$

$$\Delta P_{\text{solids6-7}} = (7)(0.0027)(1.2)(20.2)^2(5)/[(2)(0.102)] = 227 \text{ Pa}$$

$$\Delta P_{6-7} = \Delta P_{\text{gas6-7}} + \Delta P_{\text{solids6-7}} = 440 + 227 = 667 \text{ Pa}$$

$$\Delta P_{6-8} = 1000 + 667 = 1667 \text{ Pa}$$

Step 4. Calculate pressure drop in bend. With $D/R = 4$, use $B = 0.75$.

$$\Delta P_{5-6} = (0.75)(1+7)(1.2)(20.2)^2/2 = 1470 \text{ Pa}$$

$$\Delta P_{5-8} = 1470 + 1667 = 3137 \text{ Pa}$$

Step 5. Calculate pressure drop in vertical line. The line is rather long, and compared to horizontal conveying, the solids friction factor for vertical conveying is relatively large. Therefore, let's separate it into two 10-m long sections.

Since we are dealing with compressible flow, check the gas density. At 3137 Pa gauge, $\rho_g = 1.25 \text{ kg/m}^3$; $u_g = 20.1 \text{ m/s}$

$$\text{Upper section: } \Delta P_{\text{gas4}\frac{1}{2}\text{-5}} = (0.018)(1.25)(20.1)^2(10)/[(2)(0.102)] = 450 \text{ Pa}$$

$$u_p/u_g = 1 - (0.044)(0.002)^{0.3}(950)^{0.5} = 0.79$$

$$f_s = 1/[(1200)(0.79)] + 2/[(0.79)(403)] = 0.0073$$

$$\Delta P_{\text{solids4}\frac{1}{2}\text{-5}} = (7)(0.0073)(1.25)(20.1)^2(10)/[(2)(0.102)] = 1270 \text{ Pa}$$

$$\text{Pressure drop due to lift: } \varepsilon = 1 - 1.39/[(950)(0.00817)(0.79)(20.1)] = 0.989$$

$$\Delta P_{lift4\frac{1}{2}-5} = [(0.989)(1.25) + (1 - 0.989)(950)](9.81)(10) = 1150 \text{ Pa}$$

$$\Delta P_{4\frac{1}{2}-5} = 450 + 1270 + 1150 = 2870 \text{ Pa}; \Delta P_{4\frac{1}{2}-8} = 3140 + 2870 = 6010 \text{ Pa}$$

Similar calculations are performed for the lower half of the vertical section, but this time use $\rho_g = 1.3 \text{ kg/m}^3$; $u_g = 19.9 \text{ m/s}$ to account for the higher gas pressure.

$$\Delta P_{gas4-4\frac{1}{2}} = 460 \text{ Pa}; \Delta P_{solids4-4\frac{1}{2}} = 1320 \text{ Pa}; \Delta P_{lift4-4\frac{1}{2}} = 1180 \text{ Pa}$$

$$\Delta P_{4-4\frac{1}{2}} = 2960 \text{ Pa}; \Delta P_{4-5} = \Delta P_{4-4\frac{1}{2}} + \Delta P_{4\frac{1}{2}-5} = 5830 \text{ Pa}; \Delta P_{4-8} = 8970 \text{ Pa}$$

Step 6. Bend at lower elevation. You know the drill; same as last time, but this time set the gas density equal to 1.6 and the gas velocity equal to 18.4 m/s. $\Delta P_{3-4} = 1550 \text{ Pa}$; $\Delta P_{3-8} = 10520 \text{ Pa}$

Step 7. Calculate pressure drop in horizontal line following feed point. Calculate the pressure drops due to gas flow and solids flow as before, but for this section, we also need to determine the pressure drop due to the acceleration of the solids. Keep ρ_g equal to 1.3 kg/m^3 and u_g equal to 19.9 m/s .

$$\Delta P_{gas2-3} = 460 \text{ Pa}; \Delta P_{solids2-3} = 480 \text{ Pa}$$

$$\Delta P_{acc2-3} = [(1.3)(19.9)^2/2] [1 + 2(7)(0.79)] = 2990 \text{ Pa}$$

$$\Delta P_{2-3} = 3930 \text{ Pa}; \Delta P_{2-8} = 14450 \text{ Pa}$$

We should recalculate the saltation velocity to confirm that our conveying velocity is okay at the higher pressure. The Rizk equation gives $v_s = 16.6 \text{ m/s}$, so we should be fine if we don't worry about the imprecision of the Rizk equation. Again, it's best to conduct trials on a vendor's test rig.

Step 8. Calculate pressure drop between air mover and feed point. At last, an easy one! All we need to determine is the pressure drop due to air flow alone. With the higher pressure, we need to set ρ_g equal to 1.4 kg/m^3 and u_g equal to 19.7 m/s .

$$\Delta P_{1-2} = \Delta P_{gas1-2} = 470 \text{ Pa}$$

$$\Delta P_{1-8} = 14920 \text{ Pa} = 2.2 \text{ psi}$$

Results are summarized in Table 7-4.

Section	ΔP (Pa)
7-8	1000
6-7	670
5-6	1470
4-5	5830
3-4	1550
2-3	3930
1-2	<u>470</u>
Overall (1-8)	14920

The results show that the vertical lifting and acceleration of the solids are major contributions to the overall pressure drop. Also note that bends also give relatively large pressure drops, which is one of the reasons why their number should be minimized.

Our choice of a 4-in. nominal diameter pipeline gave us a reasonable pressure drop. If we had instead chosen a 2-in. nominal diameter pipe, our calculated pressure drop would have been 52 kPa (7.5 psi).

Dense-phase conveying

While design methods for dilute-phase pneumatic conveying systems are well developed, methods for designing dense-phase systems are considerably less defined. Installing a dense-phase conveying system without first conducting tests is risky, as trials need to be conducted to determine the appropriate pipe diameter and gas-loading ratio and the location and number of boosters, devices that introduce additional gas into the conveying pipeline. Compared to dilute phase, dense-phase conveying is gentle and should be considered for transport of friable particulate solids.

Transfer chutes

Chutes are used to direct the flow of bulk solids. Unlike bins, they (generally) do not have converging walls and are not completely filled with the bulk solid. They need to be properly designed to avoid problems such as plugging, excessive wear, dust generation, and particle attrition.

A chute must be sufficiently steep and low enough in friction to permit sliding and clean off. Referring to Figure 7.42, the velocity of a stream of

particles (assuming no bouncing) after impacting a chute, V_2 , relative to its velocity before impact, V_1 is:

$$V_2 = V_1(\cos\theta - \sin\theta \tan\phi') \quad (7.81)$$

where θ is the impact angle and ϕ' is the wall friction angle.

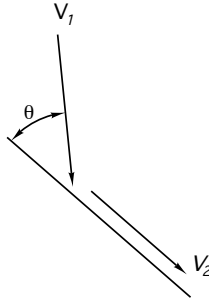


Figure 7.42. Velocity of a particle after impact on a chute.

If the particles fall freely when they are dropped onto the chute, their velocity before impact V_1 is its free-fall velocity:

$$V_1 = \sqrt{2gH} \quad (7.82)$$

where H is the drop height.

If the sum of ϕ' and θ equals 90° , the value of V_2 in Equation 7.81 is equal to zero, and the bulk material will not slide on the chute surface unless its angle of inclination is greater than a minimum value. To determine the minimum chute angle required to overcome adhesion at impact, chute tests described by Stuart and Royal [*Bulk Solids Handling*, 12, 3, 447 (1992)] can be performed. A sample of the bulk material is loaded onto a wall coupon and a load representing the impact pressure is briefly applied. The impact pressure σ is approximately equal to

$$\sigma \approx \rho_b V_1^2 \sin^2 \theta \quad (7.83)$$

The coupon is inclined about a pivot point until it just starts to slide. Usually a safety factor of 5° is applied to this minimum value to ensure clean off; if 10° greater than the minimum, the chute will remain cleaner than a Doris Day's greatest hits album.

While sliding on a straight surface, the particles will accelerate or decelerate, depending on the relative values of the chute angle α measured from horizontal and the wall friction angle ϕ' (see Figure 7.43):

$$a = g(\sin \alpha - \cos \alpha \tan \phi') \quad (7.84)$$

where a is the acceleration.

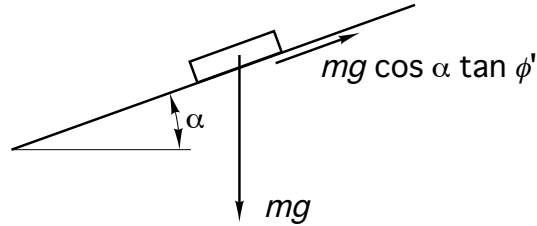


Figure 7.43. Element of bulk solid sliding on a straight chute.

With a little effort, Equation 7.84 can be rewritten as

$$a = g \cos \alpha (\tan \alpha - \tan \phi') \quad (7.85)$$

which shows that if you want to be certain that the velocity of the particles does not fall to zero, you should set the chute angle α greater than the angle of wall friction ϕ' , say 5-10° greater to be safe.

Of course it's okay for acceleration to be negative. In fact, too high a velocity can lead to the formation of dust. Also, if for example, you are discharging the material onto a moving conveyor belt, it is prudent to aim for a final velocity somewhat close to the belt speed. You just don't want the velocity to equal zero! Assuming that the chute cross section does not decrease along a distance S on the chute surface, the stream velocity V is given by:

$$V = \sqrt{V_0^2 + 2aS} \quad (7.86)$$

where V_0 is its velocity at the chute entrance.

When the velocity of the stream changes as it passes through a chute, the stream's cross-sectional area will change. To prevent flow stoppages, the chute should be sized such that it is no more than about one-third to one-half full at its minimum velocity.

While chutes can be fabricated and installed in rectangular sections, having curved surfaces upon which the material slides is advantageous. Chutes fabricated from cylindrical pipes or having rounded surfaces control the stream effectively, as they can be used to center the material allowing its momentum to keep the chute clean. The path that the bulk material will flow depends on its frictional properties and flow rate.

Flow onto a curved chute is illustrated in Figure 7.44. Dynamic equilibrium of forces gives

$$\frac{dV}{d\theta} + V \tan^2 \phi' = \frac{gR}{V} (\cos \theta - \tan \phi' \sin \theta) \quad (7.87)$$

where R is the radius of the “spoon” and θ is the angular coordinate. Fritella and Smit (search for “Chute Design Essentials” on bulk-online.com) found an analytical solution for a constant radius and wall friction angle:

$$V = \sqrt{\frac{2gR}{4 \tan^2 \phi' + 1} \left[(1 - 2 \tan^2 \phi') \sin \theta + 3 \tan^2 \phi' \cos \theta \right] + \exp(-2\theta \tan \phi')}$$

$$\cdot \left[V_i^2 - \frac{6 \tan \phi' gR}{1 + 4 \tan^2 \phi'} \right] \quad (7.88)$$

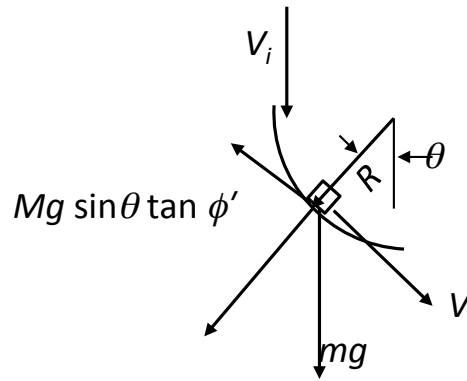


Figure 7.44. Element of bulk solid sliding on a curved chute.

When designing chutes with complicated geometries or when the solids fly off a belt before they enter the chute, Discrete Element Method (DEM)

models should be used. Rocky DEM is a good provider of DEM simulation tools.

Free fall height and sudden changes in the direction of material flow should be minimized to reduce solids impact pressures, which can result in attrition, abrasive wear, and dust generation. Since impact pressure is proportional to $\sin^2\theta$ and V_1^2 , reducing the impact angle and drop height will reduce wear, and the momentum of the flowing material will keep the chute surface cleaned off. Short drop heights also reduce the risk of segregation due to differences in particle velocities.

Dust is created when air is entrained into the flowing material. To avoid creation of dust, the chute should be designed to ensure that the material remains in contact with the chute surface, the material stream is concentrated, and the velocity through the chute remains nearly constant. If the material is to land on a belt conveyor at the exit of the chute, the velocity of the stream should be in the direction of and equal to or greater than the belt velocity.

Attrition of friable particles is most likely to occur at impact points where the impact pressures are high. Therefore, attrition can be reduced by minimizing the impact angle θ , maintaining a constant stream velocity, and ensuring that the flowing stream is concentrated and remains in contact with the chute surface.

One final note: I enjoy skiing, but I struggle whenever I attempt to snowboard. My nephew reminded me that I used to skateboard when I was in college and wondered why snowboarding was more challenging. I showed him Equation 7.85 and pointed out that the formula had two terms: α , which is related to the slope, and ϕ' , which is related to friction. When I was on a skateboard, the slope was shallow and the friction was high. My acceleration was therefore manageable. On a snowboard, however, the slope is high and the friction is low. Consequently, my acceleration could be quite high, and the only time it wasn't high was when I fell because the friction between my ass and the snow was much greater than the friction between my snowboard and the snow (see Figure 7.45). I still suck at snowboarding, but my nephew knows how to design transfer chutes.

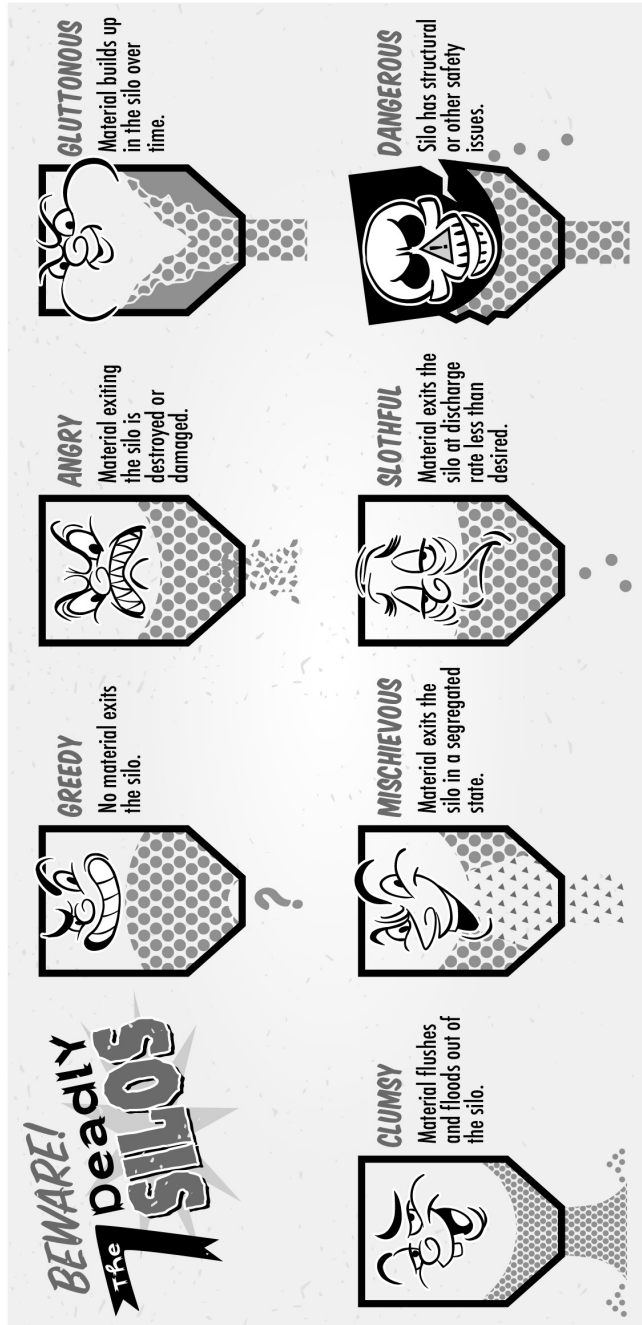


Figure 7.45. Analogy between chute design and snowboarding.

8. BETTER REFERENCES THAN THIS ONE

1. Arnold, P., A. Roberts, and A. McLean, Bulk Solids: Storage, Flow, and Handling, TUNRA, Newcastle, Australia, 1978.
2. Bates, L., User Guide to Segregation, British Materials Handling Board, Marlow, England, 1997.
3. Bates, L., Guide to the Design, Selection, and Application of Screw Feeders, Cromwell Press, Trowbridge, England, 2000.
4. Brown, C.J. and J. Nielsen, Silos, CRC Press, New York, 2019.
5. Fayed, M. and L. Otten, Handbook of Powder Science and Technology, Van Nostrand Reinhold Company, New York, 1997.
6. Jenike, A., Storage and Flow of Solids – Bulletin 123, University of Utah, Salt Lake City, Utah, 1964.
7. Klinzing, G.E., F. Rizk, R. Marcus, and L.S. Leung, Pneumatic Conveying of Solids – A Theoretical and Practical Approach, Springer, New York, 2010.
8. Kulwiec, R., Materials Handling Handbook, John Wiley and Sons, Hoboken, NJ, 1985.
9. McGlinchey, Bulk Solids Characterization, Blackwell Publishing Co., Carlton, Victoria Australia, 2005.
10. McGlinchey, Bulk Solids Handling – Equipment Selection and Operation, Blackwell Publishing Company, Ames, IA, 2008.
11. Rhodes, M. Introduction to Particle Technology, John Wiley and Sons, Hoboken, NJ, 2024.
12. Schulze, D., Powders and Bulk Solids: Behavior, Characterization, Storage and Flow, Springer, Berlin, 2021.

13. Shamiou, P., Handling of Bulk Solids – Theory and Practice, Butterworths, London, 1990.
14. Woodcock, C. and J. Mason, Bulk Solids Handling: An Introduction to the Practice and Technology, Springer Science, New York, 1987.



Courtesy of Scott Miller, Solids Handling Technologies